

**Università degli Studi di Padova**

Dipartimento di Ingegneria Industriale  
Corso di Laurea Magistrale in Ingegneria dell'Energia Elettrica

Master thesis  
**MODELLING THE LIGHTNING DISCHARGE  
INTERACTION  
WITH GROUND STRUCTURES AND AIRCRAFT**

**Students:**  
Federico Padoan

**Professors:**  
Turri Roberto  
Manu Haddad

In collaboration with



# Contents

|          |  |           |
|----------|--|-----------|
| <b>1</b> | <b>Spark discharge: Physical explanation</b>   | <b>1</b>  |
| 1.1      | Ionisation . . . . .   | 1         |
| 1.1.1    | Ionisation by impact . . . . .   | 1         |
| 1.1.2    | Thermoionization . . . . .   | 5         |
| 1.1.3    | Photoionisation . . . . .  | 5         |
| 1.2      | Generation of the charges . . . . .  | 6         |
| 1.2.1    | Electrical charge in a cell . . . . .  | 7         |
| 1.3      | Development of the leader . . . . .  | 10        |
| 1.4      | The Return Stroke . . . . .  | 13        |
| 1.5      | Lightning polarity and direction . . . . .   | 19        |
| 1.6      | Measured Characteristics of the Lightning Flash . . . . .  | 19        |
| <b>2</b> | <b>Leader models</b>   | <b>24</b> |
| 2.1      | Streamer inception . . . . .   | 24        |
| 2.2      | First streamer and streamer to leader transition . . . . .   | 25        |
| 2.2.1    | Simplified method . . . . .  | 25        |
| 2.3      | Charges extimation inside the leader corona region using a finite element<br>method software . . . . . | 31        |
| 2.3.1    | Streamer inception and dark period . . . . .   | 32        |
| 2.3.2    | Streamer-to-leader transition . . . . .  | 32        |
| 2.3.3    | Leader corona region definition . . . . .  | 33        |
| 2.3.4    | Leader corona region charger calculation . . . . .   | 33        |
| 2.3.5    | Leader channel model . . . . .   | 35        |
| 2.3.6    | Tortuous leader propagation . . . . .  | 36        |
| 2.3.7    | Methodology application . . . . .  | 39        |
| <b>3</b> | <b>Leader model for a grounded structure</b>   | <b>40</b> |
| 3.1      | Negative leader model (straight path) . . . . .  | 40        |
| 3.1.1    | Streamer Inception . . . . .   | 43        |
| 3.1.2    | First streamer formation . . . . .   | 45        |
| 3.1.3    | Streamer to leader transition . . . . .  | 49        |
| 3.2      | Positive leader model (straighth path) . . . . .   | 55        |
| 3.2.1    | Streamer inception . . . . .   | 57        |
| 3.2.2    | Streamer to leader transition . . . . .  | 59        |
| 3.2.3    | Positive leader model (tortuous path) . . . . .  | 66        |

|          |   |           |
|----------|---|-----------|
| <b>4</b> | <b>Leader model on an aircraft</b>            | <b>76</b> |
| 4.1      | Aircraft geometry . . . . .                   | 77        |
| 4.2      | Positive leader model from a radome . . . . . | 78        |
| 4.2.1    | Streamer inception . . . . .                  | 79        |
| 4.2.2    | Streamer-to-leader . . . . .                  | 79        |
| 4.3      | Radome protections . . . . .                  | 80        |
| <b>5</b> | <b>Conclusions</b>                            | <b>84</b> |

# List of Figures

|      |   |    |
|------|---|----|
| 1.1  | Attachment in $SF_6$ . . . . .  | 3  |
| 1.2  | Electron drift velocity . . . . .   | 4  |
| 1.3  | Diffusion coefficient . . . . .   | 4  |
| 1.4  | Absolute value of the net ionisation coefficient $\bar{\alpha} = \alpha - \eta$ . . . . .   | 4  |
| 1.5  | Percentage of ionised particles varying the temperature . . . . .   | 5  |
| 1.6  | Generalized diagram showing distribution of air currents and electrical charge distribution in a typical cumulonimbus cloud. . . . .  | 6  |
| 1.7  | An idealized cross section through a thunderstorm cell in its mature stage. . . . .   | 7  |
| 1.8  | Electric charge distribution inside a mature thundercloud. . . . .  | 8  |
| 1.9  | Atmospheric potential and vertical component of the atmospheric field $E_z$ . . . . .   | 9  |
| 1.10 | Orizontal component of the atmospheric field $E_x$ . . . . .  | 9  |
| 1.11 | Vertical cloud potential profile in the center of the storm and vertical electric field profile in the center of the storm. . . . .   | 9  |
| 1.12 | Stages in the development of a leader. . . . .  | 10 |
| 1.13 | The lightning leader. . . . .   | 11 |
| 1.14 | The development of a leader in the laboratory. . . . .  | 12 |
| 1.15 | Camera photograph of a lightning leader. . . . .  | 12 |
| 1.16 | Leader direction as determined from direction of branching: (a) Downward-branching leader starts at cloud. (b) Upward-branching leader starts at ground. . . . .  | 13 |
| 1.17 | Stages in the development of the return stroke. . . . .   | 14 |
| 1.18 | Phenomena associated with passage of the return stroke: (a) Current, (b) Longitudinal voltage, (c) Longitudinal resistance. . . . .   | 15 |
| 1.19 | Effect of corona cloud on velocity of propagation. (a) Distributed charge surrounding a highly conductive central core, (b) highly conductive central conductor fastened onto a series of projecting splines. . . . . | 16 |
| 1.20 | Front waveshapes of lightning currents. . . . .   | 17 |
| 1.21 | Current oscillograms from single strokes or first downward strokes. 1) Fast time-scale $t_1$ ; 2) Slow time-scale $t_2$ . . . . .   | 18 |
| 1.22 | Distribution of peak currents for first return stroke and sub-sequent strokes . . . . .   | 20 |
| 1.23 | Distribution of time to peak current. . . . .   | 20 |
| 1.24 | Distribution of rates of rise. . . . .  | 21 |
| 1.25 | Distribution of time to current half value. . . . .   | 21 |
| 1.26 | Distribution of duration of flashes to earth. . . . .   | 22 |
| 1.27 | Distribution of duration of flashes to earth. . . . .   | 22 |
| 1.28 | Distribution of duration of flashes to earth. . . . .   | 23 |
| 1.29 | Distribution of duration of flashes to earth. . . . .   | 23 |

|      |  |    |
|------|--|----|
| 2.1  | Potential distribution before and after corona formation in front of a rod. It is assumed that the rod electrode is grounded. In this case the corona zone extends from the tip of the stem $l_L$ to the coordinate $l_s$ on the discharge axis. . . . . | 26 |
| 2.2  | Schematic example of the leader advancement simulation. . . . .  | 27 |
| 2.3  | Geometrical approach of the potential distribution during the leader propagation. The shaded zone shows a detail of the used geometric area between $U_1^{(i)}$ and $U_2^{(i)}$ . . . . .  | 28 |
| 2.4  | Flow chart of the simplified leader inception model. . . . .   | 30 |
| 2.5  | Flow chart of the new methodology proposed. . . . .  | 31 |
| 2.6  | Potential distribution for a rod-plane electrode configuration. . . . .  | 33 |
| 2.7  | Spatial location of fictitious potential rings representing the LCR in front of the leader channel tip. . . . .  | 34 |
| 2.8  | Geometry built in the FEM solver for the calculation of the LCR charge using the SSM and CMM. . . . .  | 35 |
| 2.9  | Schematic representation of two consecutive leader channel segments $s_i$ and $s_j$ . Note the three different angles ( $\alpha$ , $\vartheta$ , and $\varphi$ ) used for the three-dimensional representation of the leader channel tortuosity. . . . . | 37 |
| 2.10 | PDF found for leader channel angles $\alpha$ . . . . .   | 37 |
| 2.11 | PDF found for leader channel angles $\vartheta$ . . . . .  | 38 |
| 2.12 | PDF found for leader channel angles $\varphi$ . . . . .  | 38 |
| 2.13 | From top left to bottom right: rod-to-plane, sphere-to-plane, sphere-toplane UP and sphere-to-plane SP. . . . .  | 39 |
| 3.1  | Simulation geometry. Respectively from the left: (a)domain, (b) electrode, (c)tall structure. . . . .  | 41 |
| 3.2  | 2D electrical field behavior. . . . .  | 41 |
| 3.3  | 2D electrical potential behavior. . . . .  | 42 |
| 3.4  | 1D electrical field following the line between the tower and the electrode . . . . .   | 42 |
| 3.5  | 1D electrical potential following the line between the tower and the electrode . . . . .   | 43 |
| 3.6  | Electrical field and pressure changing the altitude. . . . .   | 44 |
| 3.7  | LCR cone geometry in the first streamer. . . . .   | 46 |
| 3.8  | 2D and 1D LCR cone potential in the first streamer. . . . .  | 46 |
| 3.9  | 1D LCR cone electrical field in the first streamer. . . . .  | 47 |
| 3.10 | Electrical potential (2D) and electrical field (3D) of the approaching negative leader to the ground. . . . .  | 50 |
| 3.11 | 1D Electrical potential and electrical field of the approaching negative leader to the ground. . . . .   | 51 |
| 3.12 | Cumulonimbus geometry in Comsol Multiphysics. . . . .  | 55 |
| 3.13 | Electric field distribution 2D and 1D. . . . .   | 56 |
| 3.14 | Electric potential distribution 2D and 1D. . . . .   | 56 |
| 3.15 | Electrical field distribution in 3D, considering also the grounded structure. . . . .  | 57 |
| 3.16 | Electrical field distribution in 1D. . . . .   | 57 |
| 3.17 | Electrical field distribution in 1D and pressure changing the altitude. . . . .  | 58 |
| 3.18 | Electrical field distribution in 1D and Townsend coefficient changing the altitude. . . . .  | 58 |
| 3.19 | Leader length at each iteration (from the Matlab "Command Window"). . . . .  | 59 |
| 3.20 | Leader geometry once the simulation ended. . . . .   | 59 |

|      |   |    |
|------|---|----|
| 3.21 | 2D leader potential once the simulation ended. . . . .                                    | 60 |
| 3.22 | 1D leader electrical field once the simulation ended. . . . .                             | 60 |
| 3.23 | 1D Potential drop and superimposed potential. . . . .                                     | 61 |
| 3.24 | Resulting PDF for the $\alpha$ , $\vartheta$ and $\varphi$ angles. . . . .                | 66 |
| 3.25 | Leader geometry after the simulation. . . . .   | 69 |
| 3.26 | Leader meshing during the simulation. . . . .   | 69 |
| 3.27 | 2D electrical field. . . . .  | 70 |
| 3.28 | 1D electrical field along the z-axis . . . . .  | 70 |
| 3.29 | Potential drop in the fractal model. . . . .  | 71 |
| 4.1  | 2D electrostatic field around an aircraft in a 100 [kV/m] ambient electric field. . . . . | 76 |
| 4.2  | Jet plan drawing. . . . .   | 77 |
| 4.3  | Aircraft 3D CAD drawing in SolidWorks. . . . .  | 77 |
| 4.4  | Aircraft 3D CAD drew in SolidWorks. . . . .   | 78 |
| 4.5  | Streamers induced by approaching leader. . . . .  | 78 |
| 4.6  | Fuselage streamer development . . . . .   | 80 |
| 4.7  | Arrangement of diverter straps on non-metallic structural components. . .                 | 82 |

# Sommario

Il fulmine è un fenomeno molto affascinante che tutte le persone hanno sicuramente potuto osservare. È risaputo comunque che l'energia e la potenza che producono è enorme, causando grossi danni alle strutture, nonché un pericolo.

In particolare, in questa tesi considererò l'effetto dei fulmini su un radome di un aereo (la parte frontale del velivolo), e strutture collegate al terreno; il radome è costruito con materiali dielettrici (diversamente dalla fusoliera, composta di materiali metallici) per permettere l'emissione di segnali elettromagnetici dal radar e individuare la presenza di altri oggetti in aria. Questo è un problema, perché essendo trasparenti alle onde elettromagnetiche, la scarica potrebbe iniziare dall'antenna stessa, causando danni al radome.

Per risolverlo, implementerò un modello di scarica, cominciando dalla formazione dello streamer, per poi passare a alla sua "trasformazione" in leader, il tutto prima da una geometria connessa a terra e poi su un modello semplificato di aereo.

Per ottenere un lavoro completo, procederò in quattro step:

- I. nel primo capitolo studierò il fenomeno del fulmine da un punto di vista teorico: come si forma e sviluppa nello spazio, i processi di ionizzazione in una scarica, la formazione di cariche all'interno di una tempesta, lo sviluppo del leader nello spazio e la "scarica di ritorno" finale;
- II. nel secondo capitolo descriverò dei modelli usati per descrivere la teoria streamer. In particolare, illustrerò due metodi: uno semplificato ed uno completo che sfrutta il software *Comsol Multiphysics*;
- III. nel terzo capitolo descriverò il modello che ho scritto tenendo conto della parte teorica e di modellistica di cui ho appena accennato. Mostrerò come è stato costruito il modello usando diversi software (*Matlab*, *Comsol*, *LiveLink Matlab - Comsol*) e i risultati che ho ottenuto, implementando prima un modello con un percorso del leader lineare e poi con uno irregolare;
- IV. nel quarto e ultimo capitolo descriverò come il modello costruito nel precedente capitolo possa essere applicato anche ad un aereo. Sarà poi illustrato uno studio elettromagnetico del radome, in cui verrà evidenziato come questa parte dell'aereo sia trasparente alle onde elettromagnetiche e come l'antenna sia soggetta ad importanti campi elettrici. Questa parte è stata fatta utilizzando *Comsol* e *SolidWorks*.

Questo studio è stato fatto per valutare se il processo di scarica è possibile e per progettare delle protezioni (chiamate "strisce divertrici") per aerei, utilizzate per evitare il danneggiamento del radome.

Questo progetto verrà continuato all'Università di Cardiff, in cui questo modello verrà



implementato sarà applicato ad un dominio di dimensioni più ridotte (simulando delle condizioni di laboratorio) e poi testato con pezzi reali di radome nel "*Morgan Botti - Lightning Laboratory*" di Cardiff.

## Abstract

The lightning is a fascinating phenomena all the people can observe during their own life. But, it is well known the power it can deliver is huge, causing important damages to the structures and also a danger.

In particular, in this thesis I'll consider the effect of lightnings on an aircraft radome (the front part of the vehicle) and grounded structures; the first device is built with dielectric materials (unlike the fuselage, composed by metallic materials) to permit the emission of electromagnetic signals from the radar in order to verify the presence of other objects in the air. This is a problem, because, being transparent to electromagnetic waves, the discharge could begin from the antenna itself, causing a puncturing of the radome, and a damage on it.

To overcome this issue, I'll design a model of a discharge, starting from the streamer-leader formation from a structure connected to the ground, passing then to aircrafts.

To achieve a complete work, I'll proceed in four different steps:

- I.* in the first chapter I'll study the lightning phenomena: how it originates and develops in the space. In particular, all the ionisation processes we can find in a spark discharge, the charge formation inside a thunderstorm, the development of the leader into the space and the final "return stroke";
- II.* in the second chapter I'll describe some models used to describe the streamer inception and then the streamer to leader formation. In particular, I'll summarize two methods: a simplified method and a complete method that uses the software Comsol Multiphysics;
- III.* in the third chapter I'll illustrate the model I implemented taking into account the theoretical part and the models previously explained. I'll show you how the model was built using Matlab, LiveLink Matlab-Comsol and Comsol Multiphysics, and the results I achieved, implementing before a straight path of the leader and the tortuous path;
- IV.* in the fourth and last chapter I'll describe how the model I built could be applied on an aircraft. Then a electromagnetic study of the radome will be illustrated, showing how this part of the aircraft is transparent to the electromagnetic waves and how the antenna is subjected to the external electrical field sollecitation. This has been done using Comsol and SolidWorks.

I did this work in order to evaluate if the discharge process is possible and to design some protection (called diverted strips) for the aircraft, used to avoid the puncture of the radome.

This project will continue in Cardiff in the next month, in which this model will be applied in a smaller domain (simulating a laboratory condition) and then tested with real samples of radomes in the "*Morgan Botti - Lightning Laboratory*" in Cardiff.

# Chapter 1

## Spark discharge: Physical explanation

When we see a lighting between the clouds or from the clouds to the ground we see only a filamentary flash, but the complete process is really more complex.

Firstly, it is related to the formation of free electrical charges in the air or, more commonly, in the clouds. In fact, the most common producer of lightning is the cumulonimbus thundercloud. Lightning, however, can also occur during sand-storms, snowstorms, and in the clouds over erupting volcanos.

In all these situations, there is a charge concentration high enough to create a really strong electrical field, that helps (associated with other ionisation processes) a leader formation; This is a plasma channel, that, proceeding to the ground (or to another cloud), accumulates more charges, causing the discharge and the light we are used to see in our life.

In order to describe the phenomenon in an objective way, I'll discuss before the different kind of ionisation process [1] and then how the charges rise in a cumulonimbus, in order to achieve the conditions to obtain a streamer formation, followed by a the leader and then the final discharge.

In particular, in every gas there is a casual generation of free electrons, due to the cosmic radiation and the natural radioactivity. These electrons link to the atoms or electronegative molecules giving birth to a population of negative ions that, in normal conditions goes from 1000 to 10000 *ions/cm<sup>3</sup>* (obviously also the atmospheric conditions are important). Naturally it's impossible obtaining free electrons thanks only to the cosmic rays. So, I need to extract the valence electrons from the "cathode". How can I do it?

### 1.1 Ionisation

#### 1.1.1 Ionisation by impact

The movement of the charges (mainly electrons) follow the direction of the applied electrical field, making them collide with the neutral particles. These are divided by this impact, creating an ion and another electron.

In particular, it is possible to distinguish 2 different kind of collision:

1. **elastic**: between the particles there is only an exchange of kinetic energy, without any variation in the atomic or molecular structure;

2. **anelastic**: between the particles there are energy exchanges capable of modifying the intern energy or the nature of the particle.

This last phenomenon allows the particles to achieve a higher energy level, even if for a very short time (**excitement**) or to tear an electron apart and to leave a positive ion (**ionisation**): this last is really important in electric discharges.

In almost all cases the energy balances of these collision processes are equalized by the photons, thanks to the photoionisation, undergoing the law of the energy conservation. Considering oxygen and nitrogen (most present elements in air), it is possible to evaluate a fixed ionisation potential:

Table 1.1: Ionisation potentials.

| Material | 1° [eV] | 2° [eV] | 3° [eV] |
|----------|---------|---------|---------|
| Oxygen   | 13.61   | 35.15   | 54.9    |
| Nitrogen | 14.54   | 29.61   | 47.43   |

### Ionisation, Recombination and attachment coefficients

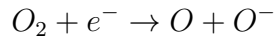
In order to evaluate the Ionisation by impact, we need a coefficient (called  $\alpha$  [ $cm^{-1}$ ]) to describe how many ionising collisions per unit length it is possible to find in a situation of high electrical field. Moreover, it is necessary taking into account also the recombination effect [3]: two particles with different polarity can, colliding, neutralize their charge. To characterize this phenomenon, generally it is used the parameter  $\rho$ , that combines the recombination speed with the concentration of positive charges ( $n^+$ ) and negative charges ( $n^-$ ):

$$\frac{dn}{dt} = \rho n^+ n^-$$

in case of  $n^+ = n^- = n$  we have

$$\frac{dn}{dt} = \rho n^2$$

Another effect is the attachment: when an electron with low energy impacts an atom or a molecule could be captured by the same particle, becoming a negative ion. Considering molecules, the attachment could be related to the molecule dissociation; for example:



After this process, the electron is associated to a particle with a really higher mass than the negative particle, with a slower mobility than the electron: we can consider the electron removed from the discharge process. The attachment is really important in the the air, because there are oxygen and other electronegative gases. This phenomenon is represented by the coefficient  $\eta$  [ $cm^{-1}$ ], the average number of attachments an electron is subjected in one centimeter path, and it depends to the nature and the energy of the electron.

The number  $dn$  of lost electrons due to the attachment along a distance  $dx$  is:

$$dn = -\eta n dx$$

integrating

$$\int_0^x dn = \int_0^x -\eta n dx \iff n = n_0 e^{-\eta x}$$

in which  $n_0$  is the initial number of electrons.

For example, considering electronegative gases as  $SF_6$ : until the energy of the electrons is around 0,1 [eV] there is the formation of  $SF_6^-$ , instead, for higher energies, there is the capture of the electrons, obtaining  $SF_5^-$  (this is why it is a really dielectric material):

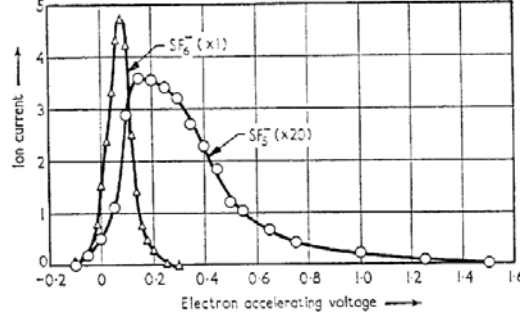


Figure 1.1: Attachment in  $SF_6$

After discussing all these parameters and phenomena, we can consider the *Townsend ionisation coefficient*  $\bar{\alpha} = \alpha - \eta$  [4]: it'll be considered a discharge in dry air, containing 80%  $N_2$  and 20%  $O_2$ , at  $p = 1$  [bar] and  $T = 300$  [K]. The electron drift velocity and electron diffusion coefficient can then be expressed in terms of the reduced electric field  $\tilde{E} = (|E|/N)/1Td$  as

$$v_e = 4.2 \cdot 10^3 [m/s] \cdot \tilde{E}^{0.74}, \quad (1.1)$$

$$D_e = 9,7 \cdot 10^{23} [1/ms] \cdot (\tilde{E}^{0.22})/N, \quad (1.2)$$

where  $N$  is the gas number density and the Townsend unit is  $1Td = 10^{-21} [Vm^2]$ . Here we assume  $N = p/(k_B T) \simeq 2,414 \cdot 10^{25} [m^{-3}]$  where the Boltzmann constant is  $k_B$ . The electron mobility follows from equation (1.1) and is given by  $\mu_e = v_e/|E|$ . The Townsend ionization coefficient ( $\bar{\alpha}$ ) it is given by

$$\bar{\alpha} = 750 \frac{T_0}{T} \left[ c_1 \left( 1 + \frac{c_2}{(\frac{|E|T}{750T_0})^3} \right) e^{\frac{c_3}{750T_0}} - \Psi \right], \quad (1.3)$$

with  $c_1 = 1,75 \cdot 10^3$ ,  $c_2 = 1,15 \cdot 10^{12}$ ,  $c_3 = -4 \cdot 10^{-4}$  and

$$\Psi = \frac{0,9}{1,49 + e^{-\frac{750T_0}{587T}}} \quad (1.4)$$

Varying the electrical field in the condition previous described we obtain the following behaviour:

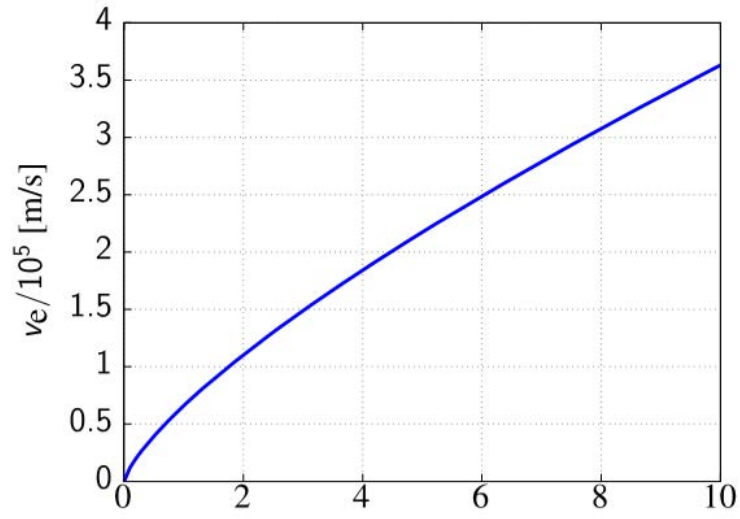


Figure 1.2: Electron drift velocity

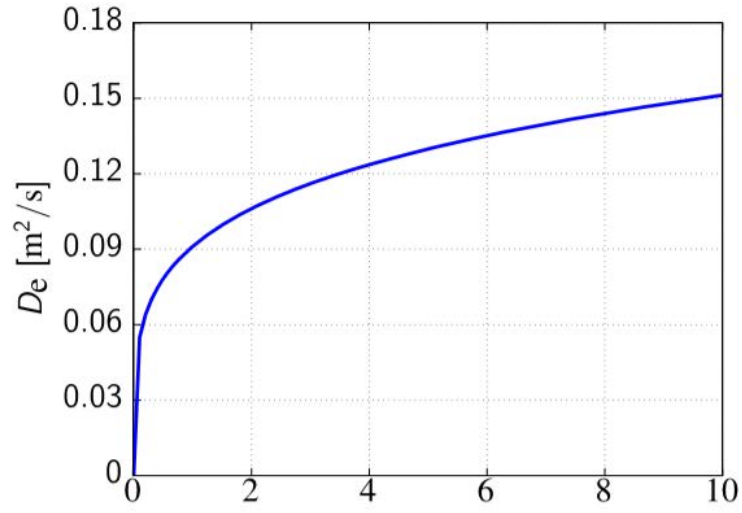


Figure 1.3: Diffusion coefficient

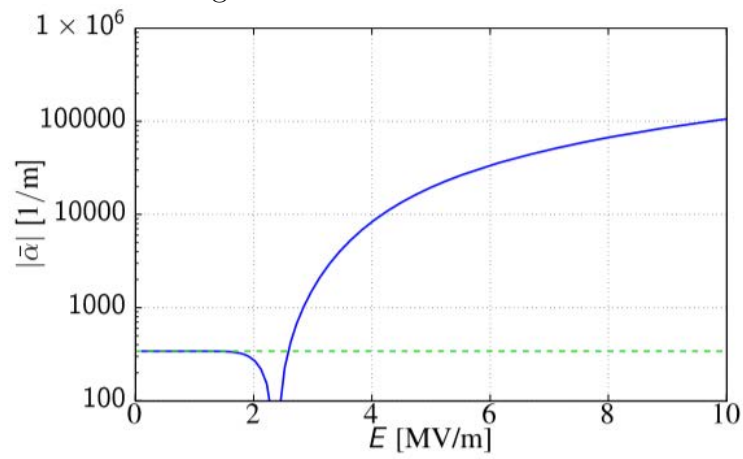


Figure 1.4: Absolute value of the net ionisation coefficient  $\bar{\alpha} = \alpha - \eta$

### 1.1.2 Thermoionization

Moving clutteringly, due to the thermal excitement, a particle can reach, after some collisions, enough energy to ionize another particle. Increasing the temperature increase the number of particles in this condition, so, also the ionisation degree increases (ratio between the number of ionized particles and total number of particles). In order to reach this process is necessary a high temperature; so, this isn't an important process in discharges in air at ambient temperature.

However, in equilibrium conditions, the ionisation degree  $x$ , fixed the pressure  $p$ , is related to the temperature with the *Sala Equation*:

$$\log\left(\frac{px^2}{1-x^2}\right) = -5040\frac{V_i}{T} + 2,5 \log(T) - 6,5 \quad (1.5)$$

in which  $V_i$  is the ionisation potential in [V].

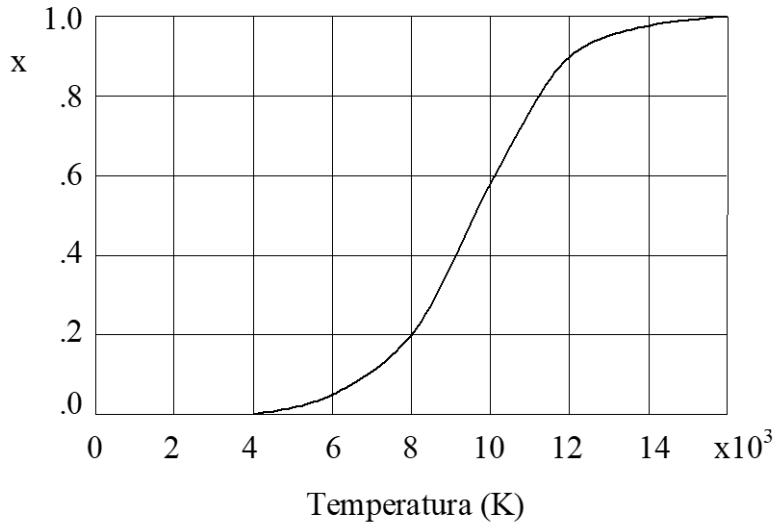


Figure 1.5: Percentage of ionised particles varying the temperature

### 1.1.3 Photoionisation

Photon energy is equal to  $h\nu$ , where  $h$  is the Planck constant ( $6.62 \cdot 10^{-34}$  [Js]) and  $\nu$  is the radiation frequency. If  $h\nu \geq eV_i$  ( $\simeq 15$  [eV]) an atom absorbing a photon could be ionised. Since  $h\nu = \frac{hc}{\lambda}$  (where  $c$  is the light speed and  $\lambda$  the photon wave length), in order to have ionisation it is necessary to have:

$$\lambda \leq \frac{12400}{V_i} \quad (1.6)$$

Introducing  $V_i = 15$  [eV] the resulting wave length is about 1000 [Å] (wavelength of an ultraviolet radiation), because oxygen and nitrogen are considered prevalent in air. This kind of radiations (called "vacuum ultraviolet") have a really high absorption coefficient, so the mean free path is really low and they are absorbed by the next gas volume.

## 1.2 Generation of the charges

The energy that produces lightning is assumed to be provided by warm air rising upwards into a developing cloud. As the air rises it becomes cooler, and at the dew point, the excess water vapor condenses into water droplets, forming a cloud. When the air has risen high enough for the temperature to drop to  $-40\text{ }^{\circ}\text{C}$ , the water vapor will have frozen to ice. At lower elevations there will be many supercooled water drops that are not frozen, even though the temperature is lower than the freezing point. In this supercooled region, ice crystals and hailstones form.

According to one theory, the cloud becomes electrically charged by the following process [2]: some of the ice crystals which have formed coalesce into hailstones. These hailstones fall through the cloud gathering additional supercooled water droplets. As droplets freeze onto a hailstone, small splinters of ice chip off. Apparently, these splinters carry away a positive electrical charge, leaving the hailstone with a net negative charge. The vertical wind currents in the cloud carry the ice splinters into the upper part of the cloud, while the hailstone, being heavier, falls until it reaches warmer air, where some portion of it melts and the remainder continues to earth. Thus, the upper part of the cloud takes on a positive charge while the lower region takes on a negative charge. In some other manner, another smaller pocket of positive charge may be formed near the front of the base of the cloud and below the main body of negative charge.

Other theories have been proposed to account for the electrification of the cloud. All of them are based on experimentally observed evidence that the charge in the top of the cloud is positive. There may also be a body of positive charge near the front of the base of the cloud. The charge in the rest of the cloud is negative. Figure 1.6 shows a typical cloud with the charge distributed as previously described. The cloud is moving to the left. The unbroken lines represent stream lines of air.

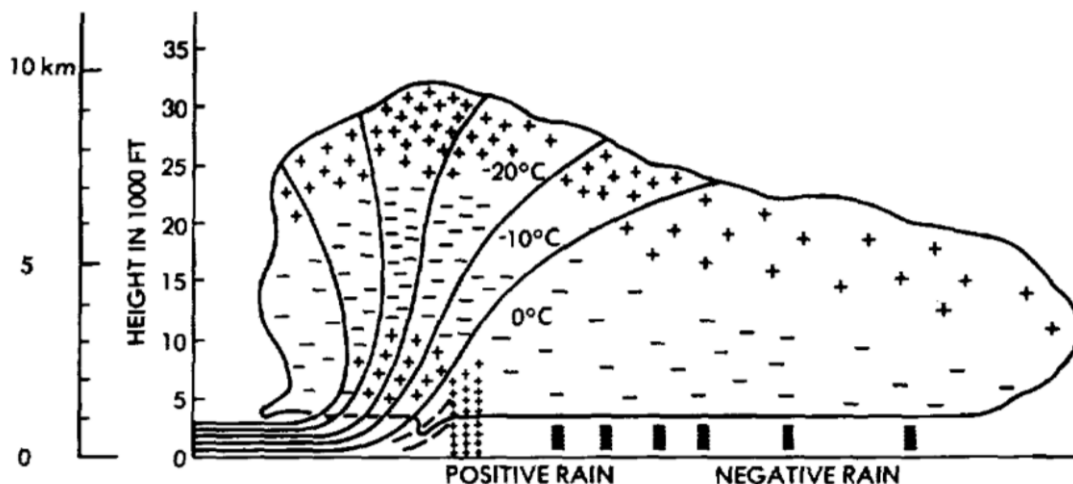


Figure 1.6: Generalized diagram showing distribution of air currents and electrical charge distribution in a typical cumulonimbus cloud.

The air currents and the electrical charges tend to be contained in localized cells and the cloud as a whole to be composed of a number of cells. A typical cloud might have the cell structure shown in Figure 1.7:



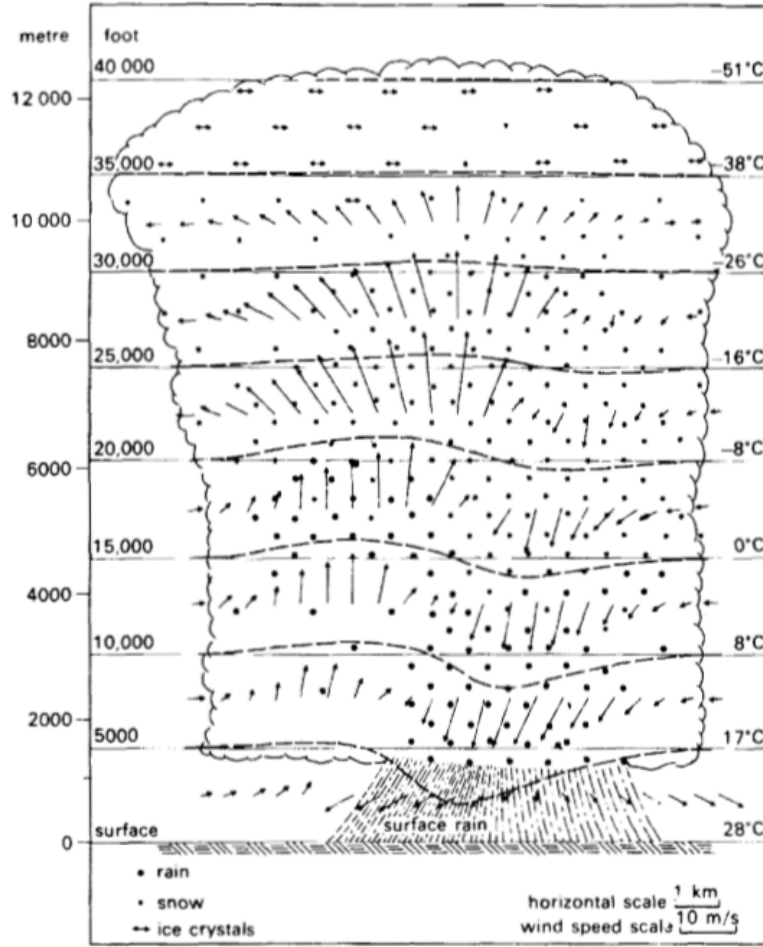


Figure 1.7: An idealized cross section through a thunderstorm cell in its mature stage.

### 1.2.1 Electrical charge in a cell

Taking account from [5] and [6] the cumulonimbus is modeled with a cylindrical geometry in order to maintain a uniform probability of lightning initiation over the active area of the storm. The variation of charges density towards the edges of space charge regions, normally found in nature, is ignored for the sake of simplicity. Charge regions have uniform densities and common borders. Thus a transition zone of mixed space charges between charge regions does not exist in this model.

In determining the dimensions of charge regions, we considered the following: a storm charge model must have maximum electric fields at two preferred altitudes where VHF radiation from the initial breakdown of cloud-to-ground and intracloud flashes is observed; these are at approximately 5 [km] and 9 [km], respectively.

As maximum electrical fields occur at the boundary between positive and negative space charge regions, the negative charges should prevail between 9 [km] altitude and the lower cloud boundaries (assumed to be at 2 [km] altitude), with positive charges ranging between 9 [km] and the top of the cloud (assumed to be at 12 [km]). The assumed radius of the charged cloud is 5 [km], a typical dimension of an isolated storm in radar reflectivity data. In view of the uncertainty in estimates of cloud charges from remote measurements, it

has been chosen their values to fall within the scale of those quoted in the literature (tens of Coulombs) but with the main negative charge much larger than the main positive one. The lower negative charge of  $-80 [C]$  extends from  $2 [km]$  to  $9 [km]$  altitude, over a region of  $5 [km]$  radius; its charge density is about  $-0,18 [nC/m^3]$ . The upper positive charge of  $50 [C]$  is  $3 [km]$  thick, also with a  $5 [km]$  radius; its charge density is  $0,21 [nC/m^3]$ . The high charge density core of  $0,5 [km]$  radius in the model corresponds to an intensive updraft region, which is the primary charge-generating region of the storm, and which is also the region where rain fall originates at the mature stage of the storm.

This core includes a small positive charge region of  $3 [C]$  which extends from the lower cloud boundary to a  $5 [km]$  altitude (with a charge density of  $1,3 [nC/m^3]$ ) and a small negative core charge region of  $10 [C]$  between  $5$  and  $9 [km]$  altitude (with a charge density of  $-3,2 [nC/m^3]$ ). The model does not take into account the corona space charges near the ground.

Figure 1.8 is a depiction of the charge model used in the present analysis:

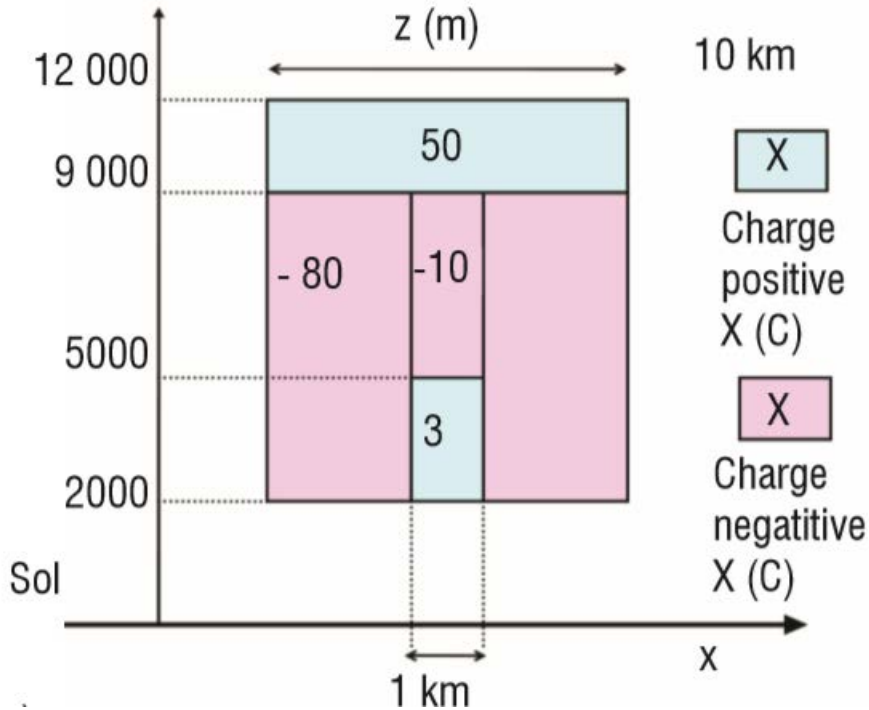


Figure 1.8: Electric charge distribution inside a mature thundercloud.

Solving the Poisson equation with this charge distribution the results obtained in [6] are reported below. In particular, it's interesting noting the electrical potential and the electrical field at the center of the storm: it could be observed there is a high electrical field at an height of  $5 [km]$ , that it's the range in which there is the most important concentration of lightnings intercepted by aircrafts.

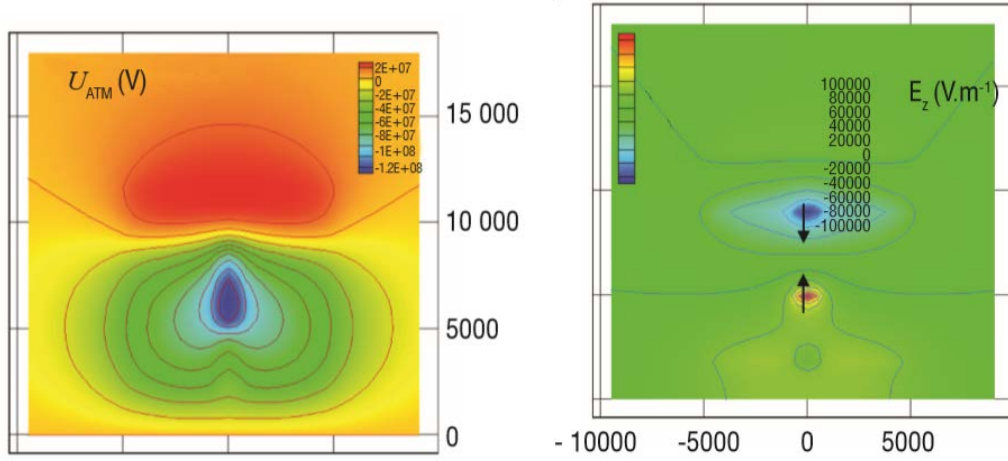


Figure 1.9: Atmospheric potential and vertical component of the atmospheric field  $E_z$

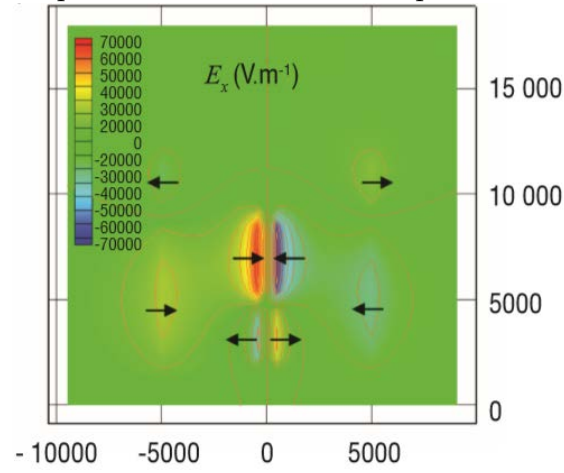


Figure 1.10: Horizontal component of the atmospheric field  $E_x$

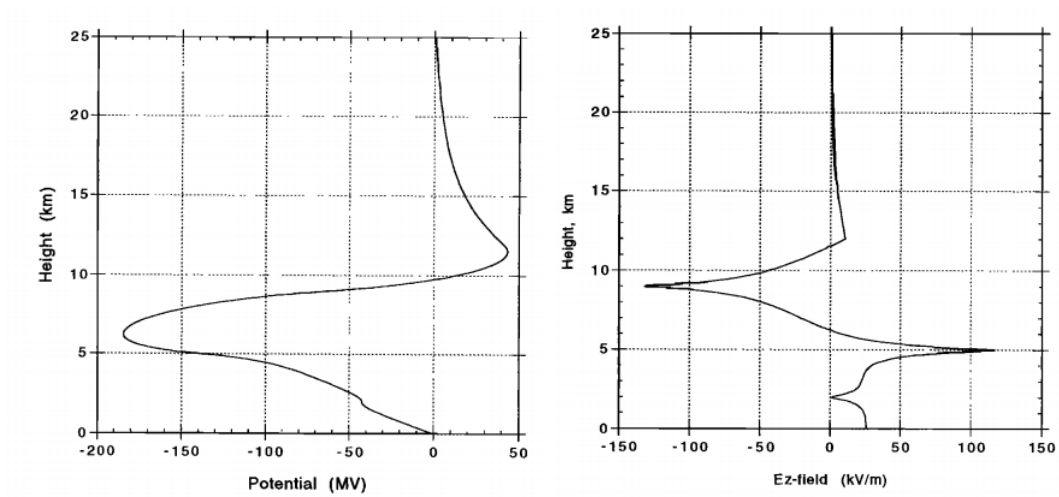


Figure 1.11: Vertical cloud potential profile in the center of the storm and vertical electric field profile in the center of the storm.

### 1.3 Development of the leader

At some state in the electrification of the cloud, a discharge towards the earth takes place. It starts as a slow-moving column of ionized air called "*the pilot streamer*". After the pilot streamer has moved perhaps 30 to 50[m], a more intense discharge called the "*step-leader*" takes place. This discharge lowers additional negative charge into the region around the pilot streamer, recharges it, and allows it to continue for another 30 to 50[m], after which the cycle repeats. A discharge propagating in this manner is called a "*streamer discharge*"; its development is illustrated in Figure 1.12.

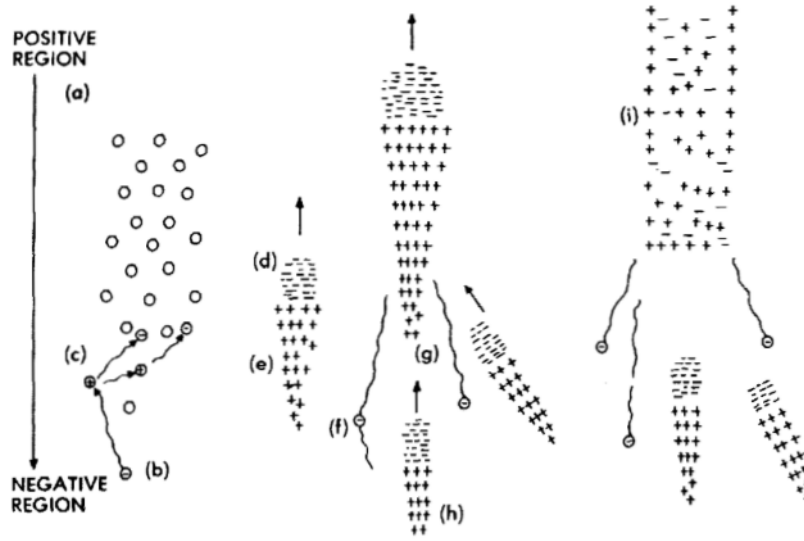


Figure 1.12: Stages in the development of a leader.

Left in the wake of these electrons will be positively charged ions (e). If the electric field is high enough, the initial avalanche will reach a critical size (approximately  $10^8$  electrons) for another avalanche of electrons (f) to be initiated by photoionization (g) from the initial discharge. The electric field that accelerates this secondary discharge is the sum of the initial electric field and that produced by the positive space charge left behind by the initial avalanche. Under the action of the total field, these successive avalanches reach the positive space charge (h), neutralize it, and leave a new positive charge a little farther on. With such a mechanism a positive charge moves step by step into the un-ionized air leaving behind it a partially ionized filament (i). This filament is a conductor, though at this stage of its development perhaps only a poor conductor. The processes just described relate to a positive electric field.

If the initial development of the leader takes place in the charged cloud, the developing streamer branches and begins to collect charges from its surroundings. Because it collects charges in this way, the streamer may be viewed as connected to the cloud and at the same potential as the cloud. As the head of the leader moves farther into the un-ionized air, charges flow down from the charged regions of the cloud, along the partially conducting filament and toward the head of the leader, thus tending to keep all parts of the leader at a very high potential. The amount of charge,  $q_0$ , lowered into the leader will be on the order of  $2$  to  $20 \cdot 10^4$  [C/m] of length. A leader 5 [km] long would then have stored within

it a charge of 1 to 10 [C].

Since the potential of the leader is very high, there will be a high radial electric field along the leader. This field will be high enough to exceed the breakdown strength of the air, and secondary streamers will branch out radially away from the central filament. The filaments will branch out radially until the field strength at the edge of the ionized region falls to about 30 [kV/cm].

It can be shown that the electric field strength at the edge of a cylinder containing a charge,  $q_0$ , per unit length is

$$E_r = \frac{1,8 \cdot 10^{10} q_0}{r} \quad (1.7)$$

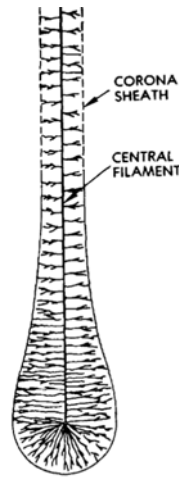


Figure 1.13: The lightning leader.

From this and the above breakdown strength of air, it can be deduced that the radius of the leader will be 1.2 to 12 m. At higher elevations the breakdown strength of air is less; hence the leader radius may be more.

The head of the leader may have a larger diameter than that of the rest of the leader, though this is difficult to prove by photographs. The head of the leader, nevertheless, is generally visible because of the optical radiation associated with the extension of the electron avalanches, But once the growth ceases, the radiation stops; consequently, the corona sheath surrounding the central conducting filament is not visible.

The process can be studied in the laboratory, albeit on a smaller scale than that of natural lightning. Figure 1.14 shows typical phenomena observed during the breakdown of the air between electrodes about 10 m apart. The sketch is based on a series of short-duration (about 1 [μs]) photographs taken at intervals of about 25 [μs] with an image-converter camera. As the electrons are attracted out of the initially ionized region at the head of the leader, the conducting filament lengthens and the corona discharge at the head of the leader occurs farther on in previously un-ionized air.

Moreover, Photographs of actual lightning leaders may be taken a camera in which the film moves relative to the camera lens. An example of such a photograph is shown in Figure 1.15. The leader is seen originating at the top left-hand corner of the picture and lengthening as time increases.

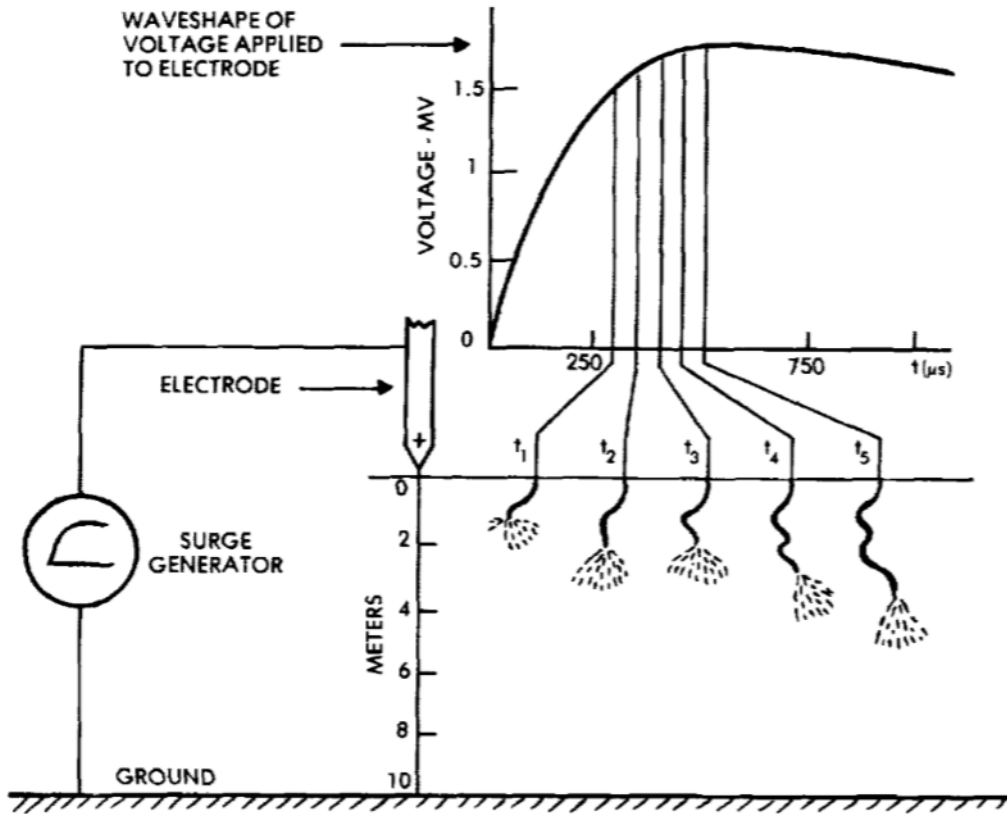


Figure 1.14: The development of a leader in the laboratory.

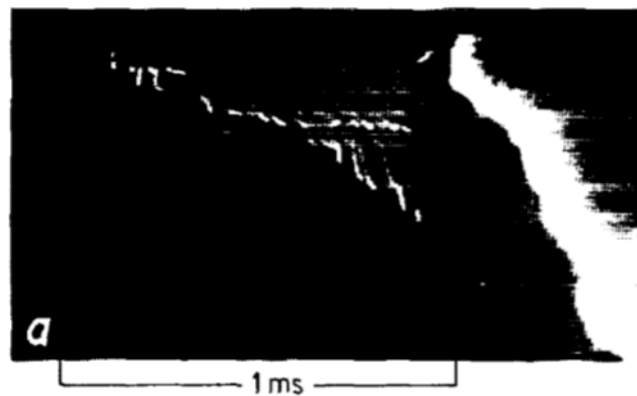


Figure 1.15: Camera photograph of a lightning leader.

From such photographs it has been learned that the leader advances at about  $1$  to  $2 \cdot 10^5 [m/s]$ , or  $0.03$  to  $0.06\%$  of the speed of light. In order that a charge of  $2$  to  $20 \cdot 10^{-4} [C]$  be deposited by a leader advancing at the rate of  $1 \cdot 10^5 [m/s]$  requires the average current in the leader,  $i_p$ , to be  $20$  to  $200 [A]$ . A current of this magnitude could be carried only in a highly conducting arc discharge, the assumed central conducting filament of the leader. Such an arc would have a diameter on the order of a few millimeters and an axial voltage gradient,  $g_p$ , of about  $5 \cdot 10^3 [V/m]$ . A leader  $4 [km]$  long would then have a voltage drop along its length of  $2 \cdot 10^7 [V]$ . The longitudinal resistance,  $R_l$ , of the conducting filament

$g_l/i_l$  would then be in the range of 40 to 400 [ $\Omega/m$ ].

While of less importance as regards aircraft, it might be noted that leaders sometimes start at the ground and work their way toward the sky. This happens most frequently from tall buildings or towers, or from buildings or towers located atop hills. Generally, one can tell from the direction of the lightning flash branching whether the leader started at the cloud or at the ground: if the branching is downward (Figure 1.16), the leader originated at the cloud; if the branching is upward, the leader originated at the ground.

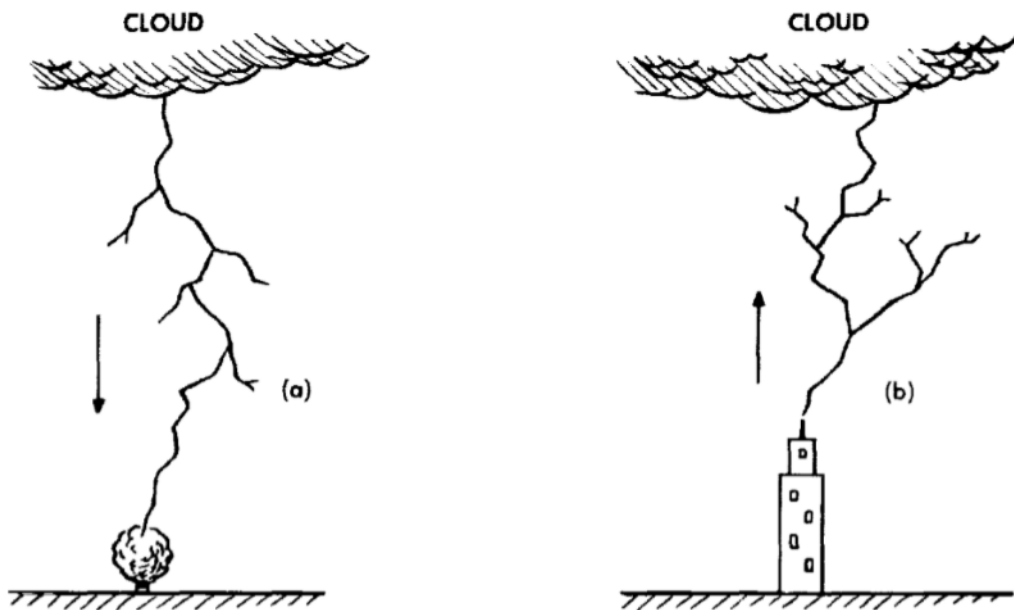


Figure 1.16: Leader direction as determined from direction of branching: (a) Downward-branching leader starts at cloud. (b) Upward-branching leader starts at ground.

## 1.4 The Return Stroke

As the negatively charged step-leader approaches the ground, positive charge accumulates in the ground underneath it or, more accurately, negative charge is repelled away from the region under the leader. At some point the electric field strength around objects on the ground becomes sufficiently high that a streamer starts at the ground and works its way toward the downward-approaching leader. When the streamers meet, the conducting filament in the center of each streamer provides a low-impedance path so that the charge stored in the head of the leader can flow easily to ground.

As the current in the central filament rises from its initial current of a few tens of amperes to higher values, it gets hotter, its diameter expands, its longitudinal gradient decreases, and it becomes an even better conductor, which in turn allows even more current to flow in the arc. As the charge in the lower part of the leader is neutralized, the heavily conducting arc reaches higher into the charged leader channel. The head of the region in which this neutralization takes place moves upwards at a rate of roughly  $100000[km/s]$  (or one-third the velocity of light) until it reaches the cloud. This heavily conducting region, called the return stroke, produces the intense flash normally associated with the

lightning stroke. Some stages in the development of the return stroke are shown in Figure 1.17.

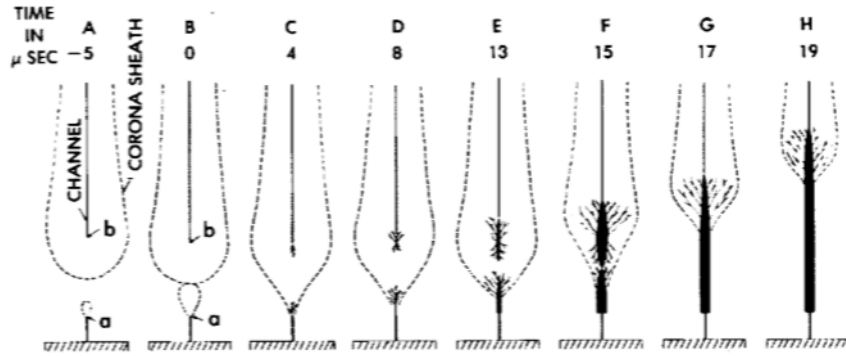


Figure 1.17: Stages in the development of the return stroke.

The velocity with which this return stroke propagates, together with the amount of charge deposited in the leader channel, determines the amount of current developed in the return stroke. Let  $v$  be the velocity of the return stroke and  $q$  be the amount of charge deposited per unit length,  $dl$ , along the leader channel. Since:

$$I = \frac{dq}{dt} \quad (1.8)$$

and

$$v = \frac{dl}{dt} \quad (1.9)$$

then

$$I = \frac{dq}{dl} \cdot v \iff I = qv \quad (1.10)$$

The velocity of the return stroke is not constant from one stroke to the next. It seems to vary with the magnitude of current that is ultimately developed. The velocity, however, may affect the surge impedance of the lightning stroke, and thus the way that the stroke interacts with a metallic conductor like an aircraft.

The velocity of propagation of the return stroke is less than that of the speed of light for two basic reasons:



- The first reason involves the longitudinal resistance of the return stroke channel: some of the factors associated with this longitudinal resistance are shown in Figure 1.18. Central to the phenomenon is the fact that the current in the lightning chan-

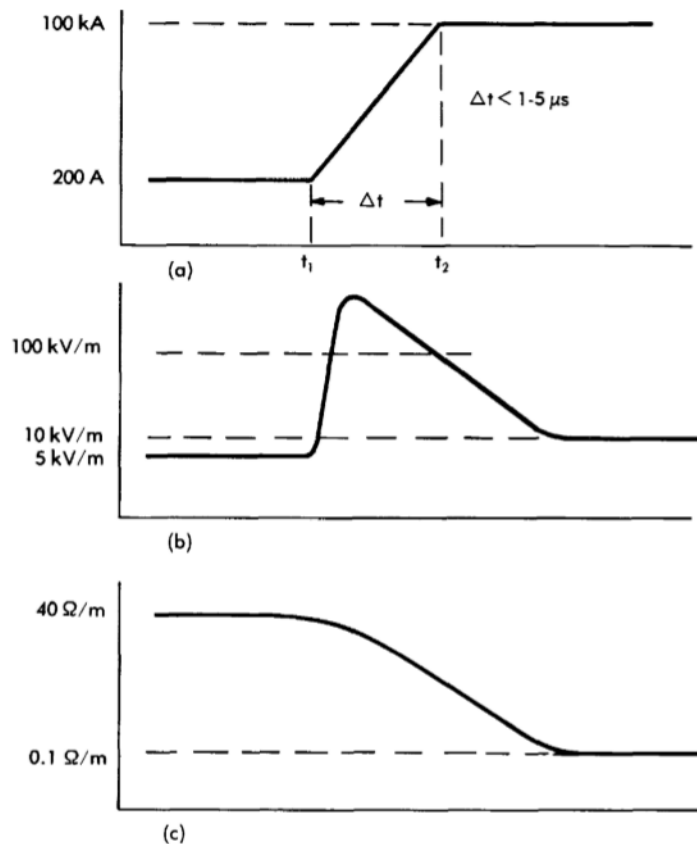


Figure 1.18: Phenomena associated with passage of the return stroke: (a) Current, (b) Longitudinal voltage, (c) Longitudinal resistance.

nel must increase fairly rapidly from the 200 [A] (approximately) current associated with the initial development of the leader to a current of perhaps 100 [kA] as the return stroke becomes fully developed.

It is a characteristic of an arc channel discharge that, if the current through the arc is increased, the arc channel expands in diameter, keeping a fairly constant current density across the channel. This channel cannot expand instantaneously, since energy must be put into the channel to cause the channel to heat up sufficiently to force it to expand. Accordingly, if the current through the arc channel is increased suddenly by a large magnitude, as in Figure 1.18(a), the longitudinal voltage gradient of the channel must suddenly increase.

Since the rate at which energy is injected into the channel is the product of the current and the longitudinal voltage gradient, the increased longitudinal voltage gradient may be taken as the mechanism forcing the arc channel to get hot enough to expand to the diameter required to carry the high currents. It is not known what the maximum longitudinal voltage gradient would be in a lightning channel, but it is known from studies of arcs in laboratories that the gradient will fall to values on the order of 100 [kV/m] in a fraction of a microsecond. Presumably in a few

microseconds, the channel diameter will have expanded to its final value, and the longitudinal volt-age gradient will have decayed back toward values on the order of 5 to 10  $[kV/m]$ . The longitudinal resistance, then, would fall from values on the order of 40  $[\Omega/m]$  to values on the order of a small fraction of an Ohm per meter, in times on the order of a few microseconds.

This collapse of longitudinal resistance, however, is far from instantaneous. The initial resistance of the leader is sufficiently high to retard the development of the upward-going return stroke and hence reduce its velocity of propagation below that of the speed of light;

- The second reason is due to the impedance: as shown in Figure 1.19(a) , the leader deposits in its wake a column of electrical charge with diameters on the order of several meters. At the center is a highly conducting core, which has a diameter of a few millimeters for the leader and which expands to a few centimeters during the passage of the return stroke.

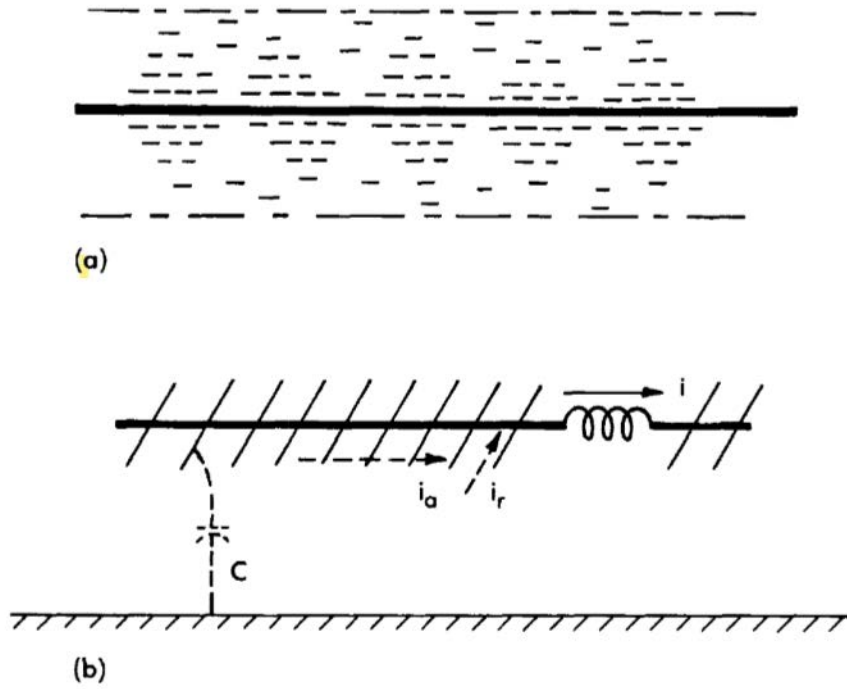


Figure 1.19: Effect of corona cloud on velocity of propagation. (a) Distributed charge surrounding a highly conductive central core, (b) highly conductive central conductor fastened onto a series of projecting splines.

The inductance of this return stroke is determined by the diameter of the highly conductive central core, and the capacitance by the diameter of the column of electrical charge. The lightning stroke may then be modeled as shown in Figure 1.19(b), in which a highly conductive central conductor is fastened onto a series of projecting splines, much like the backbone of a fish. A better analogy might be to view the lightning flash as a piece of tinsel rope for decorating a Christmas tree: a central piece of string is surrounded by a tube of fine filaments projecting radially away from the central core. In either case, the radial filaments can carry a radial current,  $i_r$ , but cannot carry an axial current,  $i_a$ . Accordingly, the lightning return stroke

has both a high capacitance and a high inductance per unit of length. In this respect it differs from a solid conductor of large diameter which, while possessing a high capacitance per unit length, simultaneously possesses a low inductance per unit length. It follows that the surge impedance, governed by the ratio of inductance to capacitance, is high while the velocity of propagation, governed by the product of inductance and capacitance, is less than that of the speed of light.

It could be concluded that the surge impedance of the lightning flash is of the order of  $3000 [\Omega]$  for return strokes of large amplitude,  $100 [kA]$ . This value is large compared to the surge impedance ( $\simeq 500 [\Omega]$ ) of a simple conductor in air and remote from a ground plane or other current return path.

The waveshapes of lightning-flash currents measured at ground level are reasonably well known. Typical waveshapes detailing the front of the initial return stroke are shown in Figures 1.20 and 1.21.

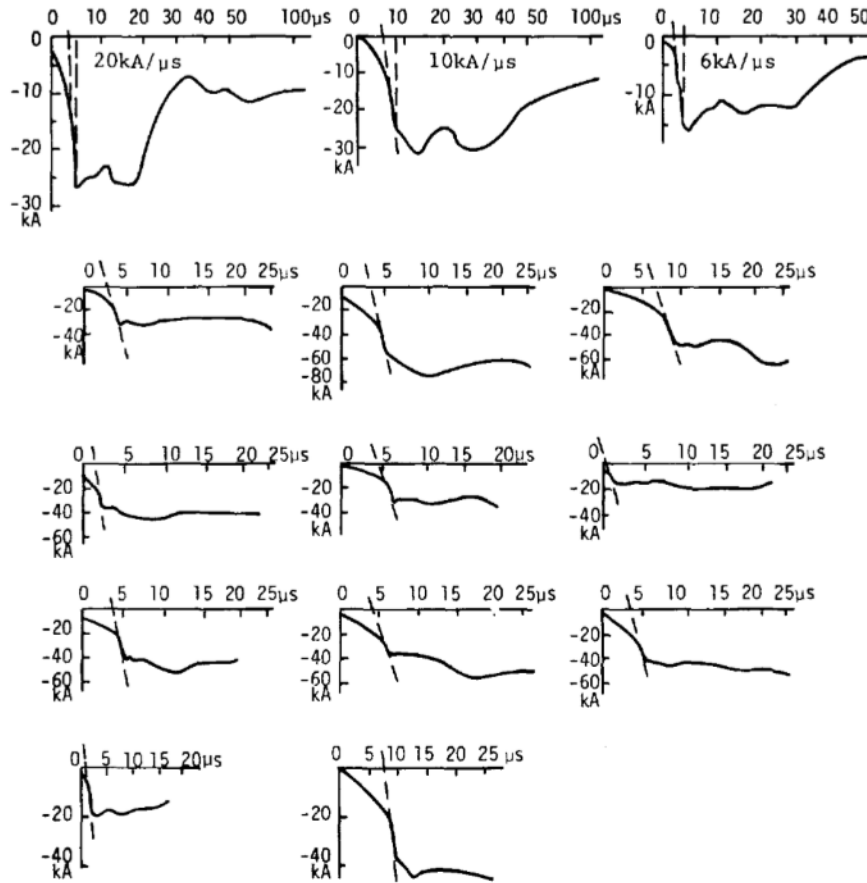


Figure 1.20: Front waveshapes of lightning currents.

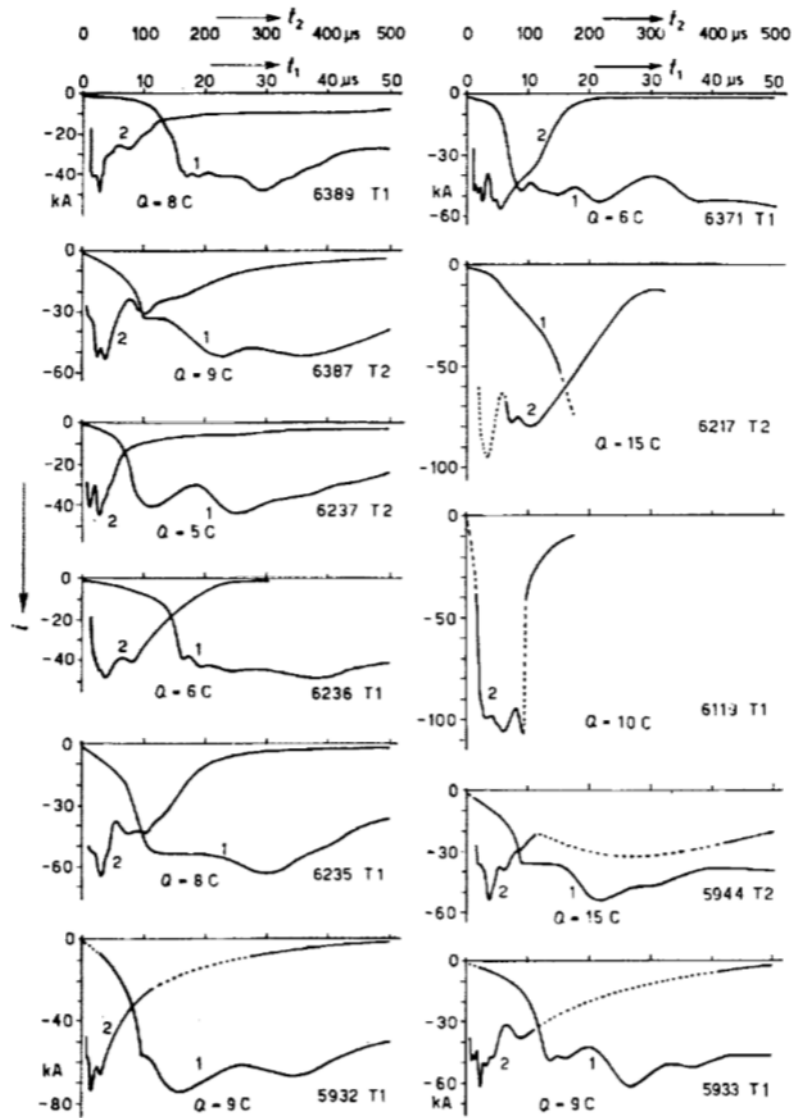


Figure 1.21: Current oscillograms from single strokes or first downward strokes. 1) Fast time-scale  $t_1$  ; 2) Slow time-scale  $t_2$

In all cases, the current is seen to have a concave front, the current initially rising slowly but then increasing to a maximum current rate of change just before crest amplitude is reached. It may be speculated that the initial slowly changing portion of these current oscillograms (which, of course, were measured at ground level) represents the growth of an upward-going leader from the lightning tower reaching upwards to contact the downward-approaching lightning leader. It can also be speculated that the maximum rate of change of current, which occurs just before crest, is most representative of the rate at which the current can increase in the lightning channel as the return stroke passes one particular point in space. This is supported by the observation that subsequent strokes in a - lightning flash, even measured at ground level, exhibit front times considerably faster than the rise time of the initial stroke in the flash.

## 1.5 Lightning polarity and direction

Most lightning flashes originate in the cloud and lower negative charge to earth. The question of direction of the lightning flash is sometimes confusing. With the intent of clarifying matters, the statement is sometimes made that lightning strikes upward and not downward. This is at least partially true; the return stroke that produces the high peak currents, thunder, and the highest intensity light, in fact does start near the ground and grow upward into the ionized channel previously established by the step-leader, thus tapping the charge in the step-leader. The step-leader, nevertheless, originated at the cloud. The source of energy is in the cloud, and the lower amplitude and longer duration currents have their origin in the charge stored in the cloud. Thus, in terms of the engineering definition of current, these flashes result in the direction of current flow from the earth to the cloud. This type is commonly called a "*negative polarity flash*".

When tall buildings or mountain tops are involved, the lightning flash often does originate at the ground; the step-leader starts at ground level and propagates upwards into the cloud. Such flashes seem to be triggered by the high electric field concentrated around the top of the building or mountain. They may be recognized by the upward direction of branching, as mentioned earlier and shown in Figure 1.16(b).

This type of flash therefore results in current flow from the cloud to the ground and is called a "*positive polarity flash*". Positive polarity flashes usually have lower peak currents than do flashes that originate at the cloud.

About 10% of all flashes are positive polarity flashes, and a fraction of these involve the highest peak currents and charge found associated with lightning. The positive flashes typically have only one high current stroke; they lack the restrike phase generally noted on flashes of negative polarity.

## 1.6 Measured Characteristics of the Lightning Flash

Lightning flashes are quite variable from one to another. Peak currents, total duration, waveshapes, number of strokes in the flash, charge transferred, etc., may all vary over wide limits, and only in general terms can one find a correlation between different parameters. Data on the characteristics of lightning are best presented in statistical terms.

One item that needs to be emphasized is that virtually all the data on lightning comes from measurements made at ground level, and these measurements may be influenced by the growth of an upward leader. Very few measurements have been made of the amplitude and waveshape of lightning currents passing through aircraft. Most of the measurements that have been made were of strokes with lower peak currents and longer times to crest than those often observed at ground level. In part this may be explained by chance and in part by the fact that many of the flashes intercepted may have been intracloud flashes and not cloud-to-ground flashes.

In any case, it could be observed that many characteristics were nearly linear when plotted as a log-normal distribution.

Figure 1.22 shows data on the peak current amplitude in lightning strokes. Regarding the damage that may be caused by lightning, this is one of the most important parameters. There are two curves shown, one for the first return stroke in a flash and one for subsequent return strokes. The first return stroke is generally of the highest amplitude. Subsequent return strokes may be represented as half the amplitude of the first return stroke. Marked on the curves are the amplitudes corresponding to the 2, 10, 50, 90 and 98% probabilities.

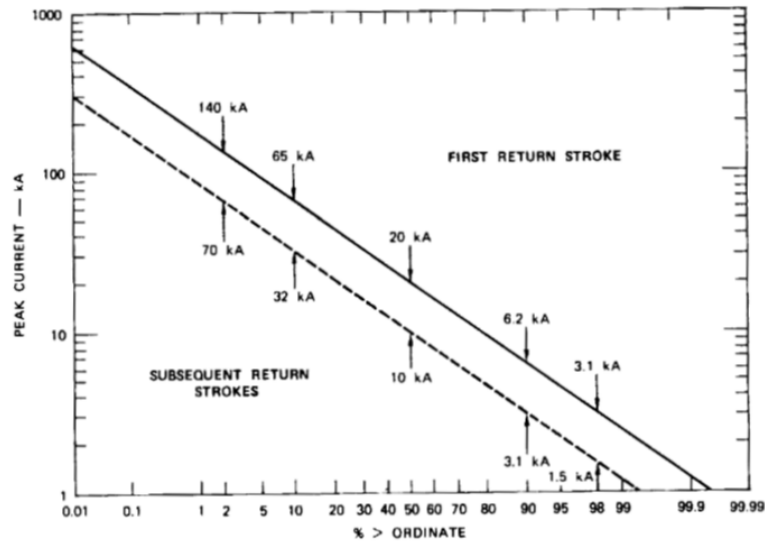


Figure 1.22: Distribution of peak currents for first return stroke and sub- sequent strokes

The peak value of the current is related to the explosive, or blasting, effect of lightning. It is also relative to the maximum voltage developed across ground resistance and hence to the risk of side flashes occurring in the vicinity of objects struck.

Figure 1.23 gives a distribution of the time for the current to reach its peak amplitude. This time is subject to considerable interpretation for any particular lightning stroke, since there is seldom a clearly definable time at which the stroke starts.

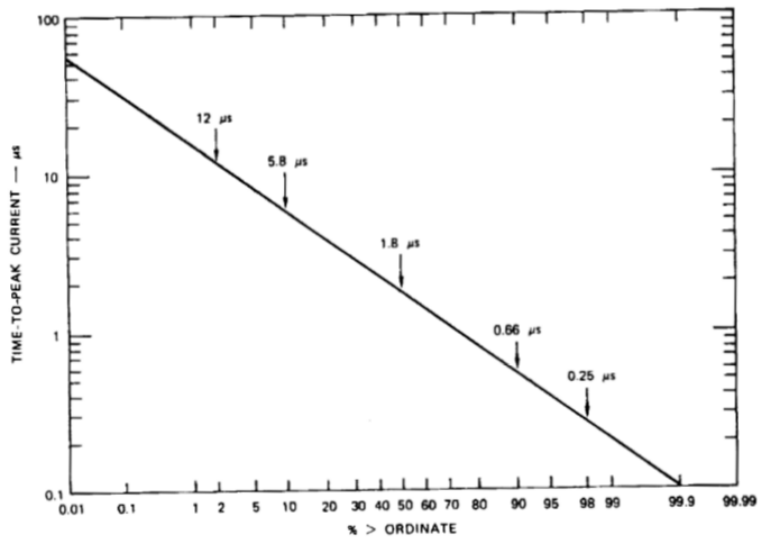


Figure 1.23: Distribution of time to peak current.

Lightning strokes typically have a concave front, starting out slowly and then rising faster as the current gets higher. Thus, the effective rate of rise of the lightning current is not directly obtained by dividing the peak current by the front time. The best summary of the effective rates of rise is given on Figure 1.24. The rate of rise of a lightning current is

an important factor in determining how much voltage is induced into electrical equipment, and in determining how many lightning conductors are needed and how they should be placed.

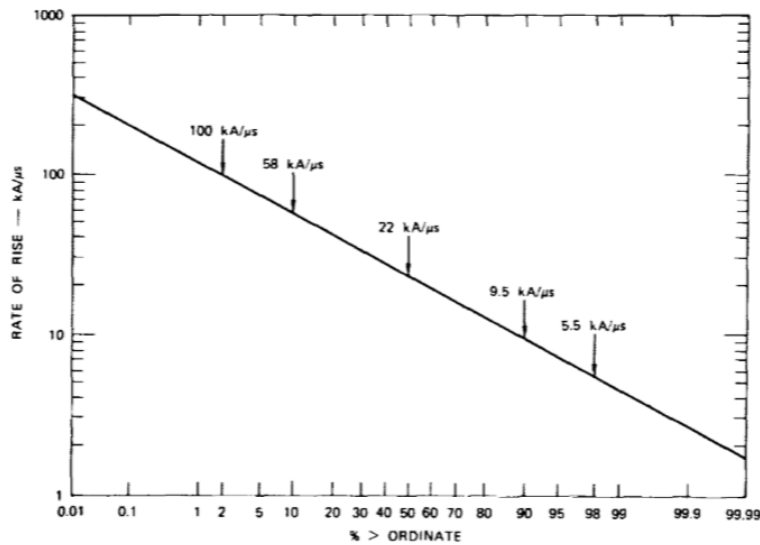


Figure 1.24: Distribution of rates of rise.

The duration of the stroke current affects the distance across which side flashes may develop, and affects how severely metal structures may be deformed by magnetic forces or the explosive libelation of energy. This distribution is shown in Figure 1.25

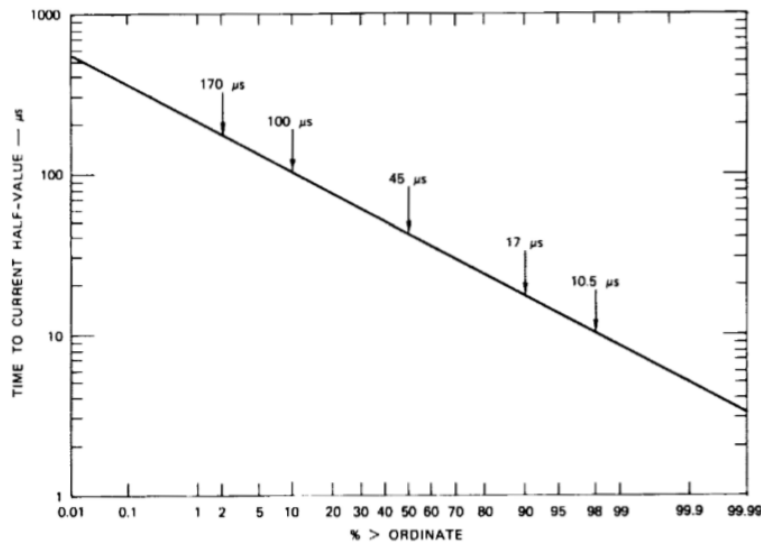


Figure 1.25: Distribution of time to current half value.

The duration of the stroke, which is measured in tens of microseconds, should not be confused with the total duration of the lightning flash. The total duration, shown in Figure 1.26, is frequently on the order of a second.

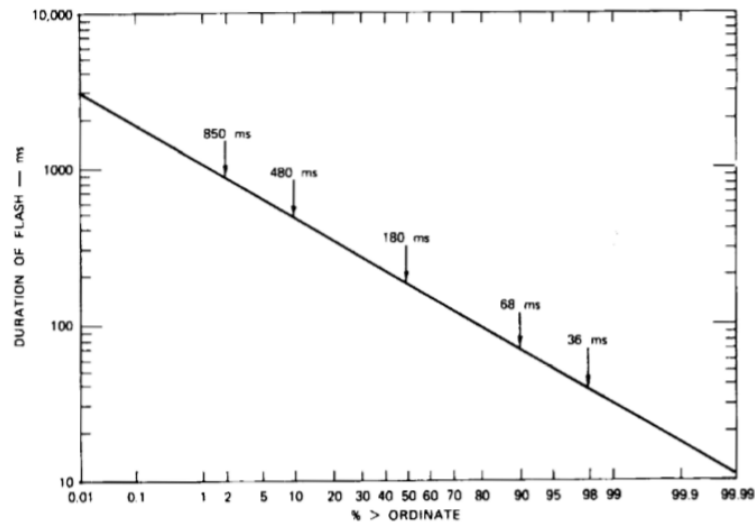


Figure 1.26: Distribution of duration of flashes to earth.

The duration of the total flash is influenced by the number of return strokes in the flash (Figure 1.27) and the time interval between strokes (Figure 1.28). Figure 1.29 gives information on the total charge transferred in the flash.

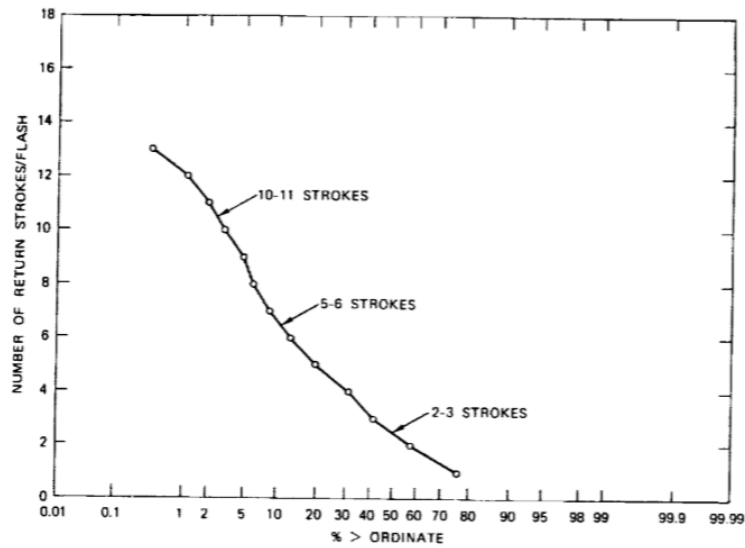


Figure 1.27: Distribution of duration of flashes to earth.



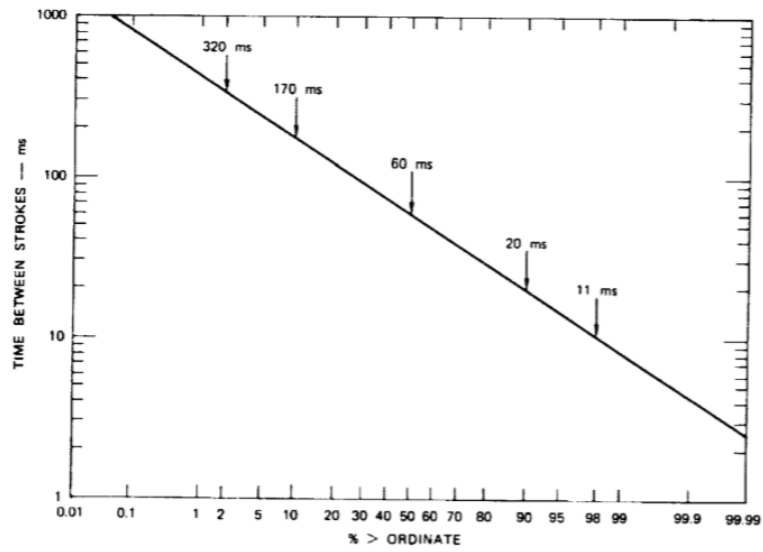


Figure 1.28: Distribution of duration of flashes to earth.

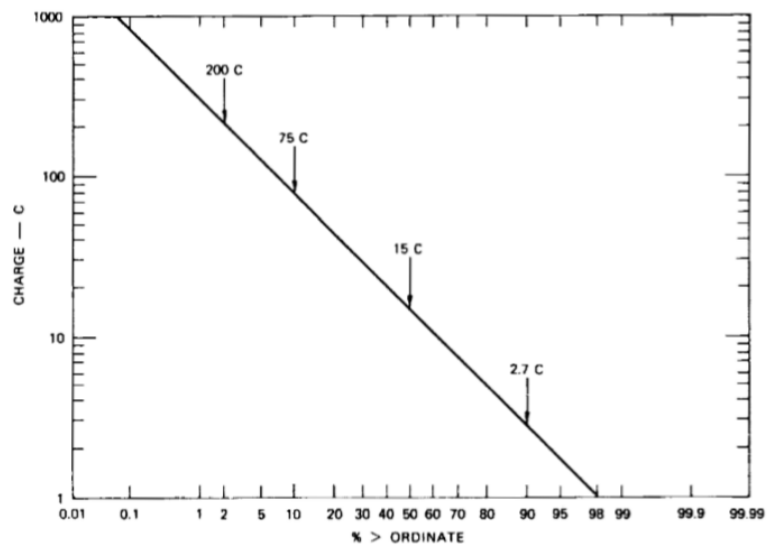


Figure 1.29: Distribution of duration of flashes to earth.

# Chapter 2

## Leader models

In order to describe the different kind of discharges, a lot of models have been designed, based on different assumptions and methods.

In any case, a common element of these models are the main stages during the discharge evolution:

- streamer inception at the high electric field-stressed electrode;
- build-up of the discharge stem at the electrode by the transition from streamer to leader channel;
- stable progression of the leader channel across the air gap fed from the electric charge produced by streamers in front of the leader channel tip at the Leader-Corona Region (LCR);
- achieving of the final jump condition once the LCR front reaches the grounded electrode.

In the next sections will be described how to modelize every step, using a finite element program to solve the Poisson Equation.

### 2.1 Streamer inception

Firstly, it is necessary verifying if the conditions to have a streamer are satisfied: it has been shown in the previous chapter (section 1.1.1) that the most important phenomena to obtain a first streamer is to have a ionisation coefficient bigger than the attachment coefficient. Therefore, these two parameter are calculated in the equation (1.3).

Then, the background electric field is calculated in the domain, considering also the pressure and temperature variation with the altitude.

Finally, the next relation is used:

$$e^{\int_{\Delta x} (\alpha - \eta) dx} \geq N_{crit} \quad (2.1)$$

where  $\Delta x$  is the size of the active region where  $(\alpha - \eta) > 0$  and  $N_{crit} = 0.55 \cdot 10^8$  is the minimum number of charges that produces a space charge field high enough to reproduce the streamer tip. The ionization and attachment coefficients are calculated as a function of the local fields.

## 2.2 First streamer and streamer to leader transition

Once the condition to have a streamer inception is verified, it is necessary to modelize the first streamer, and then the transition into a leader.

To do this, they'll be shown two different approaches:

1. a Simplified Physical Model to Determine the Lightning Upward Connecting Leader Inception [9];
2. a numerical model based on the charges extimation inside the leader corona region using a finite element method software (Comsol) [11].

### 2.2.1 Simplified method

This model is based on an iterative geometrical analysis of the background potential distribution of an earthed structure to simulate the first meters of propagation of an upward connecting leader.

When a lightning flash is initiated, a downward stepped leader is moving from the cloud to ground. As the stepped leader approaches to ground, the electric field at sharp points of structures starts increasing. Thus, stable upward leaders are pro from the elevated objects when the next conditions are fulfilled:

- a streamer discharge is incepted at the tip of the grounded structure (First corona inception);
- the streamer to leader transition occurs;
- the leader starts its continuous propagation across the gap (Stable leader inception)

These different conditions are associated to different time evolved stages of the discharge development.

The discharge process is initiated with the formation of the first corona. Once a streamer is incepted, it starts propagating from the sharp electrode and next the streamer splits into many branches within a conical volume. Thus, filamentary branched channels (streamers) are developed from a common root (stem). Depending on the curvature of the electrode, a dark period may occur before the inception of the second corona. This fact is because the injected charge by the first corona produces a field distortion that delays the second corona inception.

After the initiation of the second corona, a subsequent leader channel develops if the temperature of its stem reaches a critical value (around  $1500 [K]$ ). Then, the leader starts propagating with leader corona streamers developing in front of its head. However, if the energy input supplied by the leader corona is not high enough to sustain the thermal transition at the leader head, the leader propagation stops.

Otherwise, the leader propagates continuously across the gap. Furthermore, the corona streamer zone is modelled by using the simplified electrostatic approach. Basically, the major assumption of that approach is that the corona zone is characterized by an almost constant electric field  $E_{str}$ . In that way, the corona space charge would produce a distortion on the geometrical background potential distribution, as it is shown in Fig. 2.1.

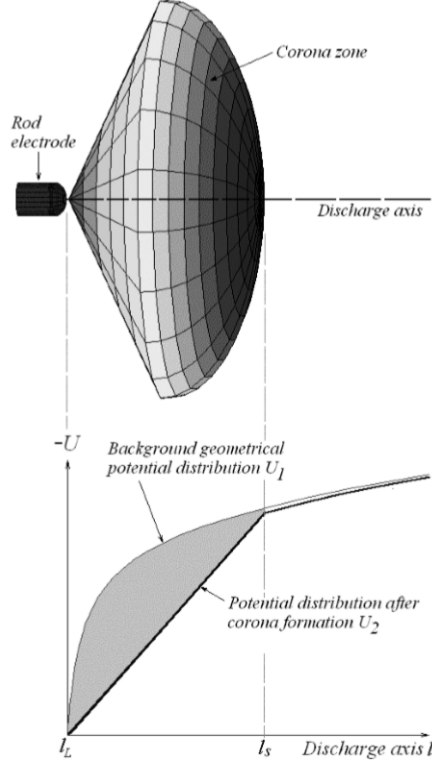


Figure 2.1: Potential distribution before and after corona formation in front of a rod. It is assumed that the rod electrode is grounded. In this case the corona zone extends from the tip of the stem  $l_L$  to the coordinate  $l_s$  on the discharge axis.

In consequence, the total corona charge required to change the geometrical potential distribution  $U_1$  to the potential distribution  $U_2$  after the corona formation is calculated, using a simplified procedure based on the assumption that the total corona charge  $\Delta Q$  can be determined from the difference between the geometrical potential distribution  $U_1$  and the potential distribution after the corona formation  $U_2$  as:

$$\Delta Q = K_Q \cdot \int_{l_L}^{l_s} U_1(l) - U_2(l) \cdot dl \quad (2.2)$$

where  $K_Q$  is a geometrical factor that takes into account the effect of all of the streamers on the total charge. The second term is the area  $S$  between  $U_1$  and  $U_2$  from  $l_L$  to  $l_s$ , as it is shown in Fig.2.1 and 2.2.

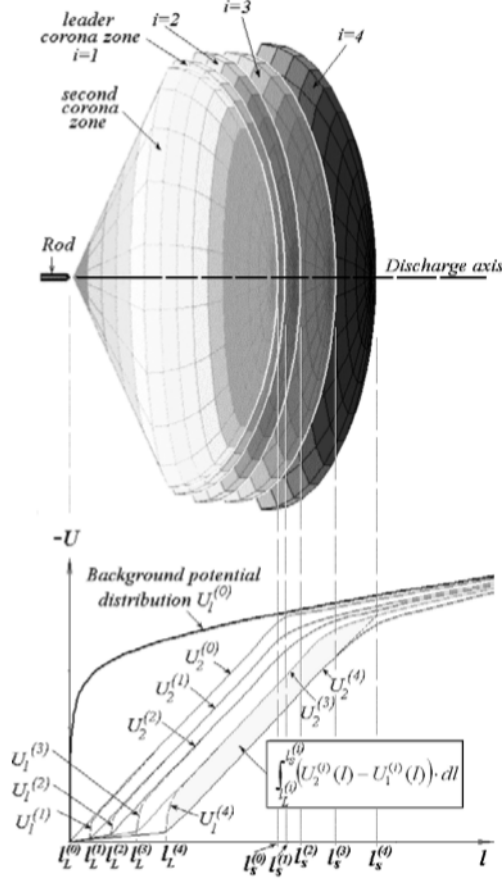


Figure 2.2: Schematic example of the leader advancement simulation.

In order to use the equation 2.2 it is necessary to determine the value of  $K_Q$  for different kind of structures: in [9] it has been derived a constant generalized value equal to  $3,5 \cdot 10^{-11} [C/Vm]$ .

### Implementation of the model

It has been assumed that the background electric field does not change considerably during the time required for the inception of the upward leader. Thus, assuming that the first corona inception condition is fulfilled, the used procedure is summarized as follows:

- (a) calculation of the background potential distribution  $U_1$ ;
- (b) calculation of the charge  $\Delta Q^{(0)}$  of the second corona zone;
- (c) if the charge  $\Delta Q^{(0)}$  is lower than  $1 [\mu C]$ , the stable leader inception condition is not fulfilled. Otherwise, go to (d);
- (d) start leader advancement simulation  $i = 1$ . Assume an initial leader length  $l_L^{(1)}$ ;
- (e) computation of the potential at the head of the leader  $U_{tip}^{(i)}$  using this relation:

$$U_{tip}^{(i)} = l_L^{(i)} \cdot E_\infty + x_0 \cdot E_\infty \cdot \ln \left[ \frac{E_{str}}{E_\infty} - \frac{E_{str} - E_\infty}{E_\infty} \cdot e^{-\frac{l_L^{(i)}}{x_0}} \right] \quad (2.3)$$

where  $l_L^{(i)}$  is the leader length at the current simulation step,  $E_{str}$  is the positive streamer gradient,  $E_\infty$  is the final quasistationary leader gradient,  $x_0$  is a constant given by the product  $v \cdot \vartheta$ , where  $v$  is the ascending positive leader speed and  $\vartheta$  is the leader time constant;

- (f) calculation of the charge  $\Delta Q^{(i)}$  of the corona zone in front of the leader channel;
- (g) computation of the leader advancement distance  $\Delta l_L^{(i)}$  and the new leader length  $l_L^{(i+1)}$  using respectively the following relations:

$$\Delta l_L^{(i)} = \frac{\Delta Q^{(i)}}{q_L} \quad (2.4)$$

where  $q_L$  is a constant that represents the charge per unit length necessary to achieve the thermal transition from the diffuse glow to the leader channel.

$$l_L^{(i+1)} = l_L^{(i)} + \Delta l_L^{(i)} \quad (2.5)$$

- (h) if the leader length  $l_L^{(i+1)}$  reaches a maximum value  $l_{max}$ , then the leader inception condition is fulfilled. If the leader advancement  $\Delta l_L^{(i)}$  starts decreasing after some steps, then the leader will stop and leader inception is not reached. Otherwise, go back to (e).

With the aim of simplifying that integral computation, a simple geometric analysis of the potential distribution before and after the leader corona formation is performed. Let us assume that several meters in front of the structure, the background potential distribution  $U_1^{(0)}$  can be approximated by a straight line, as it is shown in Fig. 2.3.

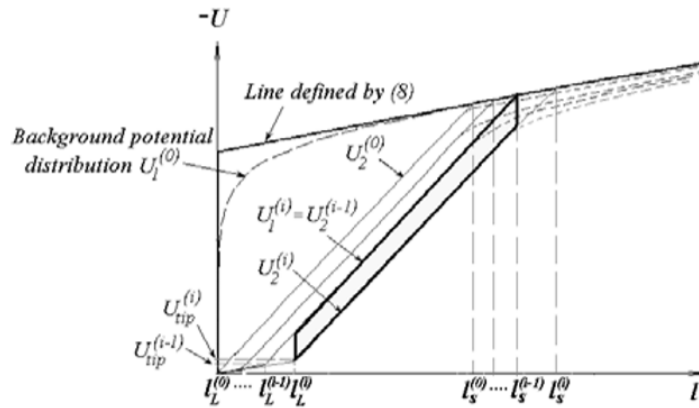


Figure 2.3: Geometrical approach of the potential distribution during the leader propagation. The shaded zone shows a detail of the used geometric area between  $U_1^{(i)}$  and  $U_2^{(i)}$ .

Therefore, the background potential distribution would be approximately defined by:

$$U_1^{(0)} \simeq E_1 \cdot l + U'_0 \quad (2.6)$$

where  $E_1$  is the slope and  $U'_0$  is the intercept of that line, both of them proportional to the background electric field  $E_{back}$ . The parameter  $l$  is the distance along the discharge axis from the tip of the structure. Additionally, the potential distribution after second corona  $U_2^{(0)}$  is assumed a line given by:

$$U_2^{(0)} = E_{str} \cdot l \quad (2.7)$$

Then, the position of the second corona zone's front  $l_s^{(0)}$  is calculated as the crossing point of the lines defined by the equations (2.6) and (2.7):

$$l_s^{(0)} = \frac{U'_0}{E_{str} - E_1} \quad (2.8)$$

and the second corona charge is computed as the product of the factor  $K_Q$  and the area defined by (2.6) and (2.7) as:

$$\Delta Q^{(0)} \simeq K_Q \cdot \frac{l_s^2}{2} \cdot (E_{str} - E_1) \quad (2.9)$$

Next, if the unstable leader inception condition is fulfilled ( $\Delta Q^{(0)} \geq 1 [\mu C]$ ), a similar geometrical analysis is performed to calculate the corona charge during the leader advancement steps. Hence, as it can be seen in Fig. 2.2, the geometrical potential distribution  $U_1^{(i)}$  at the  $i$ -th step is assumed to be approximately equal to the potential distribution after corona at the immediately previous step  $U_2^{(i-1)}$ . Furthermore, the potential distribution  $U_2^{(i)}$  at the current step is assumed to be defined by:

$$U_2^{(i)} = U_{tip}^{(i)} + E_{str} \cdot (l - l_L^{(i)}) \quad (2.10)$$

In that way, the extension of the corona zone in front of the leader's tip  $l_s^{(i)}$  is the crossing point between 2.6 and 2.10, given by:

$$l_s^{(i)} = l_s^{(0)} + \frac{E_{str} \cdot l_L^{(i)} - U_{tip}^{(i)}}{E_{str} - E_1} \quad (2.11)$$

and the corona charge produced at the leader's tip at the  $i$ -th step is approximately computed as

$$\Delta Q^{(i)} \simeq K_Q \cdot \left\{ \left( E_{str} \cdot (l_L^{(i)} - l_L^{(i-1)}) + U_{tip}^{(i-1)} + U_{tip}^{(i)} \right) \cdot \left( l_s^{(i-1)} - l_L^{(i)} \right) \right\} \quad (2.12)$$

where the term in bracket is the shaded area shown in Fig. 2.3.

Following this simplified calculation of the space charge in front of the leader channel, the procedure explained before can be easily computed. Thus, the leader inception model is reduced to an iterative geometrical analysis of the potential distribution of the analyzed structure. The flow chart for this simplified procedure is shown in Fig. 2.4.

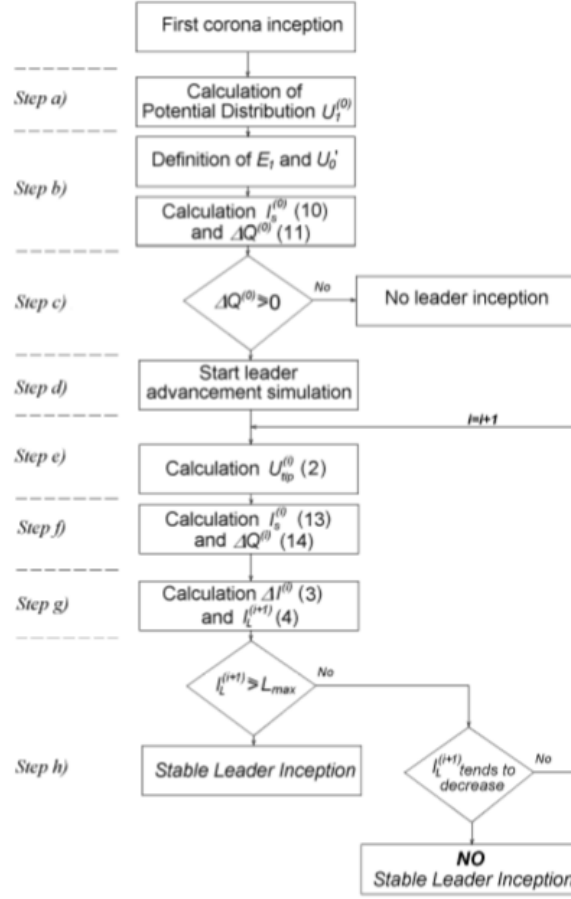


Figure 2.4: Flow chart of the simplified leader inception model.

To implement this model the following data has been used:

Table 2.1: Data used in the model.

| Symbol      | Description  | Value               | Units       |
|-------------|--|---------------------|-------------|
| $l_L^{(0)}$ | Stem length second corona zone                         | $5 \cdot 10^{-3}$   | $[m]$       |
| $l_L^{(1)}$ | Initial leader length                                  | $5 \cdot 10^{-2}$   | $[m]$       |
| $r_L$       | Leader radius  | $10^{-4}$           | $[m]$       |
| $E_{str}$   | Positive streamer gradient                             | $4,5 \cdot 10^{-5}$ | $[V/m]$     |
| $E_\infty$  | Final quasi-stationary leader gradient                 | $3 \cdot 10^4$      | $[V/m]$     |
| $v$         | Ascending positive leader speed                        | $1,5 \cdot 10^4$    | $[m/s]$     |
| $\vartheta$ | Leader time constant                                   | $50 \cdot 10^{-6}$  | $[s]$       |
| $q_L$       | Charge per unit length necessary to thermal transition | $65 \cdot 10^{-6}$  | $[C/m]$     |
| $l_{max}$   | Maximum leader length to be simulated                  | 2                   | $[m]$       |
| $\vartheta$ | Semi-angle corona zone                                 | 60                  | $[degrees]$ |



## 2.3 Charges extimation inside the leader corona region using a finite element method software

Different models, either engineering or physical, have been proposed to explain the long air gap discharge. Predictions of engineering models depart from experimental data in tests with different electrode arrangements and impulse waveshapes to predict  $U_{50\%}$ .

As it has been explained before, the following elements, based on the work of Gallimberti [12] and Goelian [13], are common to all physical models: streamer inception at the high voltage electrode; streamer-to-leader transition due to the thermalization of the electric charge from the first streamers (unstable leader channel inception); and finally propagation of the leader channel aided by the supply of charge from the LCR (stable leader channel propagation).

So, the new proposed methodology [11] consisted of a sequential execution of tasks (similar to the previous) that calculates the streamer inception, the streamer-to-leader transition and the continuous leader channel propagation until the final jump or withstand condition was achieved, as it is described in the flow diagram of Fig. 2.5:

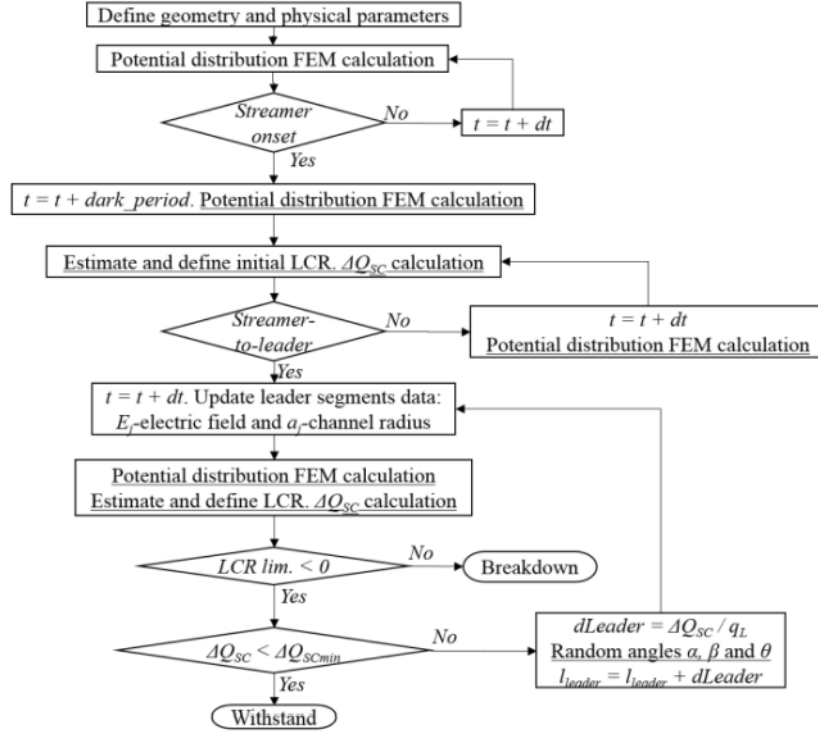


Figure 2.5: Flow chart of the new methodology proposed.

The simulation started with the definition of the geometry (electrode shape, gap distance) and other physical parameters, like  $q_L$ ,  $E_{stab}$ ,  $U_s$  (time-dependent electric potential on electrode). At several steps of the execution, it was required to calculate the electrostatic potential distribution in the simulation domain using the FEM solver COMSOL Multiphysics v.5.0.

The main advantage with this solver was the easy setting of all the simulation parameters like geometry dimensions, boundary conditions, mesh properties, etc., from an external main code that processed and stored the results during all the iterations, written

in Matlab. Regarding the meshing of geometries, it was possible to set for each single surface/domain parameters like maximum/minimum element size, growth rate, curvature factor and resolution on narrow regions [14]. In critical parts of the geometry it was possible to adjust each these mesh parameters to obtain the best results.

Once the streamer inception criterion was fulfilled, a delay for the dark period was added. The simulation continued with the evaluation of the streamer-to-leader transition criterion, where the amount of charge in front of the high voltage electrode after the streamer inception was estimated. After having reached the stable leader channel condition, the leader channel segments were updated in each iteration, and the new boundary conditions for the channel were included in the simulation domain. In each iteration within the leader channel progression loop, the LCR charge was calculated. It was also evaluated if the LCR front reached the ground for the breakdown condition or whether the estimated LCR charge was lower than a charge threshold of  $40 [nC]$ , achieving then the withstand condition. The leader channel progression consisted in adding a new segments to the leader channel, calculated as the LCR charge divided by the constant  $q_L$ . A detailed explanation of some important elements within the simulation sequence are presented in the next subsections.

### 2.3.1 Streamer inception and dark period

For the streamer inception the procedure is the same described in 2.1. Instead, regarding the dark period, it is mentioned that after the initial corona inception pulse there is a dark period before any further corona/streamer pulses or streamer-to-leader channel transition. This time delay is caused by the space charge left behind in front of electrode after the streamer inception. It increases almost linearly with the inception voltage and depends mainly on the rate of change voltage/time.

Moreover, it has been pointed out that electrodes with large curvature radius tend to have a dark period equal to zero, introducing from experimental measurements the concept of critical radius for the electrode radius. Below this critical radius, the breakdown voltage is almost unaffected by the electrode size. So, for large electrodes above the critical radius, the time delay representing the dark period was set to zero.

### 2.3.2 Streamer-to-leader transition

After the streamer inception, electric charge from the streamer discharges in front of the leader channel tip is injected to a common root where the leader channel initiates. Most of the energy from electronic collisions is transferred to vibrational energy of heavy molecules, which is slowly converted into heat. The evolution of the temperature is determined by the relaxation time of the vibrational energy levels. Once a temperature of ca.  $1500 [K]$  is reached at the channel, the negative ions lose their excess electrons.

Thus, there is a strong increment in the conductivity at the streamers common root (stem). Then, the leader channel tip behaves like a thermal transitional wave that converts the cold diffuse glow at the LCR into a hot channel.

As it has been told in the previous section, Gallimberti [12] estimates a minimum amount of LCR charge of  $1 [\mu C]$  necessary for the stem to heat above the  $1500[K]$  threshold after the first streamer pulse in atmospheric air. This LCR charge value was used as streamer-to-leader channel transition criterion. This was one of the first attempts to quantify the amount of electric charge required to achieve full streamer-to-leader transition.

### 2.3.3 Leader corona region definition

The gradient  $E_{SC}$  inside the LCR is almost constant (ca. 450 [kV/m] for atmospheric air) for streamer propagation. Goelian and Lalande [13] make use of this principle and proposed an electrostatic representation of the streamers in front of the leader channel tip. The representation consisted on superimposing the constant gradient  $E_{SC}$  over the background potential distribution, as it is presented in Fig. 2.6.

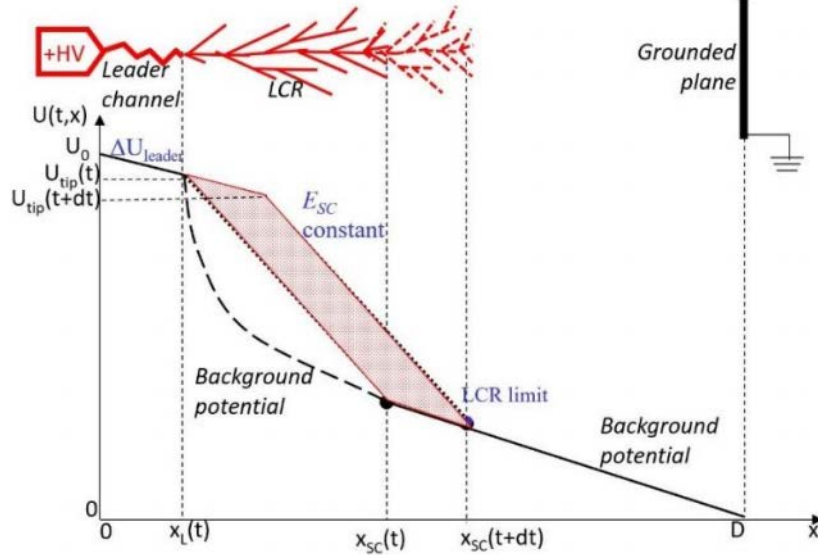


Figure 2.6: Potential distribution for a rod-plane electrode configuration.

This form of representing the LCR has also been used in the previous model. As the leader discharge propagates across the gap, the LCR was also advancing in front of the leader channel tip. When the LCR front reached the grounded plane, the discharge was at the final jump stage and thus the breakdown final step.

### 2.3.4 Leader corona region charger calculation

The three-dimensional electric potential distribution of the simulation domain, including the electrodes and the leader channel, was calculated using a FEM solver. Then, the LCR was determined in the three-dimensional region following a particular procedure: the potential distribution in the rod-to-plane geometry is calculated using the charge simulation method (CSM), including in the simulation domain the electrodes, the leader channel and the LCR, the latter represented as charge rings enclosed in a fixed cone with semiangle  $\vartheta_{SC}$  that fulfills the condition of having potential gradient higher than  $E_{stab}$ . A simplification of the methodology estimates the LCR charge as the area enclosed in the potential distribution occurring before and after the creation of a new leader channel segment; having superimposed over the background potential the  $E_{stab}$  condition between the leader channel tip and the LCR front. The charge is finally calculated by multiplying this area times a geometrical constant  $K_Q$ .

To represent the superimposed gradient  $E_{SC}$  over the background potential distribution, fictitious potential rings were located coaxially inside the LCR cone like pseudoelectrodes with fixed potential in front the leader channel tip in the simulation domain, as it can be seen in Fig. 2.7.

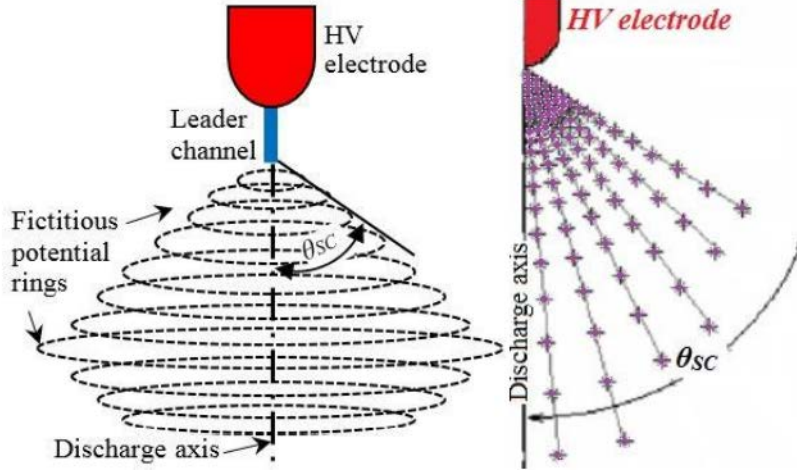


Figure 2.7: Spatial location of fictitious potential rings representing the LCR in front of the leader channel tip.

It was considered while assigning in the potential to the rings the contribution of the LCR from the previous iteration, taken from the previous iteration FEM solution and continuously overwritten during the whole leader propagation iterative process.

Once the whole geometry was built, the potential distribution was computed again in the FEM solver and the electric charge in the LCR could be estimated by two methods:

1. the first method, the Single Surface Integral (SSI) consisted in calculating the total electric flux through a Gaussian surface that encloses the LCR to evaluate the net charge:

$$Q_{LCR} = \iint_S \varepsilon_0 \vec{E} \cdot d\vec{s} \quad (2.13)$$

where  $Q_{LCR}$  is the net electric charge inside the Gaussian surface  $S$ ,  $\varepsilon_0$  is the vacuum permittivity and  $d\vec{s}$  is the differential element of surface normal to the Gaussian surface  $S$ .

2. the second method, called the Capacitance Matrix Method (CMM), the capacitance matrix elements ( $C_{ij}$ ) were calculated for all the electrodes and fictitious electrodes, by integrating the electrical energy density ( $W_E$ ) for each  $i$ -element with a potential  $U_i$  over the whole simulation domain  $\Omega$

$$C_{ii} = \frac{2}{U_i^2} \oint_{\Omega} W_E \cdot d\Omega \quad (2.14)$$

Then, the lineal system with  $i$  - equations was solved for all known  $i$  - ring potentials, so all charges  $Q_i$  for each ring can be estimated by

$$\begin{bmatrix} Q_1 \\ \vdots \\ Q_i \end{bmatrix} = \begin{bmatrix} C_{11} & \dots & C_{1i} \\ \vdots & \ddots & \vdots \\ C_{i1} & \dots & C_{ii} \end{bmatrix} \cdot \begin{bmatrix} U_1 \\ \vdots \\ U_i \end{bmatrix} \quad (2.15)$$

Thus, the total charge in the LCR was calculated by adding all the individual charges from all the  $k - fictitious$  electrodes in the LCR:

$$Q_{SC\ total} = \sum_{j=1}^{j=k} Q_j \quad (2.16)$$

The geometry elements used in the FEM solver for the calculation of the LCR charge are shown in Fig. 2.8

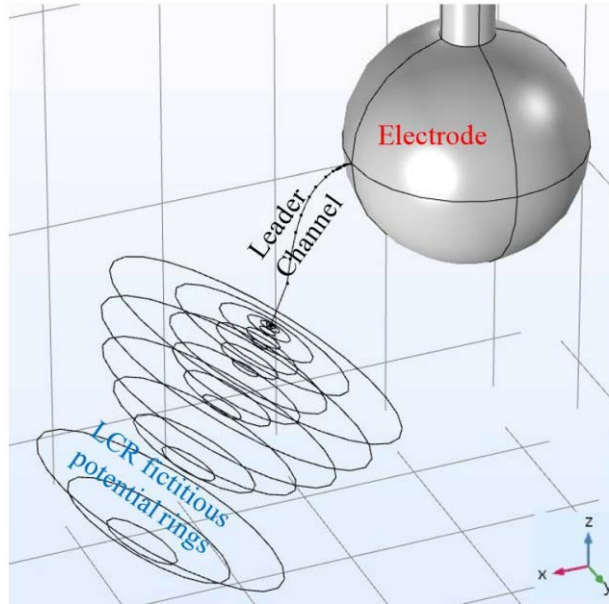


Figure 2.8: Geometry built in the FEM solver for the calculation of the LCR charge using the SSM and CMM.

### 2.3.5 Leader channel model

An important physical mechanism in long air laboratory discharges is the leader channel, which propagates long distances and grows in relatively low electric field regions, feeding itself from the electric charge produced at the LCR.

There are different theoretical approaches of how it can be represented, depending on the desired application, e.g. lightning electromagnetic radiated fields or electrostatic field calculations for insulation design. In the present work, the leader channel is represented following the model of Lalande [13], based also in the physical model of Gallimberti [12]. This model departs from thermo-hydrodynamic considerations of the channel and its energy and mass conservation equations. The channel is considered as a homogeneous cylinder surrounded by a dense shell; and over its cross section the pressure, temperature and particle density are constant.

Starting from the channel energy equations for the inner core and outer shell for an infinitesimal channel section, and making some assumptions (e.g. ideal gas behavior, loss-less boundary and constant mass expansion), the leader channel radial expansion can be expressed in the form:

$$\frac{p}{\gamma - 1} \frac{d(\pi a^2)}{dt} + p \frac{d(\pi a^2)}{dt} = EI \quad (2.17)$$

where  $p$  is pressure,  $a$  the channel radius,  $\gamma$  the constant ratio of specific heats, and  $EI$  the electric energy input to the channel section. The leader channel model proposed by Lalande [13] discretizes 2.17, then the leader channel is represented as discrete segments of length  $(\Delta x_{Lj})$  and radius  $(a_j)$ . Each segment radius and electric field are updated when new charge from the LCR is injected into the channel and a new channel segment is added.

The simplified segment radius expansion would now be:

$$a_j^2 = a_{j0}^2 + \frac{(\gamma - 1) E_j q_L \Delta x_L}{\gamma \pi p} \quad (2.18)$$

where  $a_j$  and  $a_{j0}$  are respectively the updated and previous segment radius  $\Delta x_{Lj}$ . By using the same assumptions of constant mass expansion and constant reduced field within the channel, the internal field of the  $j$  - *segment* can be calculated as:

$$E_{Lj} = \frac{E_{Lj0}}{N} N_j \quad (2.19)$$

where  $E_{Lj}$ ,  $E_{Lj0}$  and  $N_j$ ,  $N$  are respectively the updated and previous internal electric field and particle density of the segment  $\Delta x_{Lj}$ . Therefore, the leader channel tip potential can be expressed as:

$$U_{Ltip}(t) = U_0(t) - \sum_j E_{Lj} \cdot \Delta x_{Lj} \quad (2.20)$$

where  $\sum_j E_{Lj} \cdot \Delta x_{Lj}$  is the sum of the potential drops of all the  $j$  - *elements*, having internal electric field  $E_{Lj}$  and length  $\Delta x_{Lj}$ .

### 2.3.6 Tortuous leader propagation

Gallimberti [12] mentions that the main cause of breakdown voltage and time to breakdown statistical distributions are fluctuations of the leader channel propagation (tortuosity, branching, restrikes), and that the streamer inception and streamer-to-leader transition time lags play a minor role in the whole breakdown process.

The leader channel tortuous propagation can be modeled if the leader channel is divided into segments and the angles formed between them are fitted to a known probability distribution function (PDF).

The angles between two consecutive segments  $s_i$  and  $s_j$  can be described as (see Fig. 2.9):

- $\alpha$ : between two consecutive leader channel segments  $(0, \pi)$ ;
- $\vartheta$ : leader channel segment inclination with respect to the discharge axis; also known as polar angle  $(0, \pi)$ ;
- $\varphi$ : leader channel segment projection on a reference plane (e.g.  $XY$ ), also known as azimuthal  $(-\pi, \pi)$ .

From the experimental measurements presented in [15], the PDFs shown in Fig. 2.10, 2.11 and 2.12 were estimated for the tortuosity angles  $\alpha$ ,  $\vartheta$ , and  $\varphi$ .

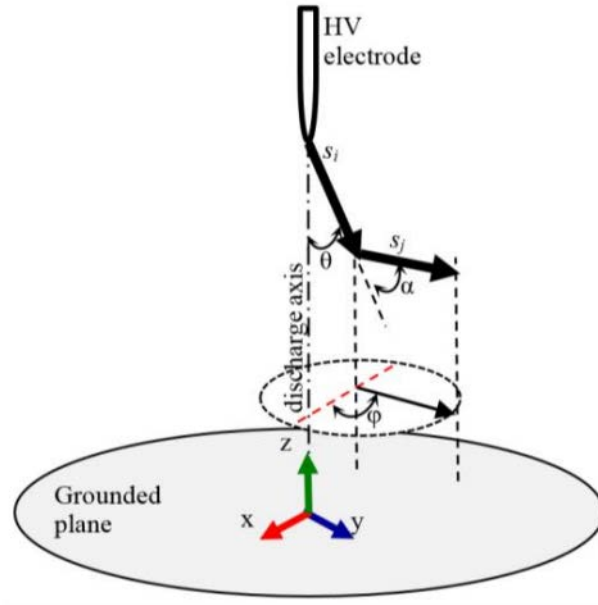


Figure 2.9: Schematic representation of two consecutive leader channel segments  $s_i$  and  $s_j$ . Note the three different angles ( $\alpha$ ,  $\vartheta$ , and  $\varphi$ ) used for the threedimensional representation of the leader channel tortuosity.

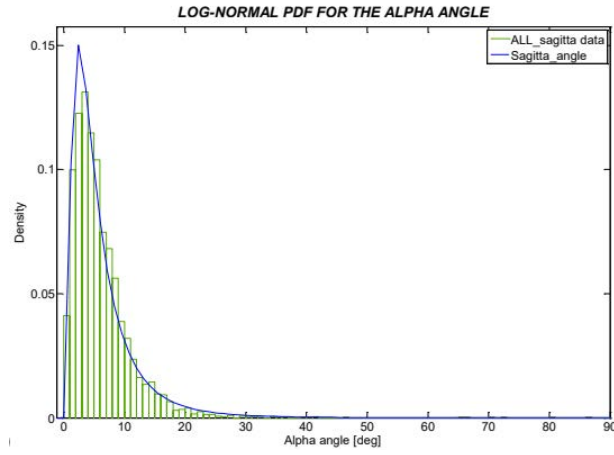


Figure 2.10: PDF found for leader channel angles  $\alpha$ .

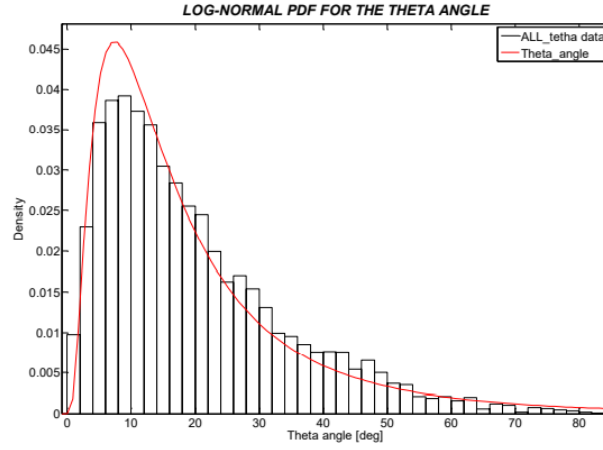


Figure 2.11: PDF found for leader channel angles  $\vartheta$ .

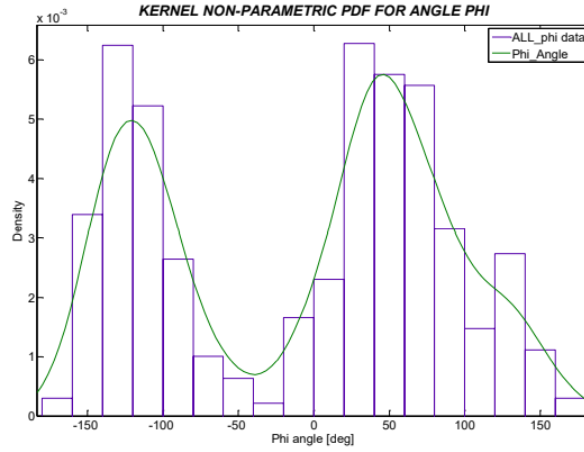


Figure 2.12: PDF found for leader channel angles  $\varphi$

The leader channel tortuosity was obtained from two still camera image records that permitted the reconstruction of the three-dimensional path followed by the leader channel during several breakdown events. After determining the path followed, the channel was divided into segments and the angles  $\alpha$ ,  $\vartheta$ , and  $\varphi$  were calculated between those segments. For 30 recorded events, ca. 400 segments were analyzed for each event. After that, ca. 12000 values for each tortuosity angle were fitted using in the Matlab distribution fitting tool. The parameter values of these PDFs are presented in Table 2.2.

Table 2.2: Probability distribution functions for leader channel segment angles

| Leader Angle | PDF type                 | Mean | Variance         |
|--------------|--------------------------|------|------------------|
| $\alpha$     | Log-normal               | 6.3  | 34.5             |
| $\vartheta$  | Log-normal               | 20.9 | 437              |
| $\varphi$    | Non-param. normal kernel |      | (bandwidth 20.3) |



### 2.3.7 Methodology application

In [11] it has been implemented this model on a electrode arrangements rod-to-plane and sphere-to-plane (with/without protrusions) were tested with 275/2500 [s] switching voltage impulses to determine the  $U_{50}\%$ .

The protrusions consisted of small cylindrical rods of 10 or 50 [mm] on the sphere surface pointing towards the grounded plane (under protrusion –UP–) or perpendicular to the main gap axis, at the sphere equatorial plane (side protrusion –SP–). In Fig. 2.13, a general view of the geometries built to simulate the experimental arrangements are presented. Note the leader channel made of segments starting at the electrode and LCR represented as a collection of rings in front of the leader tip.

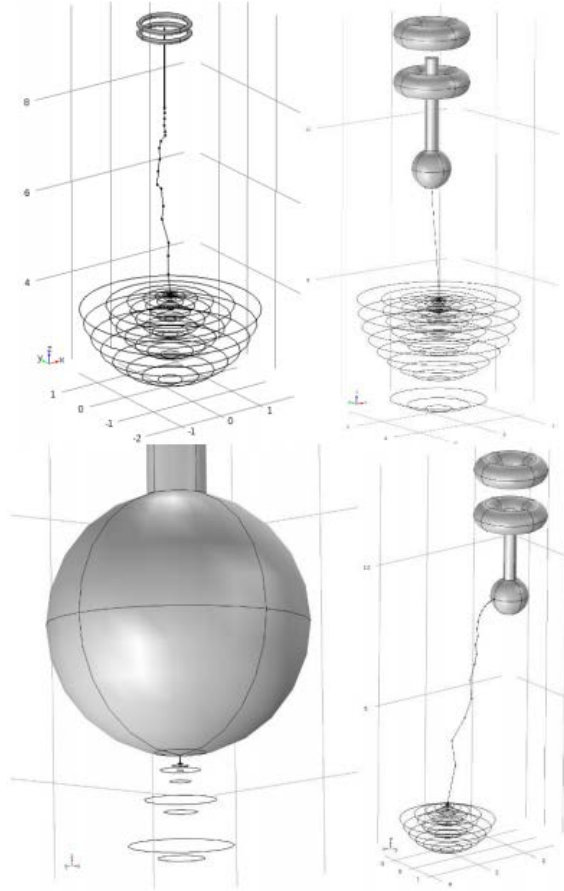


Figure 2.13: From top left to bottom right: rod-to-plane, sphere-to-plane, sphere-toplane UP and sphere-to-plane SP.

# Chapter 3

## Leader model for a grounded structure

In this chapter will be shown a model to study a leader formation in thunderstorm condition taking into account all the previous considerations

In order to achieve this result, I proceeded step by step, starting from simple simulations, and then adding more complex elements (everything using the Comsol LiveLink for Matlab):

1. negative leader to a tall strcture with a straight path;
2. positive leader from a tall structure in thunderstorm conditions with a straight path;
3. positive leader from a tall structure in thunderstorm conditions with a tortuous path;

### 3.1 Negative leader model (straight path)

As first attempt, I tried to modelize a negative leader approaching to a tall structure to the ground. I firstly elaborated the geometry, composed by (as you can see in Fig. 3.1): a 3D electrostatic Comsol simulation with a  $4 \times 4 \times 4 [km]$  domain, an electrode at a heigh of  $3800 [m]$  and a  $110 [m]$  tower connected to the ground:

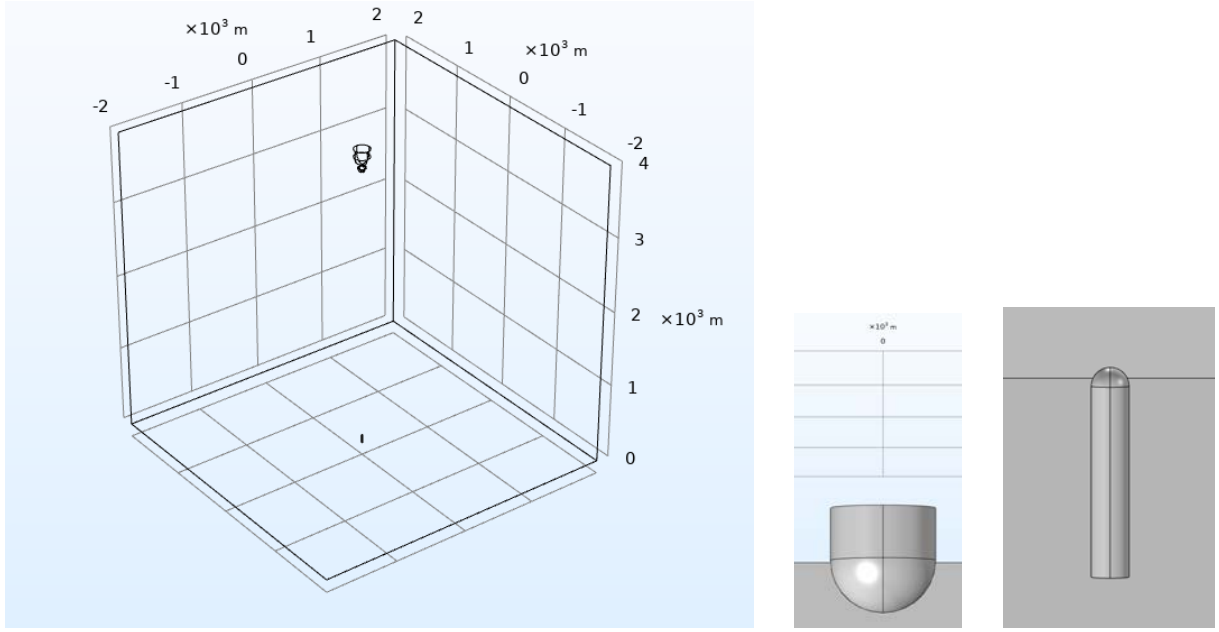


Figure 3.1: Simulation geometry. Respectively from the left: (a)domain, (b) electrode, (c)tall structure.

Then, I imposed  $0.9 \cdot 10^9 \text{ [V]}$  on the electrode and ground potential to the tower. I obtained this simple results:

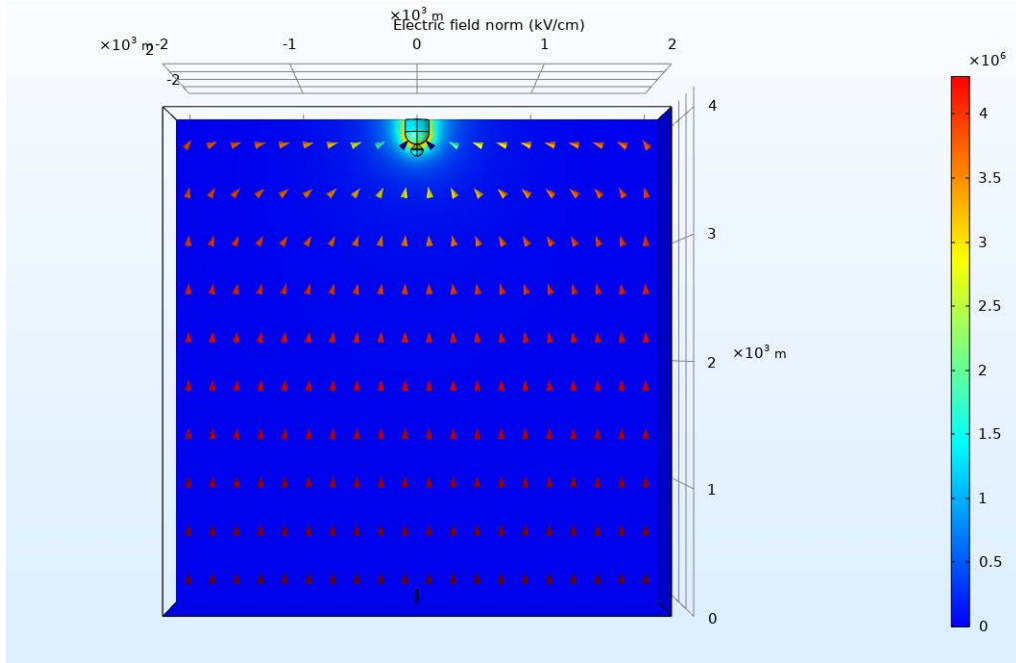


Figure 3.2: 2D electrical field behavior.

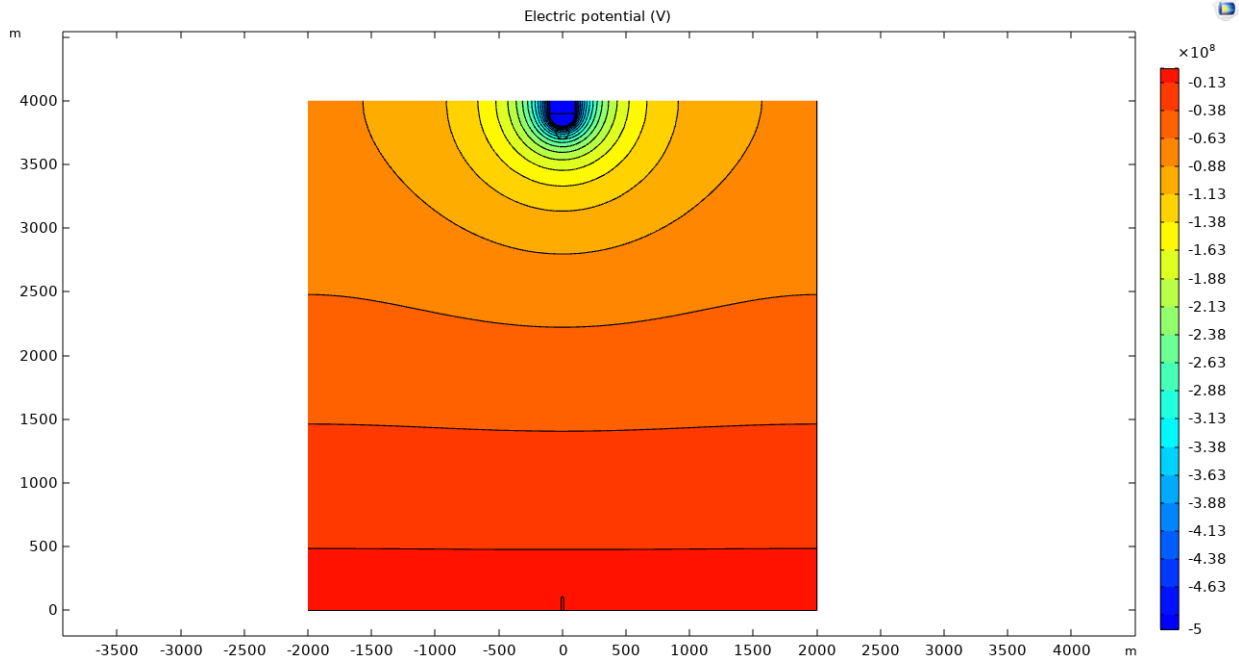


Figure 3.3: 2D electrical potential behavior.

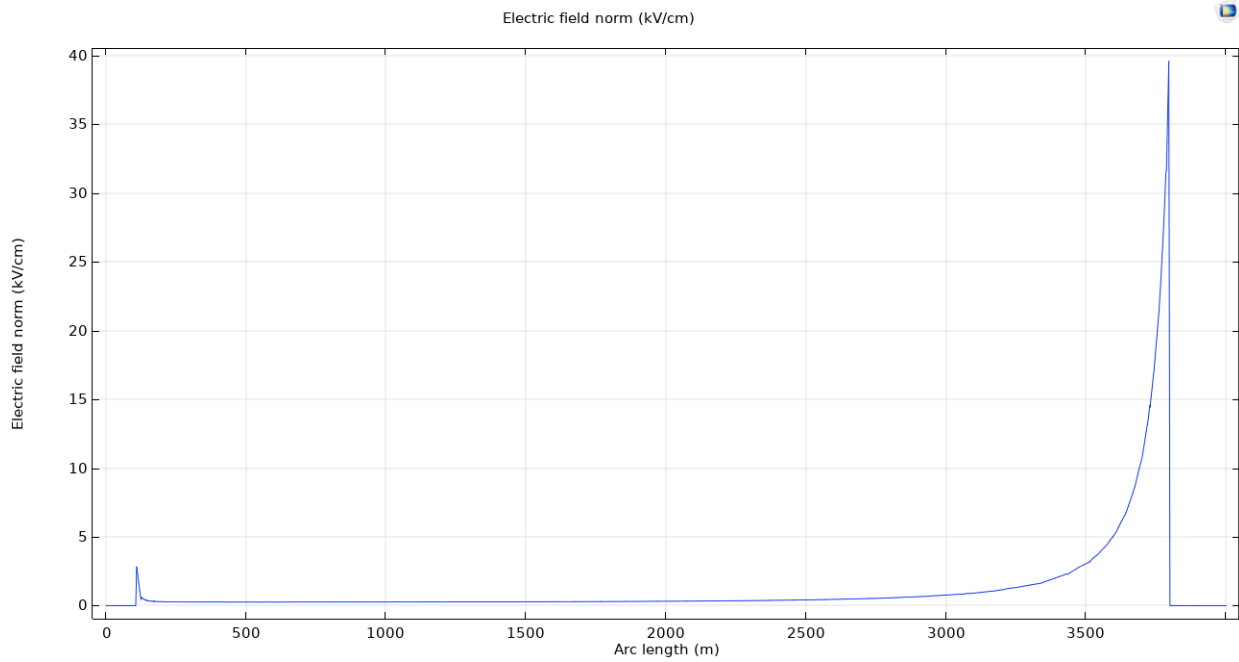


Figure 3.4: 1D electrical field following the line between the tower and the electrode

As it is possible to see in Fig. 3.4, there is an electric field peak around the electrode, due to the shape of the structure. Thus, in the next section will be shown if there are the condition to have the streamer inception (the magnitude of the electrical field is ca  $40 [kV/m]$ , more than the dielectric strength), using the LiveLink Comsol-Matlab.

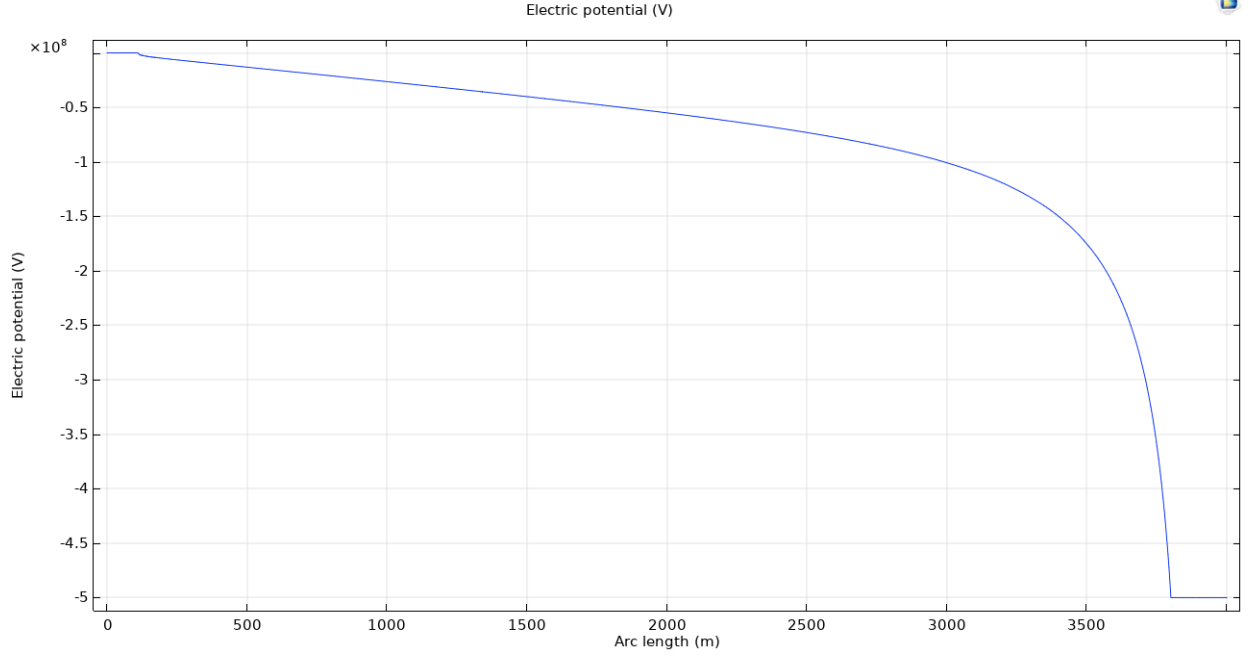


Figure 3.5: 1D electrical potential following the line between the tower and the electrode

### 3.1.1 Streamer Inception

Firstly, I uploaded the simulation on Matlab, and then, in order to evaluate the electrical field, I set a voltage of  $-0.15 \cdot 10^9 [V]$  (The streamer potential written in the code will be useful in the next section), and then I extracted the data from Comsol.

Subsequently, I wrote a function to evaluate also the pressure changing the altitude with the ipsometric formula:

$$P = 0.9887^{H/100}; \quad (3.1)$$

where  $H$  is the altitude.

To have respectively the ionisation and attachment coefficient I used the next relations taken from [1]:

$$\alpha/p = A \cdot e^{-\frac{B}{E/p}}; \quad (3.2)$$

$$\eta/p = -1.95 \cdot \frac{e^{-60 \cdot \frac{p}{E}}}{E/p}; \quad (3.3)$$

where  $A = 15$  and  $B = 365$  are two constants,  $E$  is the local electric field and  $p$  is the local pressure in  $[Torr]$ .

Applying these relation to the local electric field in Fig. 3.6 with the following code I obtained the results in Fig. :

MANCA IMMAGINE

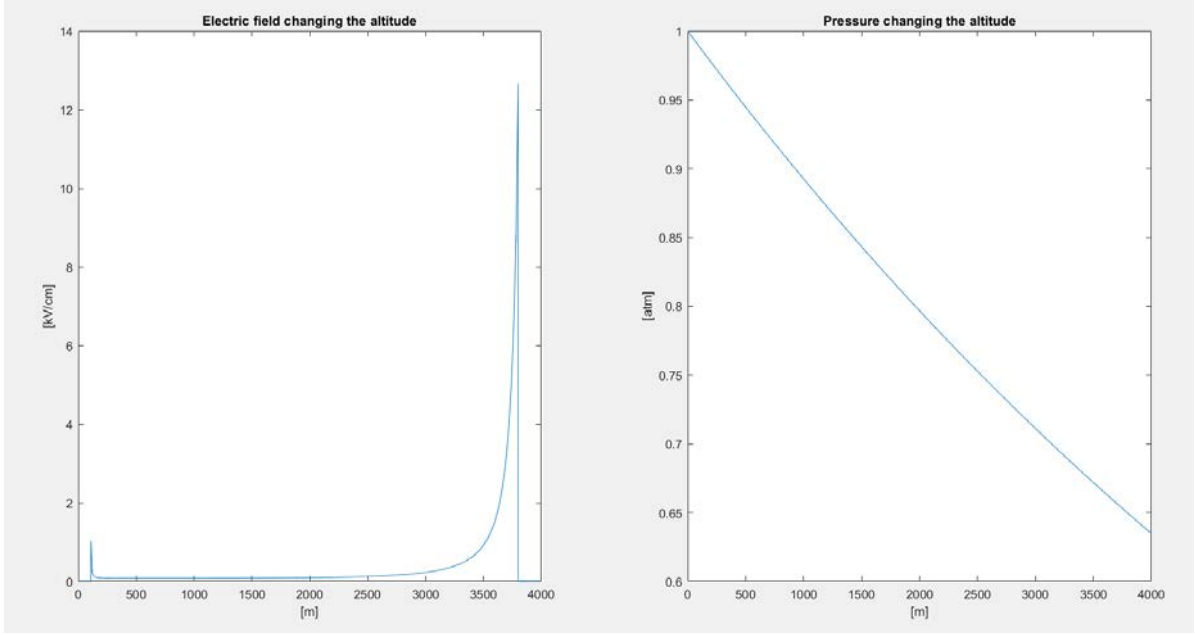


Figure 3.6: Electrical field and pressure changing the altitude.

It is possible to note that the difference between  $\alpha$  and  $\beta$  is positive near the electrode, so we have ions formation. We see in the previous sections that the condition to have a first streamer is deduced from the equation 2.1:

$$e^{\int_{\Delta x} (\alpha - \eta) dx} \geq N_{crit}$$

where  $N_{crit} = 0.55 \cdot 10^8$  [Number of particles]. I calculated this exponential and integral over the line between the electrode and the structure (using the function *trapz* of Matlab) and I obtained a bigger value than  $N_{crit}$ .

**So, we can have the first streamer.**

This is the function I wrote to have the previous results:

---

```

1 % Electric field data extraction from the z-axis
  LightningModel.result.export('data3').run
3 EP = load('Electric_Potential.txt'); %Matrix with electric fields data and
                                     %relative coordinates
5
  % Electric field data extraction along the z-axis
7 LightningModel.result.export('data2').run
  EF_line = load('Efield_line.txt'); %Matrix with electric fields data
                                     %and relative coordinates
9
11 [High,indx] = sort(EF_line(:,1)); %Different altitude point, from 0 to 4000 [m]
   %High(145:157) = []; %Removal of the terms related to the electrodes
13 Efieldno = EF_line(:,2); %Comsol gave datas in the wrong order.
   %To have the right order is necessary
15 Efield = Efieldno(indx)*10^3; %putting the ascissa in crescent order and
   %reordinate the terms of the electric field [V/cm]
17
   [HighP,indxP] = sort(EP(:,1)); %Different altitude point, from 0 to 4000 [m]
19 EPno = EP(:,2); %COMsol gave datas in the wrong order.
```

```

21 EP = EPno(indx);
%To have the right order is necessary
%putting the ascissa in crescent order and
%reordinate the terms of the electric field.
23
% Pressure from the top of the domain (4000m) to the ground
25 Press = 0.9887.^(High/100); %Pressure in function of the altitude [atm]
Presstorr = Press*760; %Pressure in Torr
27 Ratio = (Efield)./Presstorr; %Ratio between the electric field and the
%pressure (E/p [V/(cm*torr)] )
29
31 % Ionization coefficient Alpha/p
A = 15; %Constant
33 B = 365; %Constant
format long
35 alpha_p = A*exp((-B./Ratio));
% Attachment coefficient Eta/p
37 for ii = 1:length(Ratio) %Necessary to avoid the points in which
%the electric field is zero
39 if Ratio(ii) ~= 0
eta_p(ii) = -1.95.*(exp(-60*(1/Ratio(ii))))./Ratio(ii);
41 else
eta_p(ii) = 0;
43 end
end
45 eta_p = eta_p';
%Alpha/p - eta/p: if Diff < 0 no propagation. If Diff > 0 there is
47 % propagation.
Diff = alpha_p-eta_p;

```

---

The code to evaluate the equation 2.1 is:

---

```

Alpha = alpha_p.*Presstorr; %it's necessary isolate the ionisation and
%attachment coefficient
2 Eta = eta_p.*Presstorr; %to obtain a number to verify if there is
4 %the streamer inception

6 %if the next result is > Ncrit, there is the streamer inception
Ncrit = 20.7; %Minimum number of particles that cause the discharge
8 fun = (Alpha-Eta); %Subtraction between the ionisation coefficient
%and the attachment coefficient
10 Ncalc = trapz(High,fun); %this integral gives the number of particles
%that can gives birth to a discharge.

```

---

### 3.1.2 First streamer formation

In this part of the model I took as a reference both the models illustrated in section 2.2.1 and 2.3: in particular, I evaluated the length of the first streamer using the geometrical approach:

INSERIRE IMMAGINE

I built then in Comsol, through the Livelink, the LCR cone, considering an angle  $\vartheta_{SC} = 60$ , and superimposing an electrical field of  $5 [kV/cm]$ :

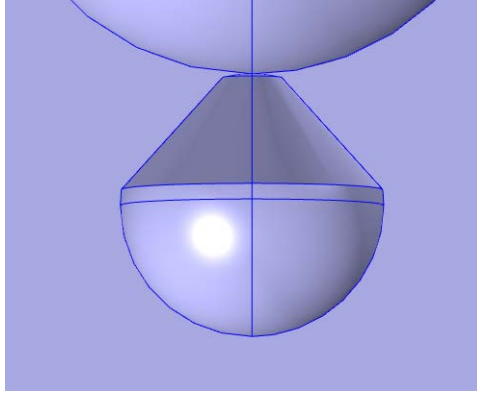


Figure 3.7: LCR cone geometry in the first streamer.

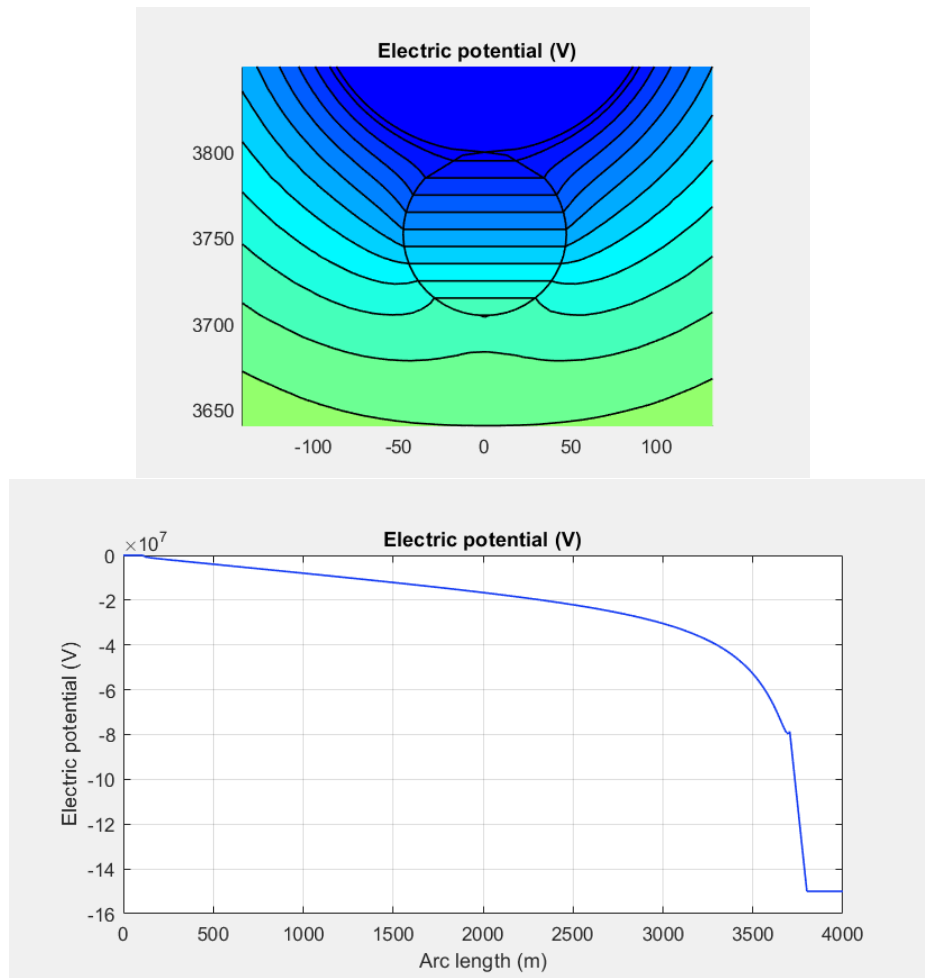


Figure 3.8: 2D and 1D LCR cone potential in the first streamer.

I evaluated then the charge inside of that region calculating (using the *geometrical approach*) the area in Fig. INSERTIRE (using the function *Quad* of *Matlab*) multiplied by  $K_Q$  (as done in 2.2.1, using the equation 2.2), and also with the second method in section 2.3.4, using the equation 2.13: I calculated the integral of the electrical field over the LCR cone surface multiplied by  $\epsilon_0$  with the "Derived values - Surface integral" available



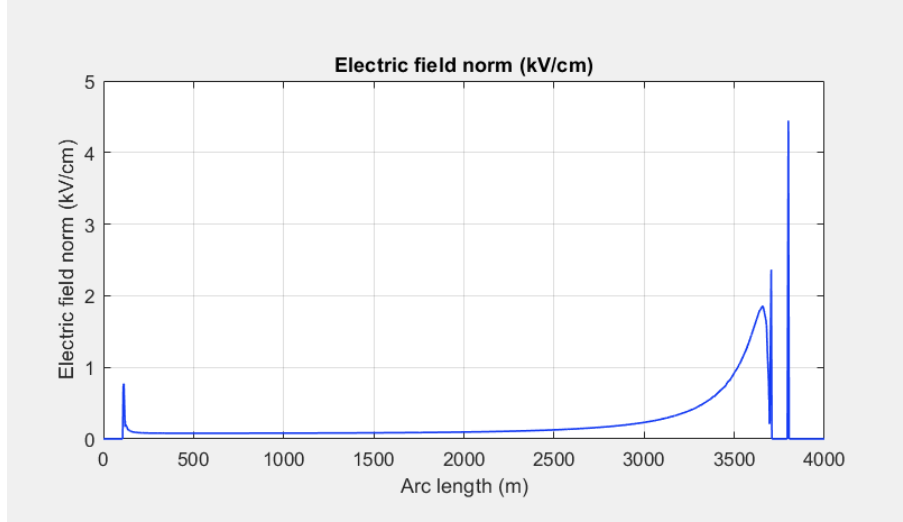


Figure 3.9: 1D LCR cone electrical field in the first streamer.

in Comsol.

I obtained two results: DA INSERIRE, with the same magnitude. I considered the result with the last method, being more accurate. We saw that if  $\Delta Q \geq 5.6 \cdot 10^{-6} [C]$  there are the condition to have a streamer to leader transition. So, I got finally the stem length of the leader using the equation 2.4:

$$\Delta l_L^{(i)} = \frac{\Delta Q^{(i)}}{q_L}$$

where the value of  $q_L$  is taken from the table 2.1.

## Matlab CODE

---

```

1  %% Streamer to Leader

3  % If the condition Ncalc > Ncrit is satisfied, we can proceed with the streamer to
4  % leader transition (we don't consider the dark period because we assume
5  % the charges in the clouds like an electrode with a big curvature,
6  % so the critical radius is not fulfilled).

7

9  %We consider the downward leader and then the upward leader, that
10 %begins when the electric field on the surface of the ground structure is
11 %high enough

12 E_1 = mean(Efield(100:200))*10^5; % Value of the electric field far from
13                                     % the electrode, supposed constant in
14                                     % the first 2000m [V/m]

15 K_q = 3.5*10^(-11);                % Geometric factor [C/V*m]

17

18 %if Ncalc > Ncrit

19 %Graphic way
20 [I] = find(abs(U0-EP) < 10000);    % Indexes in which the potential is
                                     % equal to U0

```

```

23 EP(I) = []; % Elimination of the terms related
% to the electrode
25 HighP(I) = [];
U1_0 = -E_1*HighP; % Decreasing (or increasing) of the
27 % potential far from the electrode [V]

29 Ux = +EP(end) + Estr*HighP(end); % Starting point
U2_0 = -Estr*HighP+Ux; % Imposed streamer electric field [V]
31
33 figure()
plot(HighP,U1_0)
hold on
35 plot(HighP(400:end),U2_0(400:end))
plot(HighP,EP)
37 title('Superimposition of the streamer potential')

39 EG = find(abs(EP - U2_0)<10000000); % Index Point in which the 2 curves
% have an intersection
41 Sub = U2_0(EG(1):end) - EP(EG(1):end); % Considering only the part of the
% 2 curves to subtract
43 D_Q_0 = abs(K_q*trapz(Sub)); % Area between the 2 curves
ls_0 = HighP(end) - HighP(EG(1)); % The first streamer length is the ascissa
45 % of the distance from the tip of the
% electrode and the intersection of
47 % the curves [m]

49 % Comsol way
% Now is necessary to rebuild the geometry with the LCR cone.
51 % Setting the LCR to obtain the length of the initial LCR and then the
% charge inside it.
53
% LCR parameters
55 teta_s = 60; % Internal Angle of the LCR
H_lcr = ls_0; % Length of the LCR, corresponding to the
57 % initial streamer length.
R_lcr = ls_0 * tand(teta_s); % Radius of the LCR to have the teta_s angle
59
% Parameters of the LCR for the first corona
61 % Height of the LCR
LightningModel.geom('geom1').feature('cone1').set('h', H_lcr);
63 % The LCR develops from the tip of the electrode
LightningModel.geom('geom1').feature('cone1').set('pos', [0;0; (4000 - 200 -H_lcr)]);
65 LightningModel.geom('geom1').feature('cone1').set('r', R_lcr);
% Building a sphere to do an interception with the cone, to have the right shape
67 LightningModel.geom('geom1').feature('sph5').set('r', H_lcr/2);
LightningModel.geom('geom1').feature('sph5').set('pos', [0;0; (4000 - 200 -H_lcr/2)]);
69
% Activating the terminal to give to the LCR a potential that varies linearly
71 LightningModel.physics('es').feature('term2').active(true);

73 % Constant term of the equation below, needed to intersect the potential of
% the electrode in the tip of it
75 U_x = U0 + Estr*(4000-200);
LightningModel.param.set('U_x', U_x);
77 % Superimposition of the electric field of the streamer
LightningModel.physics('es').feature('term2').set('V0', '-Estr*(z)+U_x');
79

```

```

81 % Study
LightningModel.study('std1').run;
83
% Postprocessing: Calculation of the charge inside the LCR,
85 % integrating over its surface the electric field * epsilon_0
[C] = mphint2(LightningModel,'es.normE*(8.8541878128e-12)',2,'selection','sel7');
87 figure()
subplot(2,2,1)
89 mphplot(LightningModel,'pg2');
subplot(2,2,2)
91 mphgeom(LightningModel,'geom1','entity','boundary','selection',[7:9,11]);
subplot(2,2,3)
93 mphplot(LightningModel,'pg3');
subplot(2,2,4)
95 mphplot(LightningModel,'pg4');

97 qL = 166.7e-6; % Charge per unit length necessary to thermal transition [C/m]
lL_0 = D_Q_0/qL; % Stem length second corona zone [m]
99 lL_0an = C/qL; % Stem length second corona zone using a numerical method

```

---

### 3.1.3 Streamer to leader transition

In this part I implemented an iterative cycle in order to have the negative leader approaching the tall structure to the ground. It has been possible doing it calculating at each iteration the length of the LCR, building it and then updating the leader adding a segment, following the flow chart in Fig. 2.5.

In the code, firstly I decided the initial parameters, from the table 2.1:

- $E_\infty = 0.3 \cdot 10^5$  [V/m];
- $v = 1.5 \cdot 10^4$  [m/s];
- $\vartheta = 50 \cdot 10^{-6}$  [degrees];
- $x_0 = v \cdot \vartheta$  [m]
- $\Delta Q = \Delta Q_0$  that is the charge calculated in the first streamer.

Once I've done it, I initialized a while cycle that stops only if the length of the leader is more than  $l_{Lmax} = 3000$  [m]. I followed in each iteration several steps:

(A) Updating the leader potential: I valued the potential drop along the leader using

$$\text{the equation 2.3 } (U_{tip}^{(i)} = l_L^{(i)} \cdot E_\infty + x_0 \cdot E_\infty \cdot \ln \left[ \frac{E_{str}}{E_\infty} - \frac{E_{str} - E_\infty}{E_\infty} \cdot e^{-\frac{l_L^{(i)}}{x_0}} \right]);$$

(B) I valued the electrical field along the leader:

$$E_{leader} = \frac{\Delta U}{\Delta l_L} \quad (3.4)$$

and I applied these values to the leader in Comsol;

(C) Updating the potential in the LCR: I imposed a linear decreasing potential to the LCR cone, with a slope equal to the  $E_{streamer} = 750$  [V/m] for the negative streamer;

- (D) Building a new leader segment: using the LiveLink I created the new segment with the length  $\Delta l_L^{(i)}$ ;
- (E) Updating the LCR geometry: I built a new LCR cone with the new streamer length  $l_s$ ;
- (F) Creating a new selection box: I created a box series to manage to select all the segment and give to them the right decreasing potential;
- (G) Creating a new physics for the potential in the new segment: I imposed on the new segment the new potential previous calculated;
- (H) Calculating the new charge performing the double integral over the surface;
- (I) Updating all the parameters for the next iteration and back to (A).

Once the code run, the results I obtained are the following:

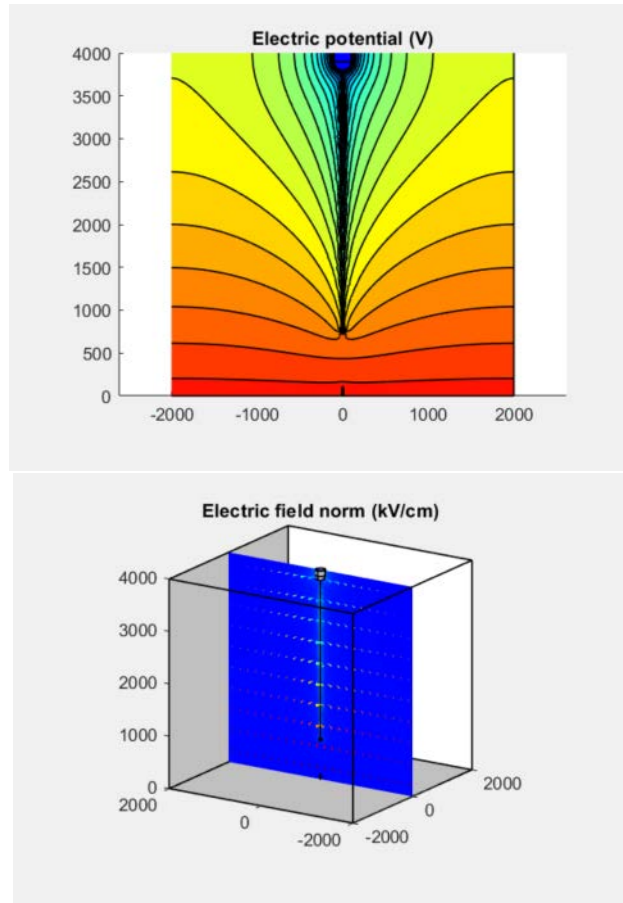


Figure 3.10: Electrical potential (2D) and electrical field (3D) of the approaching negative leader to the ground.

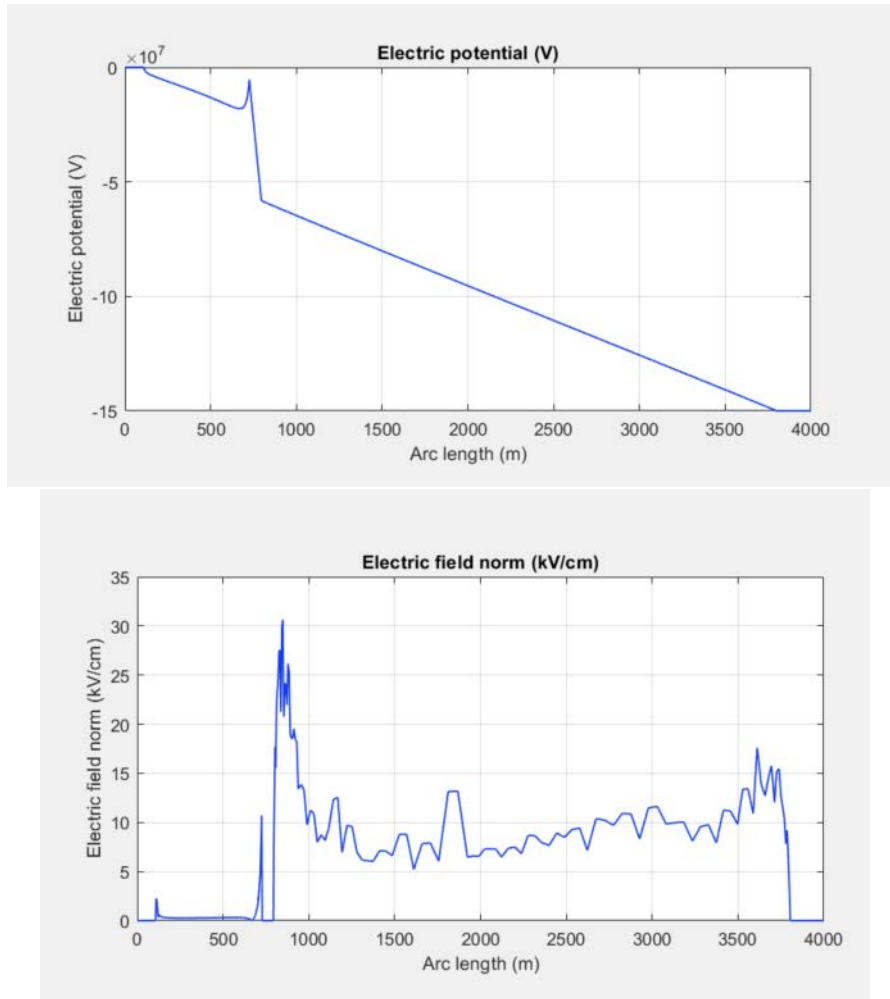


Figure 3.11: 1D Electrical potential and electrical field of the approaching negative leader to the ground.

It is possible to note in Fig. 3.11 the decreasing leader potential that proceeds to the ground and the superimposed electrical field of  $7,5 \text{ [kV/cm]}$  that produces a sharp slope of the potential after the leader tip.

Really important is the value of leader tip, that reaches a value of  $30 \text{ [kV/cm]}$ , high enough to break the dielectric strength of the air and cause the streamer propagation.

## Matlab CODE

---

```

%If the next condition is fulfilled,
2 %the stem can reach the critic temperature of 1500 [K]
if C > 5.7e-6
4
%Leader advancement simulation -- Iterative cycle
6 %Parameters for the cycle
iter = 1;          lLmax = 3000; %maximum leader length to be simulated
8 Einf = 0.3e5;      %Final quasi-stationary leader gradient [KV/cm]
v = 1.5e4;          %Leader speed (supposed constant)
10 teta = 50e-6;     %Leader time constant
x_0 = v*teta;       %Constant

```

```

12 DQ = D_Q_0; %Initializing charge parameter to begin the cycle

14 %Initializing length parameter to begin the cycle
    %lL = 0;
16 Utipprev = U0;      Utip = Utipprev;
    ls = ls_0;
18 lLprev = 0;      lL = lLprev;      DlL = lL_0an;
    DU = 0;      DUprev = 0;
20 Ux_2prev = [];      E_leadprev = [];
    U_xprev = [];      U_x = U_xprev;
22
    figure()
24 hold on
    while lL <= lLmax
26
        %E_lead = (DU)/lL_0; %Electric field of the Leader
        % (supposed linear) - negative value
28
30 %Updating the leader potential
    %Leader voltage drop
32 DU = (-DlL*Einf - x_0*Einf*log(Estr/Einf - ((Estr-Einf)/Einf)*exp(-DlL/x_0)));
    DUtot = DUprev+DU;
34 Utip = U0 - DUtot; %Voltage at the top of the leader
    E_lead = (DU)/DlL; %Electric field of the Leader
    % (supposed linear) - negative value
36
    E_leadvet = [E_leadprev E_lead];
38 %LightningModel.param('default').paramCase(tag4).set('E_lead', E_leadvet(end));
    N_EL = 'E_lead%d';
40 NAME_E_lead = sprintf(N_EL,iter);
    LightningModel.param('default').set(NAME_E_lead, E_leadvet(end));
42
    Ux_2 = Utipprev - E_lead*(4000 - 200 - lLprev) ; %Constant term of the equation below
    %needed to intersect the potential
    %electrode with the tip of it
44
46 Ux_2vet = [Ux_2prev Ux_2];
    N_UX2 = 'Ux_2%d';
48 NAME_UX2 = sprintf(N_UX2,iter);
    LightningModel.param('default').set(NAME_UX2, Ux_2vet(end));
50
    lL = lLprev + DlL;
52 lLNAME = 'The length of the leader at the iteration %d is %f[m]\b' ;
    fprintf(lLNAME,iter,lL)
54
    %Updating the potential in the LCR
56 U_x = Utip + Estr*(3800-lL);
    U_xvet = [U_xprev U_x];
58 N_UX = 'U_x%d';
    NAME_UX = sprintf(N_UX,iter);
60 LightningModel.param('default').set(NAME_UX, U_xvet(end));
    N_LCR = '-Estr*(z)+U_x%d';
62 NAME_LCR = sprintf(N_LCR,iter);
    LightningModel.physics('es').feature('term2').set('V0', NAME_LCR);
64
    Ustr = -Estr*(HighP)+U_x;
66 EG = find(abs(EP - Ustr)<200000);
    ls = 3800-lL - HighP(EG(1));
68

```

70

*%Building a new leader segment*

72

tag = LightningModel.geom('geom1').feature().uniquetag('ls');  
LightningModel.component("comp1").geom("geom1").feature().create(tag, "LineSegment");

74

LightningModel.geom('geom1').feature(tag).set('specify1', 'coord');  
LightningModel.geom('geom1').feature(tag).set('specify2', 'coord');

76

*% The upper part of the new segment, corresponding to the tip of the leader  
% in the previous iteration*

78

LightningModel.geom('geom1').feature(tag).set('coord1', [0;0;4000-200-1Lprev]);

*% Lower part of the leader*

80

LightningModel.geom('geom1').feature(tag).set('coord2', [0;0;4000-200-(1L)]);  
LightningModel.geom('geom1').run(tag);

82

*%Updating the LCR*

84

LightningModel.geom('geom1').feature('cone1').set('h', ls);

*%The position is the top minus the electrode, the leader and the height of the LCR*

86

*%(the cone coordinates start from the bottom)*

LightningModel.geom('geom1').feature('cone1').set('pos', [0;0; (4000 - 200 -ls -(1L)]

88

*%To obtain a cone with an angle of teta\_s*

LightningModel.geom('geom1').feature('cone1').set('r', ls \* tand(teta\_s));

90

LightningModel.geom('geom1').feature('sph5').set('r', ls/2);

LightningModel.geom('geom1').feature('sph5').set('pos', [0;0; (4000 - 200 -ls/2 -(1L)]

92

*%Creating a new selection box*

94

tag2 = LightningModel.selection.uniquetag('sel');

LightningModel.selection.create(tag2, 'Box');

96

LightningModel.selection(tag2).set('xmin', 0);

LightningModel.selection(tag2).set('ymin', 0);

98

LightningModel.selection(tag2).set('zmin', 4000-200-1L);

LightningModel.selection(tag2).set('xmax', 0);

100

LightningModel.selection(tag2).set('ymax', 0);

LightningModel.selection(tag2).set('zmax', 4000-200-1Lprev);

102

LightningModel.selection(tag2).set('entitydim', 1);

LightningModel.selection(tag2).set('condition', 'allvertices');

104

*%creating a new physics for the potential in the new segment*

106

tag3 = LightningModel.component("comp1").physics("es").feature.uniquetag('pot');

LightningModel.component("comp1").physics("es").create(tag3, "ElectricPotential", 1)

108

LightningModel.physics('es').feature(tag3).selection.named(tag2);

N\_LEAD = 'E\_lead%d\*z+Ux\_2%d';

110

NAME\_LEAD = sprintf(N\_LEAD, iter, iter);

LightningModel.physics('es').feature(tag3).set('VO', NAME\_LEAD);

112

114

LightningModel.study('std1').run;

116

*%Charge in the new LCR*

118

[C] = mphant2(LightningModel, 'es.normE\*(8.8541878128e-12)', 2, 'selection', 'sel7');

120

if C < 5.7e-6

break

122

end

124

D1L = C/qL; *%Stem length second corona zone [m]*

126

*%Updating the parameters*

```

128 DUprev = DUtot;
    Utipprev = Utip;
130 lLprev = lL;
    Ux_2prev = Ux_2vet;
132 E_leadprev = E_leadvet;
    U_xprev = U_xvet;
134 mphsave(LightningModel,'Light_final')
    iter = iter+1;
136
    %plotting the potential for each iteration
138 mphplot(LightningModel,'pg3');
    plot(HighP, EP)
140
    end
142 hold off

144 Plots2(LightningModel)
    end

```

---



## 3.2 Positive leader model (straighth path)

In order to achieve a more complex model, I simulated a positive leader model from a tall structure, but in this case in a thunderstorm condition. To modelize that situation I studied a cumulonimbus charge distribution from [5] and [6]. Taking into account the data from those articles (dimensions and charges into the thunderstorm) I built a domain and a geometry as in Fig. 3.12:

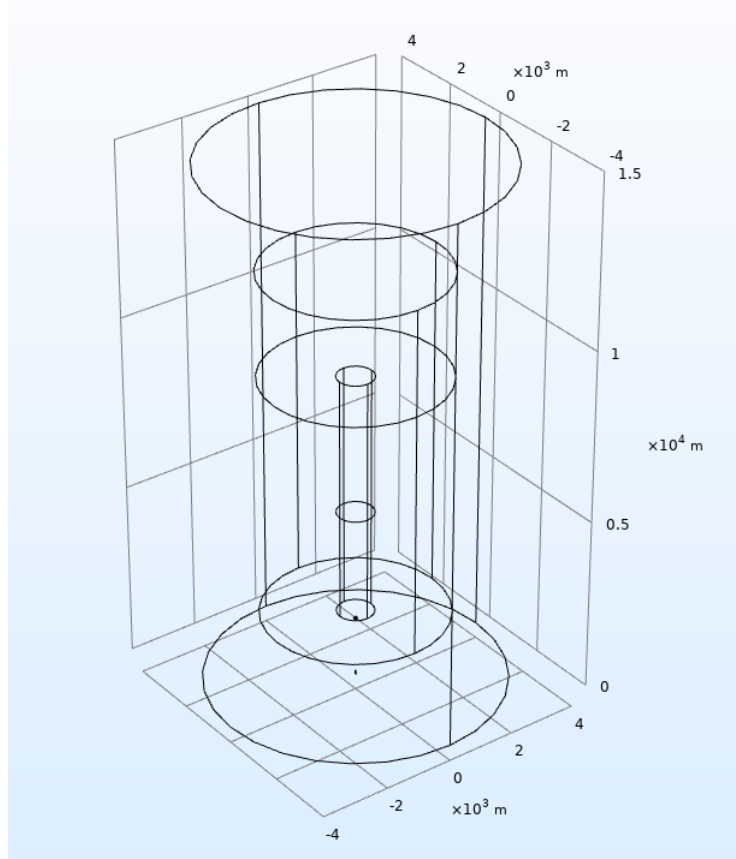


Figure 3.12: Cumulonimbus geometry in Comsol Multiphysics.

I considered a charge distribution in order to obtain a situation as in Fig. 1.8 (section 1.2.1). Running the electrostatic simulation these are the results:

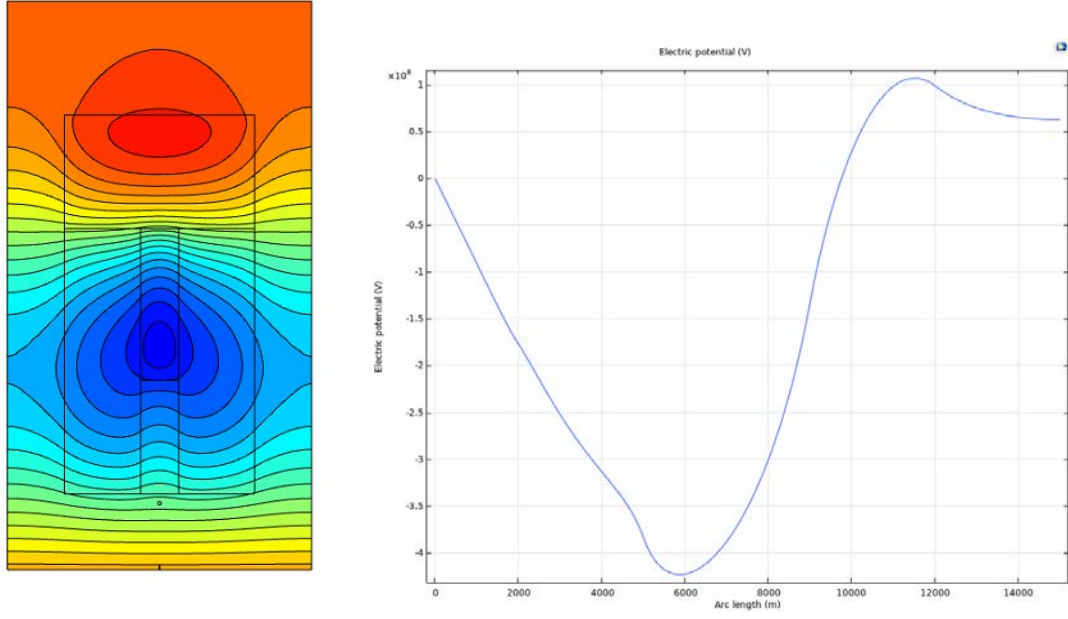


Figure 3.13: Electric field distribution 2D and 1D.

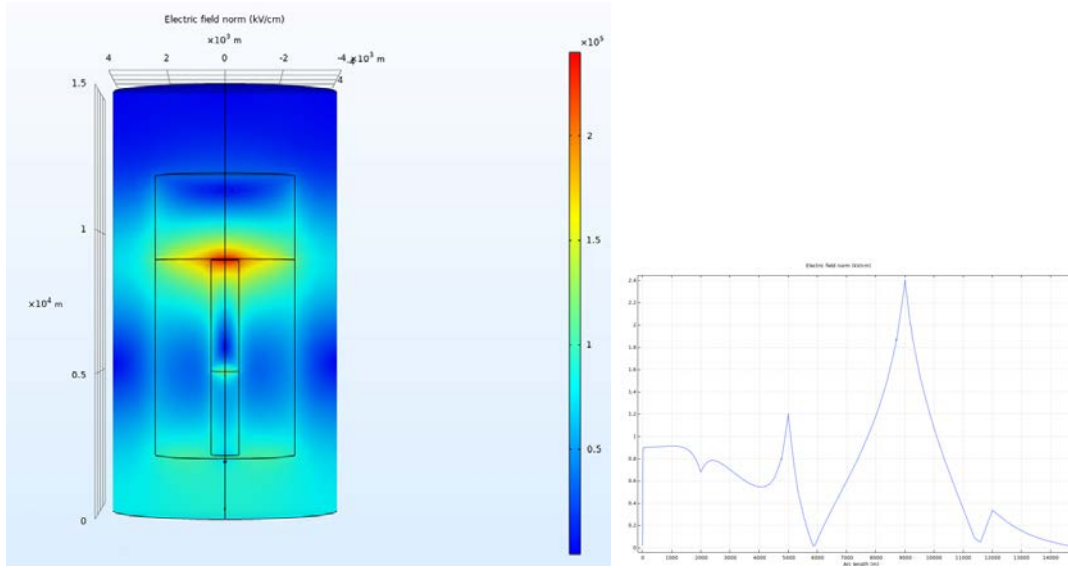


Figure 3.14: Electric potential distribution 2D and 1D.

As it is possible to note in Fig. 3.13 and 3.14, these graphs show the same results of the simulation elaborated in section 1.2.1.

Once the electrical field in a thunderstorm condition is identified, I studied if the streamer formation is possible, taking into account that there are some points in this domain in which the electrical field is really high, so a discharge could be possible from the ground or from a flying object. These considerations will be discussed in the next sections.

### 3.2.1 Streamer inception

As it has been done in section 3.1.1, I performed an electrostatic simulation, taking into account also the grounded structure in thunderstorm conditions. The results are reported below:

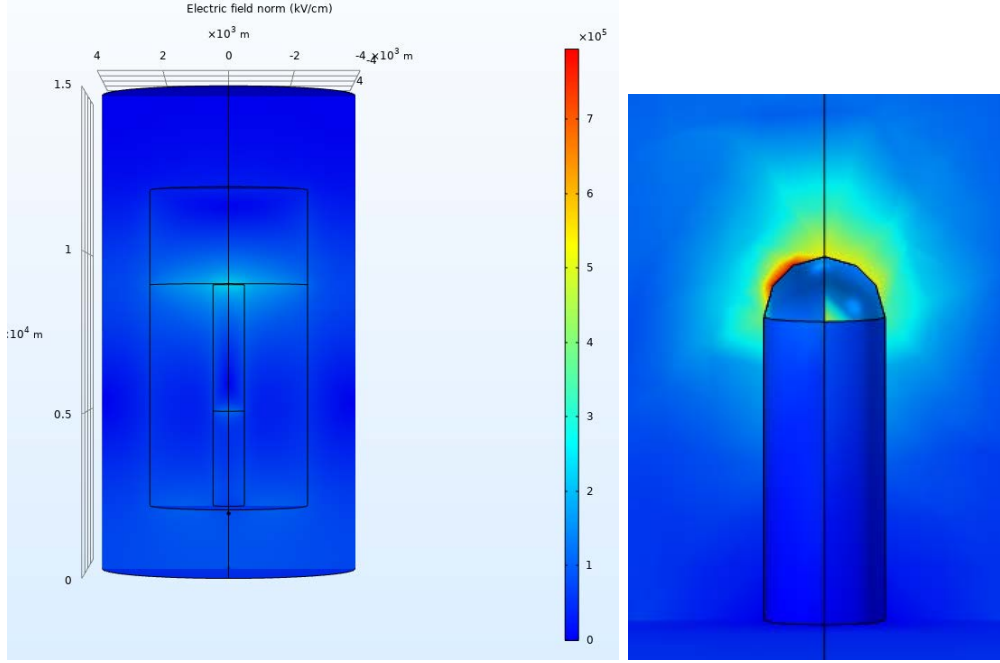


Figure 3.15: Electrical field distribution in 3D, considering also the grounded structure.

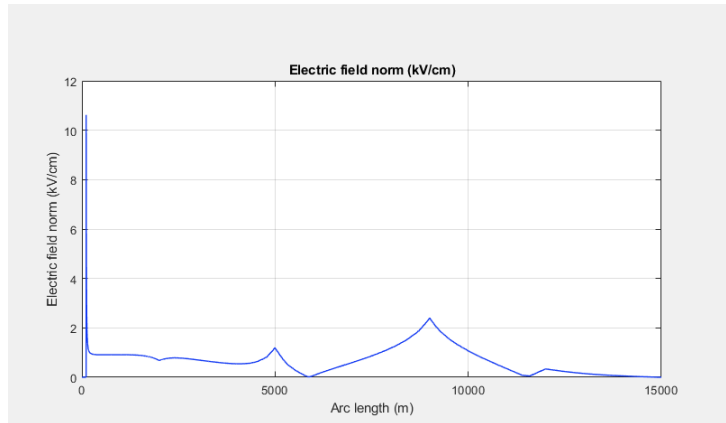


Figure 3.16: Electrical field distribution in 1D.

The electrical field at tip of the tall structure is really high, so I studied if there are the conditions in order to have a first streamer and then a positive leader propagation approaching to the clouds. To verify this, I followed the same procedure of the section 3.1.1, evaluating the ionisation coefficient  $\alpha$  and the attachment coefficient  $\eta$ , varying the electrical field with the pressure.

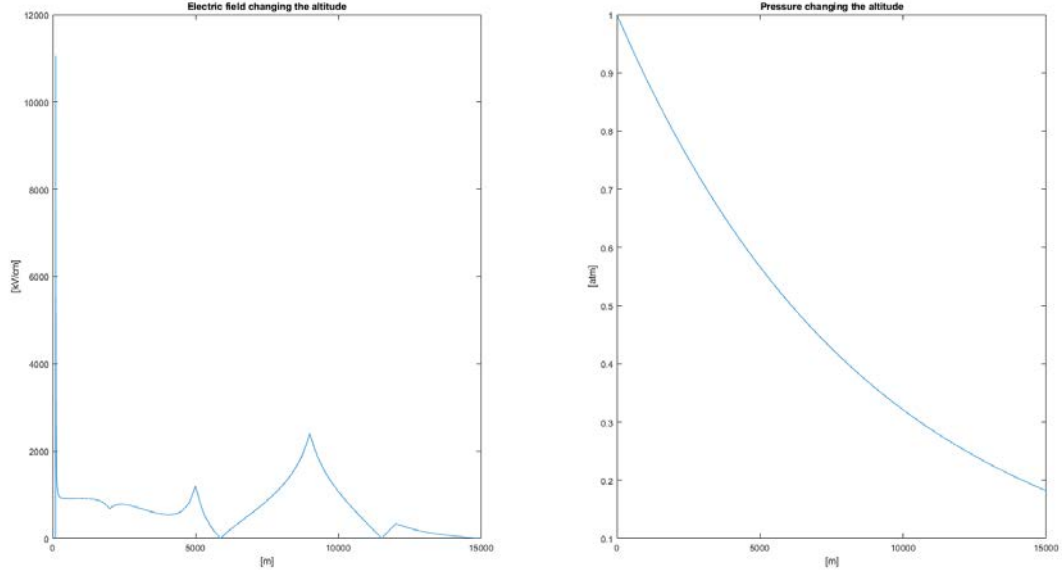


Figure 3.17: Electrical field distribution in 1D and pressure changing the altitude.

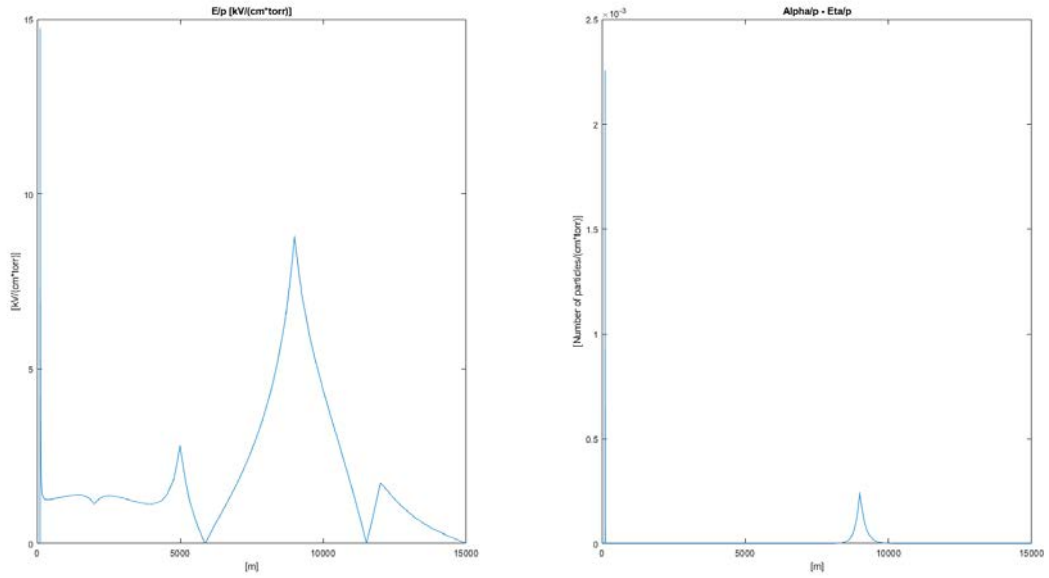


Figure 3.18: Electrical field distribution in 1D and Townsend coefficient changing the altitude.

It can be noticed the difference between  $\alpha$  and  $\eta$  is positive near the structure tip and at 4000 [m]. Thus, I finally used the relation 2.1, verifying there is a streamer inception.

### 3.2.2 Streamer to leader transition

I previously verified the streamer inception conditions. It is possible now to elaborate the positive streamer propagation from the tip of the tall structure. The procedure is similar to the negative leader formation, following the same steps of section 3.1.3, but the potential in this case is positive and decreasing. Running the simulation, the length of the leader increased at each cycle, as we expected:

```
The length of the leader at the iteration 1 is 19.454895 [m]
The length of the leader at the iteration 2 is 47.289986 [m]
The length of the leader at the iteration 3 is 89.518981 [m]
The length of the leader at the iteration 4 is 150.471746 [m]
The length of the leader at the iteration 5 is 236.800376 [m]
The length of the leader at the iteration 6 is 371.478103 [m]
The length of the leader at the iteration 7 is 603.622098 [m]
The length of the leader at the iteration 8 is 1070.763856 [m]
The length of the leader at the iteration 9 is 2266.675892 [m]
```

Figure 3.19: Leader length at each iteration (from the Matlab "Command Window").

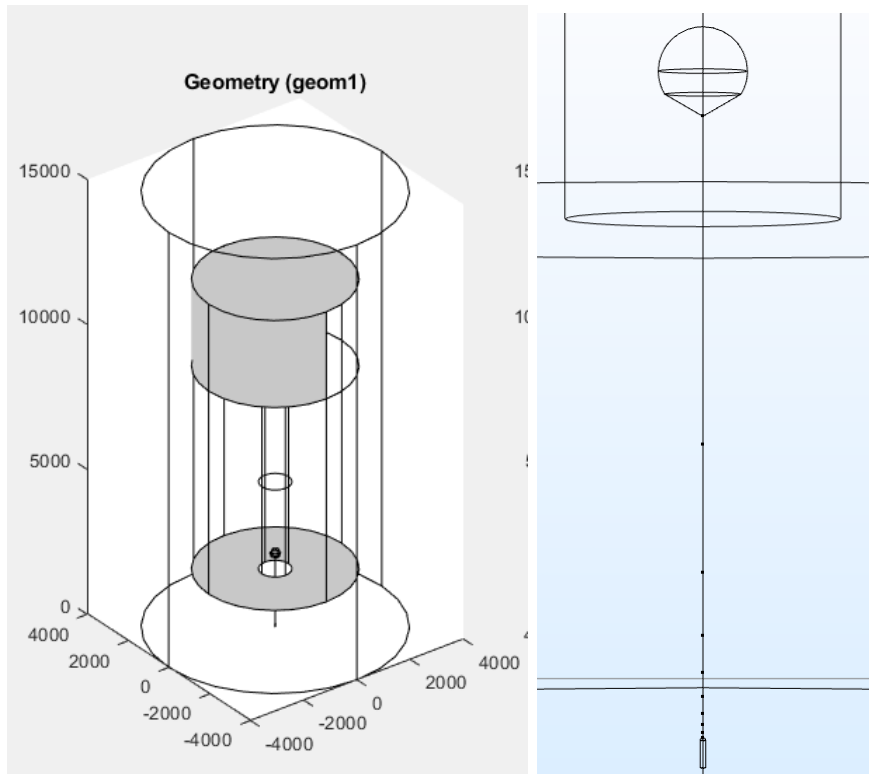


Figure 3.20: Leader geometry once the simulation ended.

The increasing leader length at each iteration means an increasing in the leader velocity and charge at each cycle.

Moreover, the resultant potential and electrical field graphs are really similar to the results derived by R. Morrow and J. J. Lowkein in [10], in which at the tip of the leader the electrical field is high enough to permit the discharge advancing into the space:

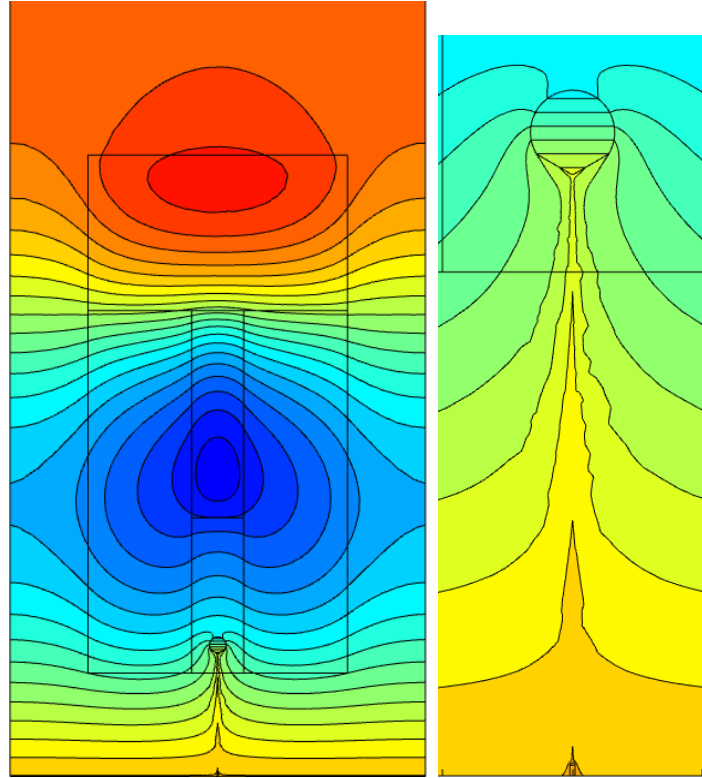


Figure 3.21: 2D leader potential once the simulation ended.

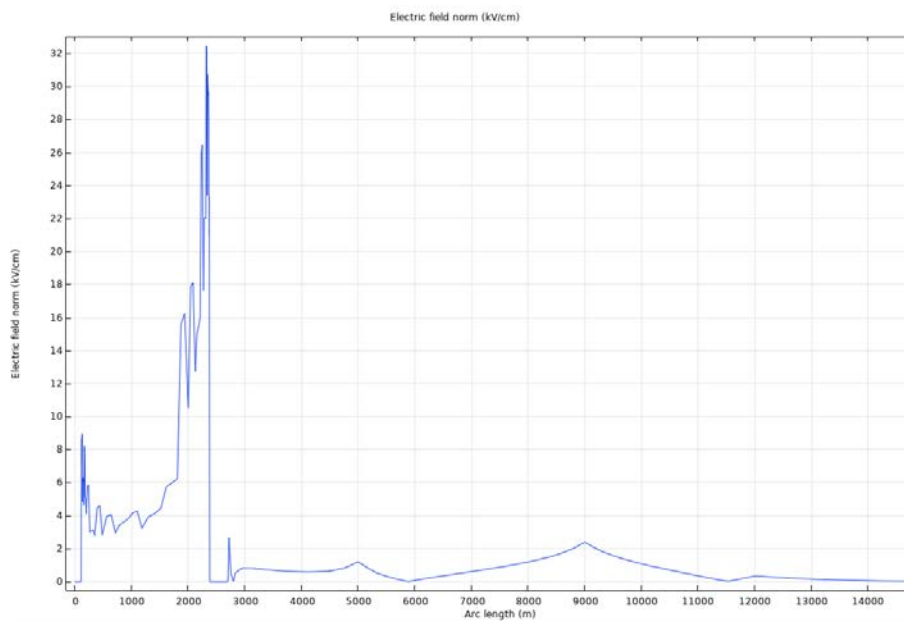


Figure 3.22: 1D leader electrical field once the simulation ended.

These are the leader drop and superimposed potential at each cycle:

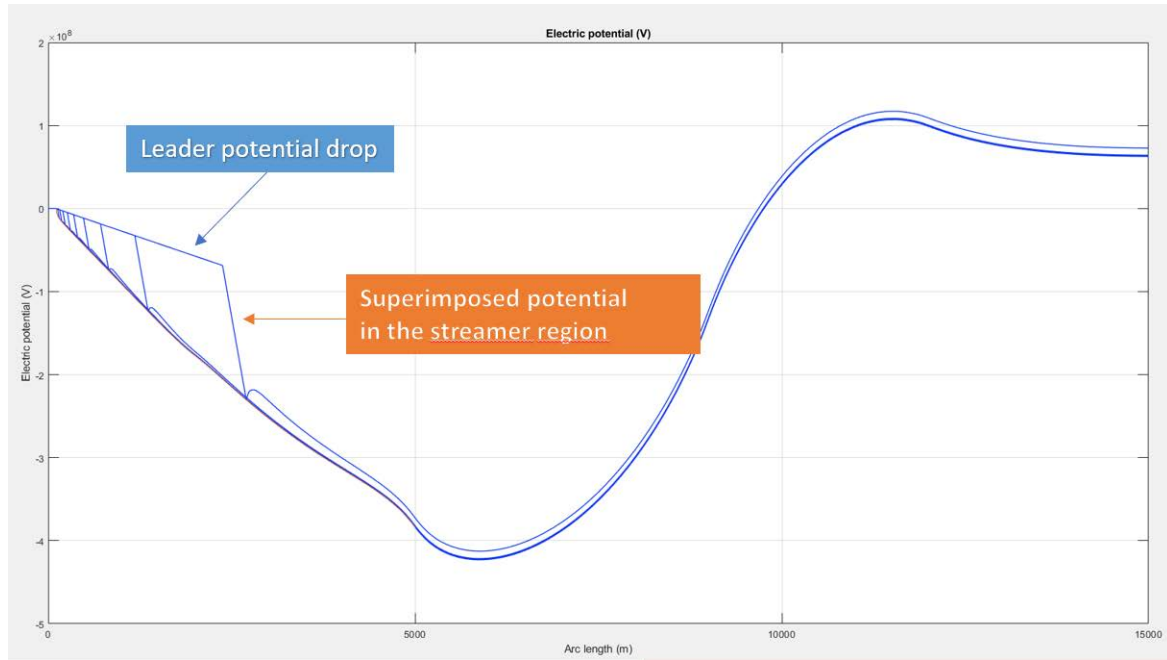


Figure 3.23: 1D Potential drop and superimposed potential.

The potential is modified by the leader progression, causing an increasing on the electrical field while the plasma channel proceeds.

The code to achieve this simulation is presented below:

## Matlab CODE

```

%% Streamer to Leader
2 % If the condition Ncalc > Ncrit is satisfied, we can proceed with the
  % streamer to leader transition (we don't consider the dark period
4 % because we assume the charges in the clouds like an electrode
  % with a big curvature, so the critical radius is not fulfilled).
6
  % We consider the downward leader and then the upward leader, that
8 % begins when the electric field on the surface of the ground structure is
  % high enough
10
  E_1 = mean(Efield(100:200))*10^2; % Value of the electric field far from the
12                                     % electrode, supposed constant in the first
                                     % 2000m [V/m]
14 K_q = 3.5*10^(-11); % Geometric factor [C/V*m]

16 if Ncalc > Ncrit

18 %Graphic way
  [I] = find(abs(HighP - 5000) < 1); % Isolating only the height until to 5000 [m]
20 EP(I:end) = []; % Elimination of the terms with an height more than 5000 [m]
  HighP(I:end) = [];
22 [I_2] = find(abs(EP) < 1);
  EP(I_2) = [];
24 HighP(I_2) = [];

```

```

    Ux = Estr*(HighP(1)); % Starting point for
26  U2_0 = -Estr*(HighP)+Ux; % Imposed streamer electric field [V]

28  figure()
    hold on
30  plot(HighP,U2_0)
    plot(HighP,EP)
32  title('Superimposition of the streamer potential')

34  EG = find(abs(EP - U2_0)<500000); % Index Point in which the 2 curves
                                     % have an intersection
36  Sub = -U2_0(1:EG(end)) + EP(1:EG(end)); % Considering only the part of
                                     % the 2 curves to subtract
38  D_Q_0 = abs(K_q*trapz(Sub)); % Area between the 2 curves
    ls_0 = HighP(EG(end))-110; % The first streamer length is the ascissa
40                                     % of the distance from the tip of the
                                     % electrode and the intersection of
42                                     % the curves [m]

44  % Comsol way
    % Now is necessary to rebuild the geometry with the LCR cone.
46  % Setting the LCR to obtain the length of the initial LCR and then the
    % charge inside it.

48  % LCR parameters
50  teta_s = 60; % Internal Angle of the LCR
    H_lcr = ls_0; % Length of the LCR, correspondig to the initial streamer length.
52  R_lcr = ls_0 * tand(teta_s); % Radius of the LCR to have the teta_s angle

54  %Parameters of the LCR for the first corona
    % Height of the LCR
56  LightningModel.geom('geom1').feature('cone1').set('h', H_lcr);
    %The LCR develops from the tip of the electrode
58  LightningModel.geom('geom1').feature('cone1').set('pos', [0;0; (HighP(1))]);
    LightningModel.geom('geom1').feature('cone1').set('r', 5);
60  LightningModel.geom('geom1').feature('cone1').set('rtop', R_lcr); ;
    % Building a sphere to do an interception with the cone, to have the right shape
62  LightningModel.geom('geom1').feature('sph5').set('r', H_lcr);
    LightningModel.geom('geom1').feature('sph5').set('pos', [0;0; (HighP(1))]);
64

66  % Activating the terminal to give to the LCR a potential that varies
    % linearly
    LightningModel.physics('es').feature('term2').active(true);
68

70  % Constant term of the equation below, needed to intersect the potential
    % of the electrode in the tip of it
    U_x = Estr*(HighP(1));
72  LightningModel.param.set('U_x', U_x);
    %Superimposition of the electric field of the streamer
74  LightningModel.physics('es').feature('term2').set('V0', '-Estr*(z)+U_x');

76

78  % Study
    LightningModel.study('std1').run;

80  % Postprocessing: Calculation of the charge inside the LCR,
    %integrating over its surface the electric field * epsilon_0
82  [C] = mphint2(LightningModel,'es.normE*(8.8541878128e-12)',2,'selection','sel7');

```



```

figure()
84 subplot(2,2,1)
    mphplot(LightningModel,'pg2');
86 subplot(2,2,2)
    mphgeom(LightningModel,'geom1','entity','boundary','selection',[7:9,11]);
88 subplot(2,2,3)
    mphplot(LightningModel,'pg3');
90 subplot(2,2,4)
    mphplot(LightningModel,'pg4');
92
    qL = 166.7e-6; % Charge per unit legth necessary to thermal transition [C/m]
94    lL_0 = D_Q_0/qL; % Stem length second corona zone [m]
    lL_0an = C/qL;
96    mphsave(LightningModel,'Light_final')
    % If the next condition is confirmed, the stem can reach the
98    %critic temperature of 1500K

100    if C > 5.7e-6

102    % Leader advancement simulation -- Iterative cycle
    % Parameters for the cycle
104    iter = 1;      lLmax = 2000; % Maximum leader length to be simulated
    Einf = 0.3e5; % Final quasi-stationary leader gradient [KV/cm]
106    v = 1.5e4; % Leader speeded (supposed constant)
    teta = 50e-6; % Leader time constant
108    x_0 = v*teta; % Constant
    DQ = D_Q_0; % Initializing charge parameter to begin the cycle

110    % Initializing length parameter to begin the cycle
112    Utipprev = 0;      Utip = Utipprev;
    ls = ls_0;
114    lLprev = 0;      lL = lL_0an;      DlL = lL_0an;
    DU = 0;      DUprev = 0;
116    Ux_2prev = [];      E_leadprev = [];
    U_xprev = [];      U_x = U_xprev;

118
    figure()
120    hold on

122    while lL <= lLmax

124    % Adding a new piece of leader
    lL = lLprev + DlL;
126    lLNAME = 'The length of the leader at the iteration %d is %f[m]\n' ;
    fprintf(lLNAME,iter,lL)

128    %Updating the leader potential
130    % Leader voltage drop at the iteration considered
    DU = -((DlL*Einf + x_0*Einf*log(Estr/Einf - ((Estr-Einf)/Einf)*exp(-DlL/x_0))));
132    DUtot = DUprev+DU; % Total Leader voltage drop
    Utip = DUtot; % Voltage at the top of the leader
134    % Electric field of the Leader (supposed linear) - negative value
    E_lead = (DU)/DlL;
136    % Vector containing all the leader electric field values
    E_leadvet = [E_leadprev E_lead];
138    % Updating the name at each iteration
    N_EL = 'E_lead%d';
140    NAME_E_lead = sprintf(N_EL,iter);

```

```

LightningModel.param('default').set(NAME_E_lead, E_leadvet(end));
142
% Constant term of the equation below, needed to intersect the potential
144 % of the electrode with the tip of it
Ux_2 = Utipprev - E_lead*(lLprev + HighP(1));
146 Ux_2vet = [Ux_2prev Ux_2]; % Vector containing all the constant values
% Updating the name at each iteration
148 N_UX2 = 'Ux_2%d';
NAME_UX2 = sprintf(N_UX2,iter);
150 LightningModel.param('default').set(NAME_UX2, Ux_2vet(end));

152 % Building a new leader segment
% Needed to create a new segment at each iteration
154 tag = LightningModel.geom('geom1').feature().uniquetag('ls');
LightningModel.component("comp1").geom("geom1")...
156 ... .feature().create(tag, "LineSegment");
LightningModel.geom('geom1').feature(tag).set('specify1', 'coord');
158 LightningModel.geom('geom1').feature(tag).set('specify2', 'coord');
% The lower part of the new segment, corresponding to
160 % the tip of the leader in the previous iteration
LightningModel.geom('geom1').feature(tag).set('coord1', [0;0;HighP(1)+lLprev]);
162
% Upper part of the leader
164 LightningModel.geom('geom1').feature(tag).set('coord2', [0;0;HighP(1)+lL]);
LightningModel.geom('geom1').run(tag);
166
% Creating a new selection box: inside of it there is the segment
168 % taking into account in the iteration considered
tag2 = LightningModel.selection.uniquetag('sel');
170 LightningModel.selection.create(tag2, 'Box');
LightningModel.selection(tag2).set('xmin', 0);
172 LightningModel.selection(tag2).set('ymin', 0);
LightningModel.selection(tag2).set('zmin', HighP(1) + lLprev);
174 LightningModel.selection(tag2).set('xmax', 0);
LightningModel.selection(tag2).set('ymax', 0);
176 LightningModel.selection(tag2).set('zmax', HighP(1) + lL);
LightningModel.selection(tag2).set('entitydim', 1);
178 LightningModel.selection(tag2).set('condition', 'allvertices');

180 % Creating a new physics for the potential in the new segment
tag3 = LightningModel.component("comp1").physics("es").feature.uniquetag('pot');
182 LightningModel.component("comp1").physics("es")...
... .create(tag3, "ElectricPotential", 1);
184 LightningModel.physics('es').feature(tag3).selection.named(tag2);
% Updating the potential name
186 N_LEAD = 'E_lead%d*z+Ux_2%d';
NAME_LEAD = sprintf(N_LEAD,iter,iter);
188 LightningModel.physics('es').feature(tag3).set('VO',NAME_LEAD);

190 % Updating the potential in the LCR
% Constant term of the equation below, needed to intersect the potential
192 % of the Lcr with the tip of the leader
U_x = Utip + Estr*(lL+HighP(1));
194 U_xvet = [U_xprev U_x];
% Updating the name
196 N_UX = 'U_x%d';
NAME_UX = sprintf(N_UX,iter);
198 LightningModel.param('default').set(NAME_UX, U_xvet(end));

```

```

N_LCR = '-Estr*(z)+U_x%d';
200 NAME_LCR = sprintf(N_LCR,iter);
LightningModel.physics('es').feature('term2').set('V0', NAME_LCR);
202
Ustr = -Estr*(HighP)+U_x;
204 EG = find(abs(EP - Ustr)<500000);
ls = HighP(EG(end))-(1L+HighP(1));
206
% Updating the LCR
208 LightningModel.geom('geom1').feature('cone1').set('h', ls);
% The position is the top of the building, the leader and the
210 % heigth of the LCR (the cone coordinates start from the base of it)
LightningModel.geom('geom1').feature('cone1')...
212 ... .set('pos', [0;0; (HighP(1) +1L)]);
LightningModel.geom('geom1').feature('cone1').set('r', 5);
214 % To obtain a cone with an angle of teta_s
LightningModel.geom('geom1').feature('cone1')...
216 ... .set('rtop', ls * tand(teta_s));
% Intersecting a sphere
218 LightningModel.geom('geom1').feature('sph5').set('r', ls/2);
LightningModel.geom('geom1').feature('sph5')...
220 ... .set('pos', [0;0; (HighP(1) + ls/2 +(1L))]);

222
LightningModel.study('std1').run;
224 mphsave(LightningModel,'Light_final')
% Charge in the new LCR, with a double integral over the
226 %LCR surface multiplied by eps_0
[C] = mphint2(LightningModel,'es.normE*(8.8541878128e-12)',2,'selection','sel7');
228
if C < 5.7e-6 % Stop the cycle in these conditions
230 break
end
232
D1L = C/qL; % Stem length second corona zone [m]
234

236 % Updating the parameters
DUprev = DUtot;
238 Utipprev = Utip;
1Lprev = 1L;
240 Ux_2prev = Ux_2vet;
E_leadprev = E_leadvet;
242 U_xprev = U_xvet;
mphsave(LightningModel,'Light_final')
244 iter = iter+1;

246 % Plotting the potential for each iteration
mphplot(LightningModel,'pg3');
248 plot(HighP, EP)

250 end
hold off

252
% Plotting
254 Plots2(LightningModel)
end

```

---

### 3.2.3 Positive leader model (tortuous path)

Once the positive leader simulation worked with a straight path, I performed a code in order to achieve the tortuous path.

#### Creation of the PDF (Probability density function)

To achieve a realistic model I used the *Probability density functions* presented in [15], taken from experimental results, as previously explained in section 2.3.6. The analytical equations for the angles for the spherical coordinates  $\alpha$  and  $\vartheta$  are:

$$f(\vartheta) = 2,24 \cdot 10^{-2} \cdot \frac{0,035\vartheta + 1}{0,01\vartheta^2 - 0,13\vartheta + 1} \quad (3.5)$$

$$f(\varphi) = 8,7 \cdot 10^{-3} \cdot \frac{9,6 \cdot 10^{-2} + 1}{1,06 \cdot 10^{-2}\varphi^2 - 0,18\varphi + 1} \quad (3.6)$$

For each iteration it is necessary to have an angle value  $\vartheta$  and  $\varphi$  with a probability taken from the equation 3.5 and 3.6; to achieve that result:

- I wrote the previous relations having  $\alpha$  and  $\vartheta$  spacing from 0 to 180 [*degrees*] and  $\varphi$  from  $-180$  to  $180$  [*degrees*];
- I considered from [15] 10000 samples, so I multiplied the PDF (in which the subtended area is 1) for that value. Plotting it, I obtained the following results:

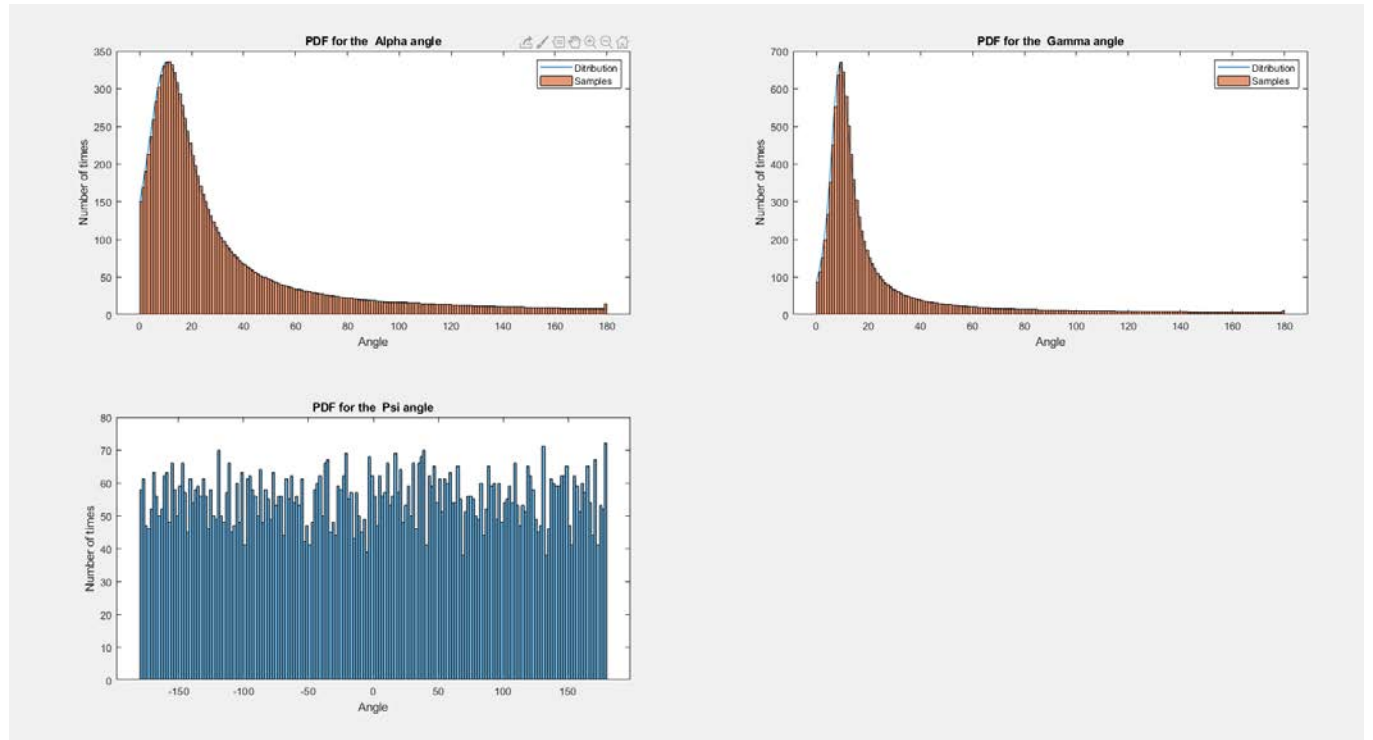


Figure 3.24: Resulting PDF for the  $\alpha$ ,  $\vartheta$  and  $\varphi$  angles.

It is simple to note these results are in close agreement with those in section 2.3.6;

- I created a vector in which there are all the samples (10000) and each angle value ( $0 - 180$  [degrees]) is repeated a number of times given by the PDF in Fig. 3.24 (i.e. considering the alpha angle, from the graph it is possible to see that 20 [degrees] appears ca 200 times. So, in the vector, 20 will be repeated 200 times).

Having such a vector, taking in each iteration a casual value from one of the three vectors created, (using the *Matlab* function "rand") there is exactly the probability to have an angle value given by the probability distribution.

### Code written in the function "Angles"

---

```

1 function [Alpha,Gamma,Psi] = Angles()

3 Angle = linspace(0,180,181); %Values of the angles of Alpha and Gamma
  N_cases = 10000; %Number of samples took to see lightning path
5
  %% Alpha: leader channel segment inclination with respect to the
7 %%discharge axis (0,pi)

9 % Probability distribution multiplied by the number of total cases
  % considered
11 Distr_Alpha = N_cases*(1.49e-2*((0.035*Angle+1)./(0.005*Angle.^2-0.09*Angle+1)));

13 % Vector of data: needed to obtain a vector in which there are all the
  %samples
15 Alpha = [];
  for ii = 1:length(Angle)
17 Distr_Alpha_round(ii,:) = round(Distr_Alpha(ii)); % The "ones" vector doesn't
                                                    % work with decimal numbers
19 % Creating a vector that repeat the value of the angle the times in that
  %iteration there is that value of distribution
21 v = Angle(ii)*ones(Distr_Alpha_round(ii),1);
  Alpha = [Alpha ;v]; % Adding new values at each iteration
23 end

25 %Plotting the results
  figure()
27 subplot(2,2,1)
  plot(Angle,Distr_Alpha)
29 title('PDF for the Alpha angle')
  xlabel('Angle')
31 ylabel('Number of times')
  hold on
33 histogram(Alpha,180);
  legend('Ditribution','Samples')
35 hold off

37 %% Gamma: angle between 2 consecutive leader segments (0,pi)

39 % Probability distribution multiplied by the number of total cases
  % considered
41 Distr_Gamma = N_cases*(8.7e-3*((9.26e-2*Angle+1)./...
  ... (1.06e-2*Angle.^2-0.18*Angle+1)));
43
  %Vector of data: needed to obtain a vector in which there are all the
45 %samples
  Gamma = [];

```

```

47 for ii = 1:length(Angle)
    Distr_Gamma_round(ii,:) = round(Distr_Gamma(ii)); % The "ones" vector doesn't
49 % work with decimal numbers
    % Creating a vector that repeat the value of the angle the times in that
51 % iteration there is that value of distribution
    v = Angle(ii)*ones(Distr_Gamma_round(ii),1);
53 Gamma = [Gamma ;v]; % Adding new values at each iteration
    end
55
    %Plotting the results
57 subplot(2,2,2)
    plot(Angle,Distr_Gamma)
59 title('PDF_for_the_Gamma_angle')
    xlabel('Angle')
61 ylabel('Number_of_times')
    hold on
63 histogram(Gamma,180);
    legend('Ditribution','Samples')
65 hold off

67 %% Psi: leader channel segment projection on a reference plane, also known
    %%as azimuthal ( $-\pi,\pi$ )
69
    % Random number between -180 and 180 [degrees]
71 Psi = randi([-180,180], 1,10000);

73 % Plotting the results
    subplot(2,2,3)
75 histogram(Psi,180)
    title('PDF_for_the_Psi_angle')
77 xlabel('Angle')
    ylabel('Number_of_times')
79
    end

```

---

Written this function, as I previously explained, I built a new leader segment in each iteration, but this time the direction is determined by the value of the spherical coordinates angles  $\vartheta$  and  $\varphi$ .

The code become more complex, due to the tortous path, making the evaluation of the leader and streamer potential more difficult to evaluate in Comsol Multiphysics.

The results are reported below:

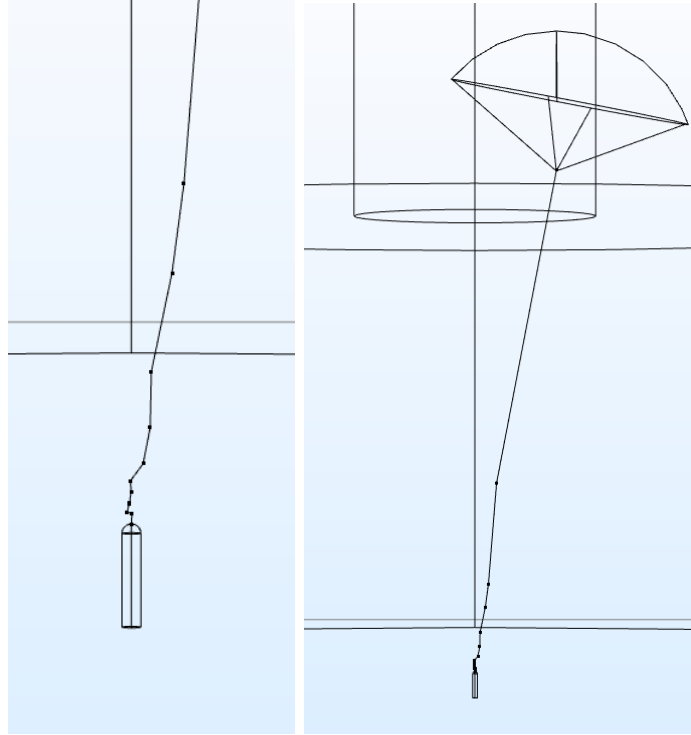


Figure 3.25: Leader geometry after the simulation.

The leader path in this case is tortuous. This is a casual geometry, in which the angle of the segment direction is given by the PDF explained above. If I ran another simulation, I would obtain a different path.

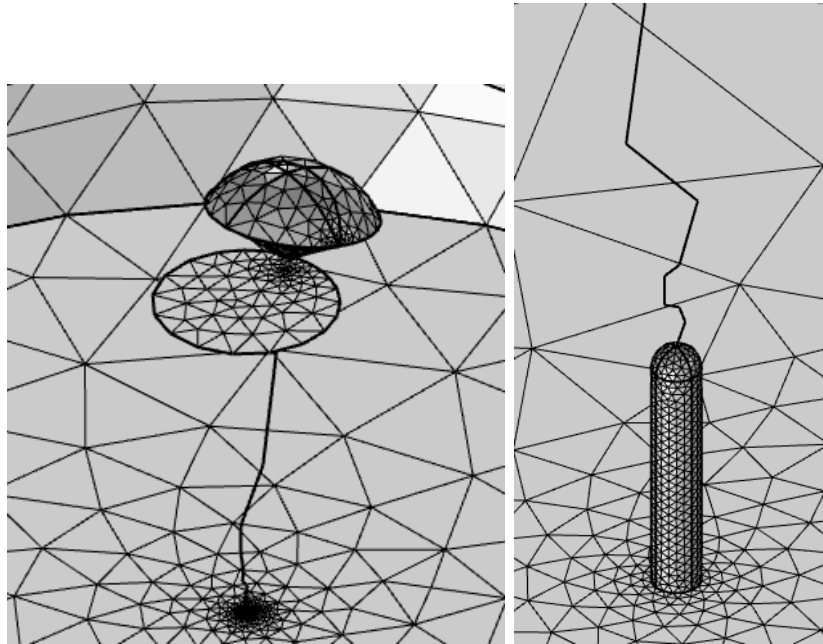


Figure 3.26: Leader meshing during the simulation.

It was necessary setting the mesh in order to have a good resolution of the tall structure, the LCR cone and the leader. In Fig. 3.26 is possible to see how fine is the mesh around the "critical parts".

Finally, these are the results for the electrical potential and field:

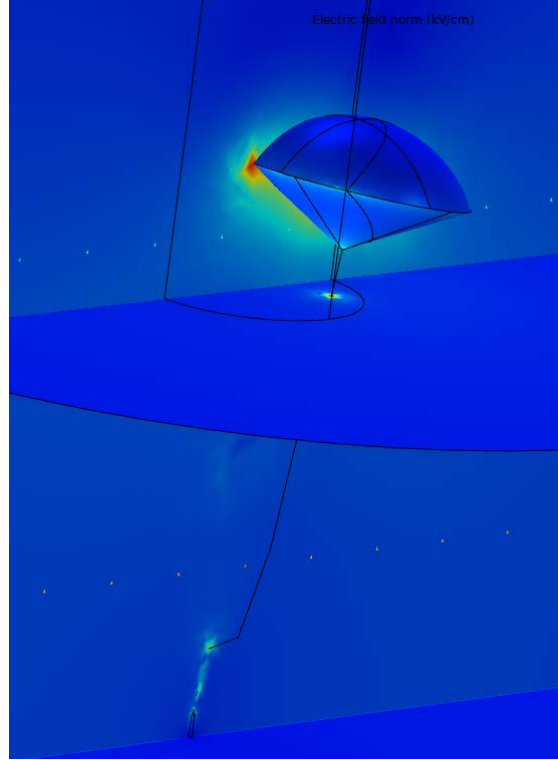


Figure 3.27: 2D electrical field.

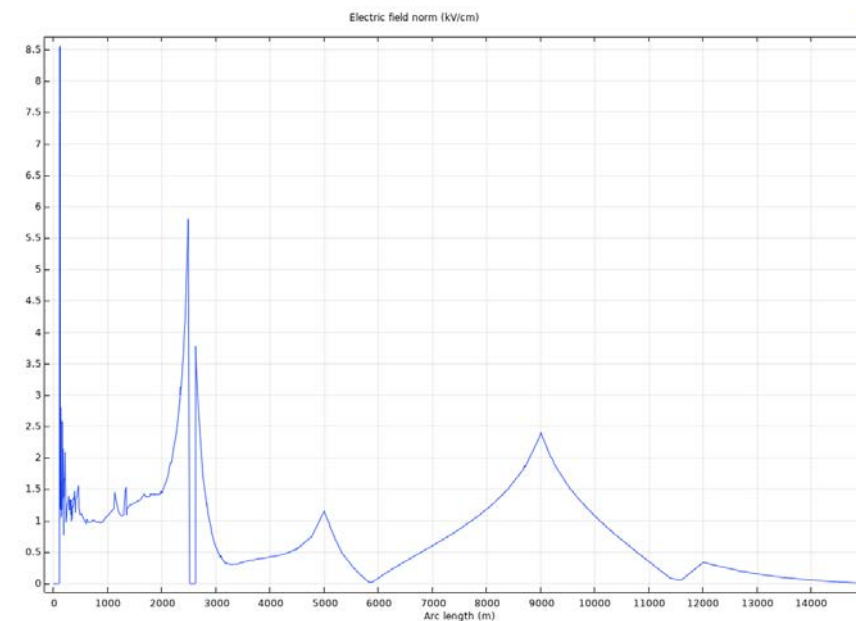


Figure 3.28: 1D electrical field along the z-axis



Evaluating the electrical field, the charge inside the LCR cone, the potential drop and other elements was more difficult, because of the 3D geometry. In order to verify the results it was necessary in Comsol building a number of evaluating lines as the leader segments, with the same direction but a different length. In this way the code can impose the potential drop along the segment and superimpose the  $E_{str}$ :

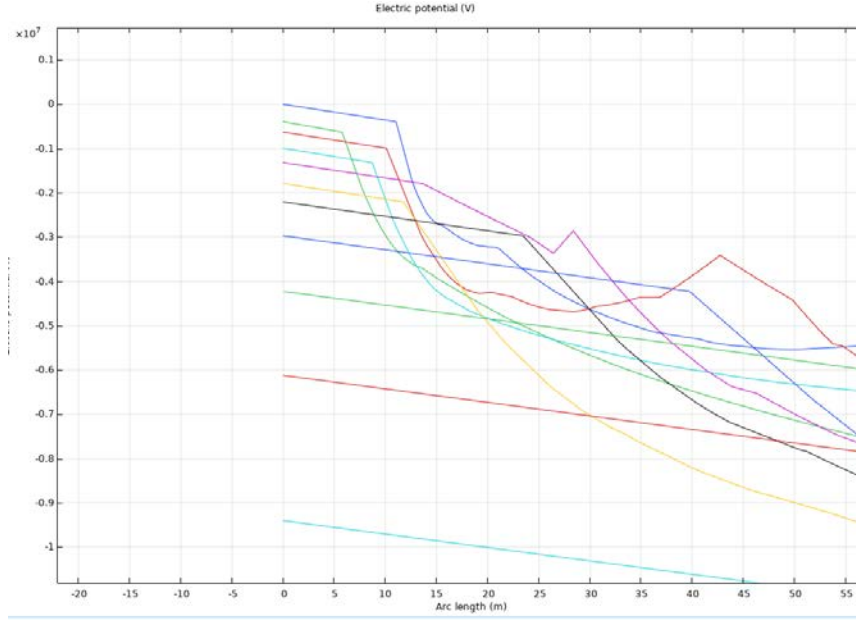


Figure 3.29: Potential drop in the fractal model.

Fig. 3.29 is not simple to understand: each line represent an iteration, and, more precisely, the evaluation of the potential along the evaluating line previously defined. In each iteration it is possible to note that there is a linear decreasing part, corresponding to the linear potential drop of the leader. The rest of it is the evaluation of the potential along the line into domain. It is important to note that the end of the linear decreasing part of each line has the same magnitude of the beginning of the next line: this means that the potential in a segment leader tip corresponds with the potential of the next leader segment.

### Matlab CODE for the fractal model

---

```

% Data samples vector to implement the leader fractal model, based
2 % on statistical data
[Alpha,Gamma,Psi] = Angles();
4
% Spherical coordinates
6 x_in = 0;    xprev = x_in;
  y_in = 0;    yprev = y_in;
8  z_in = 110; zprev = z_in;
  xvec = [];
10 yvec = [];
   zvec = [];
12 V_point = 0;

14 %ITERATIVE CYCLE

```

```

while lL <= lLmax
16
    % Adding a new piece of leader
18    lL = lLprev + DlL;
    lLNAME = 'The length of the leader at the iteration %d is %f[m]\n' ;
20    fprintf(lLNAME,iter,lL)

22    %Updating the leader potential
    % Leader voltage drop at the iteration considered
24    DU = -((DlL*Einf + x_0*Einf*log(Estr/Einf - ((Estr-Einf)/Einf)*exp(-DlL/x_0))));
    DUtot = DUprev+DU; % Total Leader voltage drop
26    Utip = DUtot; % Voltage at the top of the leader
    NUTip = 'Utip%d'; NUTip = sprintf(NUTip,iter);
28    LightningModel.param('default').set(NUTip, Utip);
    % Electric field of the Leader (supposed linear) - negative value
30    E_lead = (DU)/DlL;
    % Vector containing all the leader electric field values
32    E_leadvet = [E_leadprev E_lead];
    % Updating the name at each iteration
34    N_EL = 'E_lead%d';
    NAME_E_lead = sprintf(N_EL,iter);
36    LightningModel.param('default').set(NAME_E_lead, E_leadvet(end));

38    % Constant term of the equation below, needed to intersect the potential of
    %the electrode with the tip of it
40    Ux_2 = Utipprev - E_lead*(lLprev + HighP(1));
    Ux_2vet = [Ux_2prev Ux_2]; % Vector containing all the constant values
42    % Updating the name at each iteration
    N_UX2 = 'Ux_2%d';
44    NAME_UX2 = sprintf(N_UX2,iter);
    LightningModel.param('default').set(NAME_UX2, Ux_2vet(end));
46

    % Spherical coordinates
48    randAlpha = Alpha(randperm(length(Alpha),1));
    randPsi = Psi(randperm(length(Psi),1));
50

52    x = xprev + DlL*sind(randAlpha)*cosd(randPsi);
    y = yprev + DlL*sind(randAlpha)*sind(randPsi);
54    z = zprev + DlL*cosd(randAlpha);

56    xvec = [xvec x];
    yvec = [yvec y];
58    zvec = [zvec z];

60    % Building a new leader segment
    % Needed to create a new segment at each iteration
62    tag = LightningModel.geom('geom1').feature().uniquetag('ls');
    LightningModel.component("comp1").geom("geom1").feature()...
64    ... .create(tag, "LineSegment");
    LightningModel.geom('geom1').feature(tag).set('specify1', 'coord');
66    LightningModel.geom('geom1').feature(tag).set('specify2', 'coord');
    LightningModel.geom('geom1').feature(tag).set('selresult', 'on');
68    % The lower part of the new segment, corresponding to
    % the tip of the leader in the previous iteration
70    LightningModel.geom('geom1').feature(tag).set('coord1', [xprev;yprev;zprev]);
    % Upper part of the leader
72    LightningModel.geom('geom1').feature(tag).set('coord2', [x;y;z]);

```

```

LightningModel.geom('geom1').run(tag);
74
% Creating a new selection cylinder: inside of it there is the segment
76 % taking into account in the iteration considered
tag2 = LightningModel.selection.uniquetag('sel');
78 LightningModel.selection.create(tag2, 'Cylinder');
LightningModel.selection(tag2).set('entitydim', 1);
80
LightningModel.selection(tag2).set('axistype', 'spherical');
82 LightningModel.selection(tag2).set('axis', [randAlpha;randPsi]);
LightningModel.selection(tag2).set('bottom', 0);
84 LightningModel.selection(tag2).set('condition', 'intersects');
LightningModel.selection(tag2).set('pos', [xprev;yprev;zprev]);
86 LightningModel.selection(tag2).set('r', '2');
LightningModel.selection(tag2).set('top', D1L);
88 LightningModel.selection(tag2).set('condition', 'allvertices');

90 % Creating a new physics for the potential in the new segment
tag3 = LightningModel.component("comp1").physics("es").feature.uniquetag('pot');
92 LightningModel.component("comp1").physics("es")...
... .create(tag3, "ElectricPotential", 1);
94 LightningModel.physics('es').feature(tag3).selection.named(tag2);
% Updating the potential name
96 LightningModel.param('default').set('x0', x);
LightningModel.param('default').set('y0', y);
98 LightningModel.param('default').set('z0', z);

100 Nxprev0 = 'xprev0%d'; Nxprev0 = sprintf(Nxprev0,iter);
Nyprev0 = 'yprev0%d'; Nyprev0 = sprintf(Nyprev0,iter);
102 Nzprev0 = 'zprev0%d'; Nzprev0 = sprintf(Nzprev0,iter);
LightningModel.param('default').set(Nxprev0, xprev);
104 LightningModel.param('default').set(Nyprev0, yprev);
LightningModel.param('default').set(Nzprev0, zprev);
106 N_Vp = 'Vp%d'; NAME_VP = sprintf(N_Vp,iter);
LightningModel.param.set(NAME_VP, V_point);
108
NUtipprev = 'Utipprev%d'; NUtipprev = sprintf(NUtipprev, iter);
110 LightningModel.param('default').set(NUtipprev, Utipprev);
N_LEAD = 'E_lead%d*sqrt((x-xprev0%d)^2+(y-yprev0%d)^2+(z-zprev0%d)^2)+Utipprev%d';
112
NAME_LEAD = sprintf(N_LEAD,iter,iter,iter,iter,iter);
114 LightningModel.physics('es').feature(tag3).set('V0',NAME_LEAD);

116 % Updating the potential in the LCR
% Constant term of the equation below,
118 %needed to intersect the potential of the Lcr with the tip of the leader
%U_x = Utip + Estr*(lL+HighP(1));
120 %U_xvet = [U_xprev U_x];
% Updating the name
122 %N_UX = 'U_x%d'; NAME_UX = sprintf(N_UX,iter);
%LightningModel.param('default').set(NAME_UX, U_xvet(end));
124
tag6 = LightningModel.result().dataset().uniquetag('cln');
126 LightningModel.result().dataset().create(tag6, "CutLine3D");
LightningModel.result().dataset(tag6).setIndex("genpoints", xprev, 0, 0);
128 LightningModel.result().dataset(tag6).setIndex("genpoints", yprev, 0, 1);
LightningModel.result().dataset(tag6).setIndex("genpoints", zprev, 0, 2);
130 LightningModel.result().dataset(tag6).setIndex("genpoints", x + ...

```

```

... 1000*sind(randAlpha)*cosd(randPsi), 1, 0);
132 LightningModel.result().dataset(tag6).setIndex("genpoints", y + ...
... 1000*sind(randAlpha)*sind(randPsi), 1, 1);
134 LightningModel.result().dataset(tag6).setIndex("genpoints", z + ...
... 1000*cosd(randAlpha), 1, 2);
136
tag7 = LightningModel.result.export.uniquetag('data');
138 LightningModel.result.export.create(tag7, 'Data');
LightningModel.result.export(tag7).set('data', tag6);
140 LightningModel.result.export(tag7).set('expr', {'V'});
LightningModel.result.export(tag7).set('location', 'regulargrid');
142 LightningModel.result.export(tag7).set('regulargridx1', '10000');
LightningModel.result.export(tag7).set('filename', 'D:\Utenti\padofed18199\...
144 ..._Desktop\Tesi\Lightning_model\Electric_Potential_Fractal.txt');
LightningModel.result.export(tag7).run;
146 EPfrac = load('Electric_Potential_Fractal.txt');

148 Ustr = -Estr*(EPfrac(:,1)-DlL)-DU;
EG = find(abs(EPfrac(:,2) - Ustr)<400000);
150 %         figure()
%         plot(EPfrac(:,1),EPfrac(:,2))
152 %         hold on
%         plot(EPfrac(:,1),Ustr)
154 ls = EPfrac(EG(end))-DlL;

156 Nx0 = 'x0%d'; Nx0 = sprintf(Nx0,iter);
Ny0 = 'y0%d'; Ny0 = sprintf(Ny0,iter);
158 Nz0 = 'z0%d'; Nz0 = sprintf(Nz0,iter);
LightningModel.param('default').set(Nx0, x);
160 LightningModel.param('default').set(Ny0, y);
LightningModel.param('default').set(Nz0, z);
162 N_LCR = '-Estr*(sqrt((x-x0%d)^2+(y-y0%d)^2+(z-z0%d)^2))+Utip%d';
NAME_LCR = sprintf(N_LCR,iter,iter,iter,iter);
164 LightningModel.physics('es').feature('term2').set('V0', NAME_LCR);

166
% Updating the LCR
168 LightningModel.geom('geom1').feature('cone1').set('h', ls);
% The position is the top of the building, the leader and the height of the
170 % LCR (the cone coordinates start from the base of it)
LightningModel.geom('geom1').feature('cone1').set('pos', [x; y; z]);
172 LightningModel.geom('geom1').feature('cone1').set('r', 10);
% To obtain a cone with an angle of teta_s
174 LightningModel.geom('geom1').feature('cone1').set('rtop', ls * tand(teta_s));
LightningModel.geom('geom1').feature('cone1').set('axistype', 'spherical');
176 LightningModel.geom('geom1').feature('cone1').set('axis', [randAlpha;randPsi]);
LightningModel.geom('geom1').feature('sph5').set('r', ls); % Intersecting a sphere
178 LightningModel.geom('geom1').feature('sph5').set('pos', [x; y; z]);

180
LightningModel.study('std1').run;
182 mpshsave(LightningModel,'Light_final')

184 % Postprocessing

186 % Creating a new selection ball: inside of it there is a point
% taking into account the iteration considered
188 tag5 = LightningModel.selection.uniquetag('sel');

```

```

    LightningModel.selection.create(tag5, 'Ball');
190 LightningModel.selection(tag5).set('posx', x);
    LightningModel.selection(tag5).set('posy', y);
192 LightningModel.selection(tag5).set('posz', z);
    LightningModel.selection(tag5).set('r', 1);
194 LightningModel.selection(tag5).set('entitydim', 0);

196 Vpoint = mpheval(LightningModel,'V','selection', tag5);
    V_point = Vpoint.d1;
198

200 % Charge in the new LCR, with a double integral over the LCR surface
    % multiplied by eps_0
202 [C] = mphint2(LightningModel,'es.normE*(8.8541878128e-12)',2,'selection','sel7');

204 if C < 5.7e-6 % Stop the cycle in these conditions
    break
206 end

208 D1L = C/qL; % Stem length second corona zone [m]

210
    % Updating the parameters
212 DUprev = DUtot;
    Utipprev = Utip;
214 lLprev = lL;
    Ux_2prev = Ux_2vet;
216 E_leadprev = E_leadvet;
    % U_xprev = U_xvet;
218 mphsave(LightningModel,'Light_final')
    iter = iter+1;
220 xprev = x;
    yprev = y;
222 zprev = z;
    % Plotting the potential for each iteration
224 mphplot(LightningModel,'pg3');
    plot(HighP, EP)
226
end

```

---

# Chapter 4

## Leader model on an aircraft

On average every commercial airliner gets struck by lightning at least once per year. Thus, the test and design criteria of a new aircraft are becoming important, since the aircraft safety is increasingly dependent on fail-safe electronic equipment.

According to statistics an airplane is struck by lightning on average every 1,000 to 3,000 flight hours. For commercial aircraft, that is equivalent to one lightning strike per year. The aircraft must be able to withstand such a strike without failure of critical electronic equipment and/or without any impairment of flight characteristics.

To study this problem, once I performed the model on a grounded structure, I applied the model on an aircraft. In order to do so, the inception conditions became different due to the fact that the temperature and pressure are different when you are at an height of 4000 [m].

Moreover, in order to evaluate where the electrical field is higher, it is necessary building a geometry of an aircraft.

The same has been done by C. Karch in [16], in which it is possible to read that one the most critical parts of the aircraft is the radome. In particular, in Fig. 2 the enhancement of the ambient electric field is presented around the radome area (a detail from Fig. 4.1).

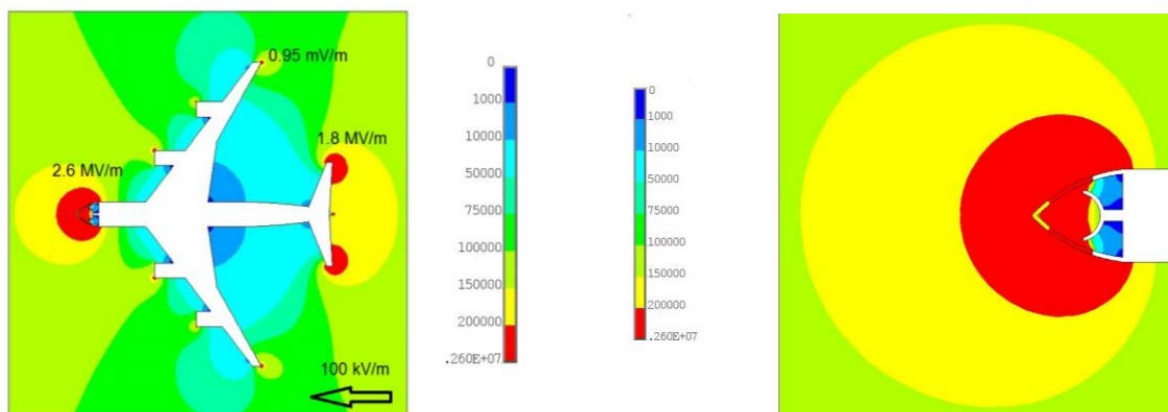


Figure 4.1: 2D electrostatic field around an aircraft in a  $100 [kV/m]$  ambient electric field.

It is clearly shown, that the dielectric radome structure cannot shield the external electric field. A partial shielding effect is here caused by the solid diverter strips only. These last consist of solid metal bars or a series of closely spaced buttons of conductive material. In many ways, diverter strips function like a lightning rod.

In this model, I built a 3D electrostatic simulation in which I included in the thunderstorm an aircraft at an height of 4000 [m]. Firstly it was necessary building the aircraft. I did it using the software *SolidWorks*.

## 4.1 Aircraft geometry

To build the geometry using *SolidWorks* I needed to take as a reference a plan drawing of an aircraft, in order to have all the measures for the 3D CAD project. It is represented in Fig. 4.2:

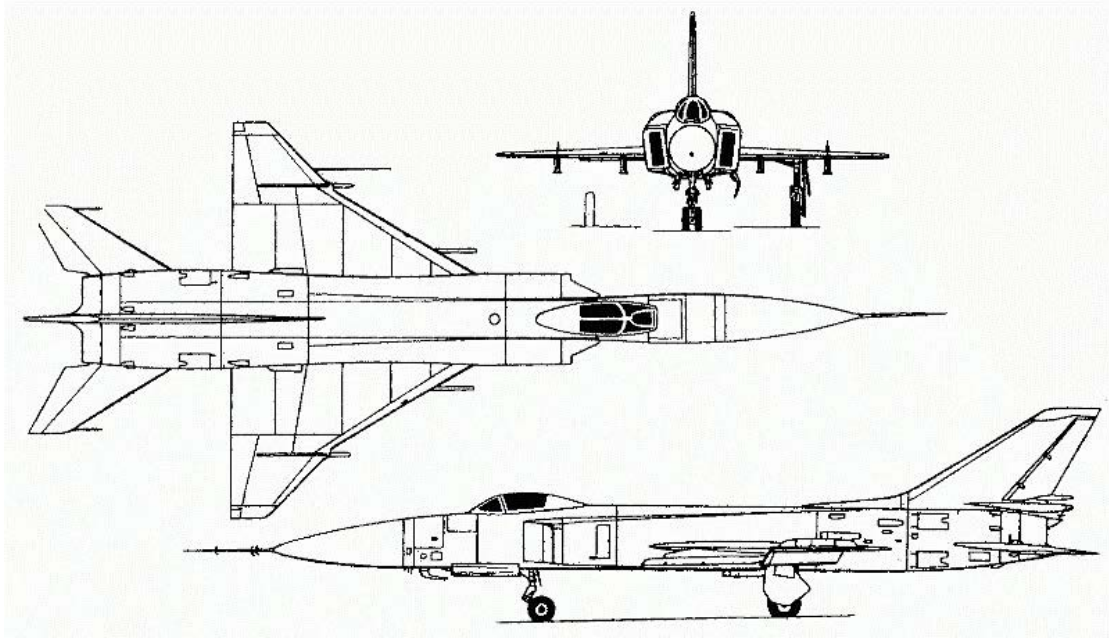


Figure 4.2: Jet plan drawing.

I obtained the following geometry:



Figure 4.3: Aircraft 3D CAD drawing in SolidWorks.

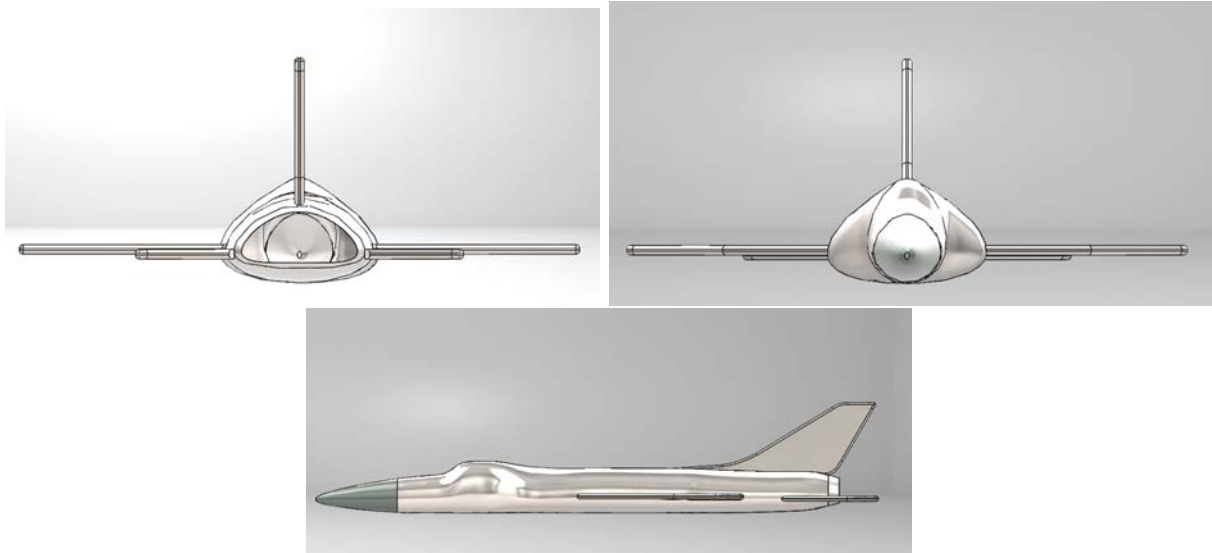


Figure 4.4: Aircraft 3D CAD drew in SolidWorks.

## 4.2 Positive leader model from a radome

In Chapter 1, we described the basic lightning breakdown process.

As noted there, when the intense electric field created by the oncoming leader reaches the ionization potential of air in the neighborhood of extremities and sharp edges on the aircraft, ionization occurs and streamers propagate outward from the aircraft in the direction of the oncoming leader.

Since fiberglass has no electrical conductivity, the electric field passes directly through it, which phenomenon can cause streamers to originate from objects inside as well as outside of the fiberglass structure. What happens may be viewed as a race between streamers propagating from conducting objects inside and outside of the fiberglass structure, as shown in Figure 4.5.

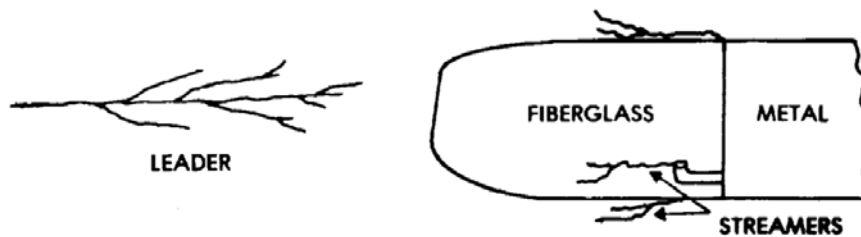


Figure 4.5: Streamers induced by approaching leader.



Both the voltage withstand capability of the fiberglass and the distances along alternate breakdown paths are important in establishing whether puncture or external flashover will occur.

Usually, of course, a higher intensity electric field is necessary to permit the internal streamer to puncture the fiberglass wall and contact the leader than would be necessary merely to draw the external streamer through the air to the leader. As the leader approaches, the field intensity increases until one of the streamers reaches and joins the leader.

Once the geometry has been drawn, it is possible to study (as it has been previously done in section 3.2.1) the streamer inception, considering the different temperature and pressure conditions.

#### **4.2.1 Streamer inception**

Taking account the same equations used in sections 3.1.1 and 3.15 I performed firstly an electrostatic simulation, proving that there is a really high electrical field near the tip of the aircraft. I evaluated then the ionisation and attachment coefficients, verifying that there is a streamer inception in the point in which the electrical field is higher on the aircraft surface.

#### **4.2.2 Streamer-to-leader**

Once the streamer inception is verified, it is possible to study the streamer to leader transition. In order to do it, I evaluated the point on the radome in which the electrical field is higher and I started from there the first streamer, passing then to other leader segments.

The results are reported in Fig. 4.6

The leader proceeds in a random way, given from the PDF studied in section 3.2.3. It was necessary taking into account a simplified geometry in order to have a faster simulation. Using the model of the aircraft, there were some imperfections and the code took too much time.

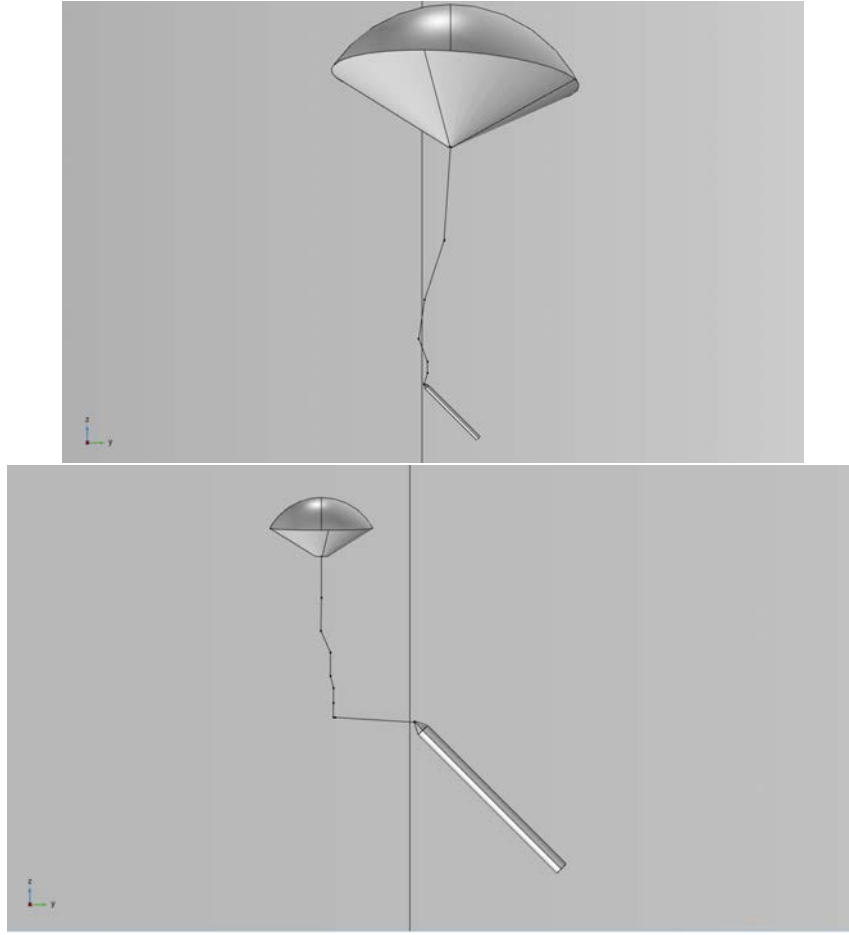


Figure 4.6: Fuselage streamer development

### 4.3 Radome protections

It has been shown how the materials radome is built are transparent to the electrical fields. Most of the times they are in fiberglass components, so, in order to avoid punctures of them there is a need for external conductors that will inhibit internal streamer formation and provide external points from which streamers can originate. Such external conductors, called diverters, also shorten the surface flashover paths. If properly placed, diverters make puncture of a fiberglass skin unlikely. The following guidelines and tests should be followed to orient and space diverters properly on a fiberglass structure:

- I.* orient the diverters as nearly as possible in the line of flight so that flashes which originally strike the diverter can reattach farther aft on the same diverter as the aircraft moves forward;
- II.* while the fore-aft arrangement recommended in Guideline *I.* is desirable for reattachment purposes, an adequate path must also be provided for lightning current to be conducted into the airframe. This requirement usually calls for some of the diverters to be oriented perpendicularly to the line of flight. Examples of preferred arrangements incorporating both of these guidelines are shown in Figure 4.7;
- III.* the surface flashover voltage from any point over the external surface to the nearest diverter strap must be less than the maximum voltage required to puncture the

skin and attach to a conducting object beneath. Thus, the diverter must be within a maximum displacement distance from a point on the skin directly opposite the enclosed conductor. This relationship is defined as follows:

$$\text{Max displacement distance} \leq \frac{\text{Skin puncture voltage [kV]}}{\text{Surface flashover voltage [kV/cm]}} \quad (4.1)$$

- IV. The maximum voltage drop from the original attachment point to any other point on a lightning arc swept aft directly above a nonconducting surface must not exceed the skin puncture voltage from that point through the skin to any conducting objects inside.

The maximum arc voltage drop will occur during a restrike formation in a multiple-stroke flash and can be assumed to be equal to or less than the free air breakdown voltage, or about  $500 \text{ [kV/m]}$  of arc length. Since this voltage will be applied from a point directly above the surface, instead of from an approaching leader, this swept-stroke environment may be more severe than one produced by an initial strike;

- V. The inductive voltage rise,  $V_L$ , along any diverter segment carrying lightning-stroke currents to conducting structure must be less than the skin puncture voltage between the diverter and the nearest conducting object inside the structure. The inductive voltage rise,  $V_L$ , may be expressed as follows:

$$V_L = L \frac{dI_L}{dt} \quad (4.2)$$

Where:  $L$  is the diverter segment inductance  $[H]$ ,  $I_L$  is the lightning current  $[A]$  and  $t$  the time  $[s]$ .

In practice,  $L$  may be assumed to be  $1 \text{ [pH/m]}$  for most diverter straps or foils, and  $dI_L/dt$  may be assumed to be  $100000 \text{ [A/}\mu\text{s]}(1 \cdot 10^{11} \text{ [A/s]})$ .

The intent of Guideline III. is to assure that sufficient diverters are utilized to prevent punctures resulting from initial strikes. Guideline IV. extends this criterion for swept strokes, and Guideline V. is aimed at preventing punctures resulting from inductive voltages that arise when lightning currents flow through the diverter.

This means that a diverter strap can, in fact, be too close to the internal conductor it is supposed to protect.

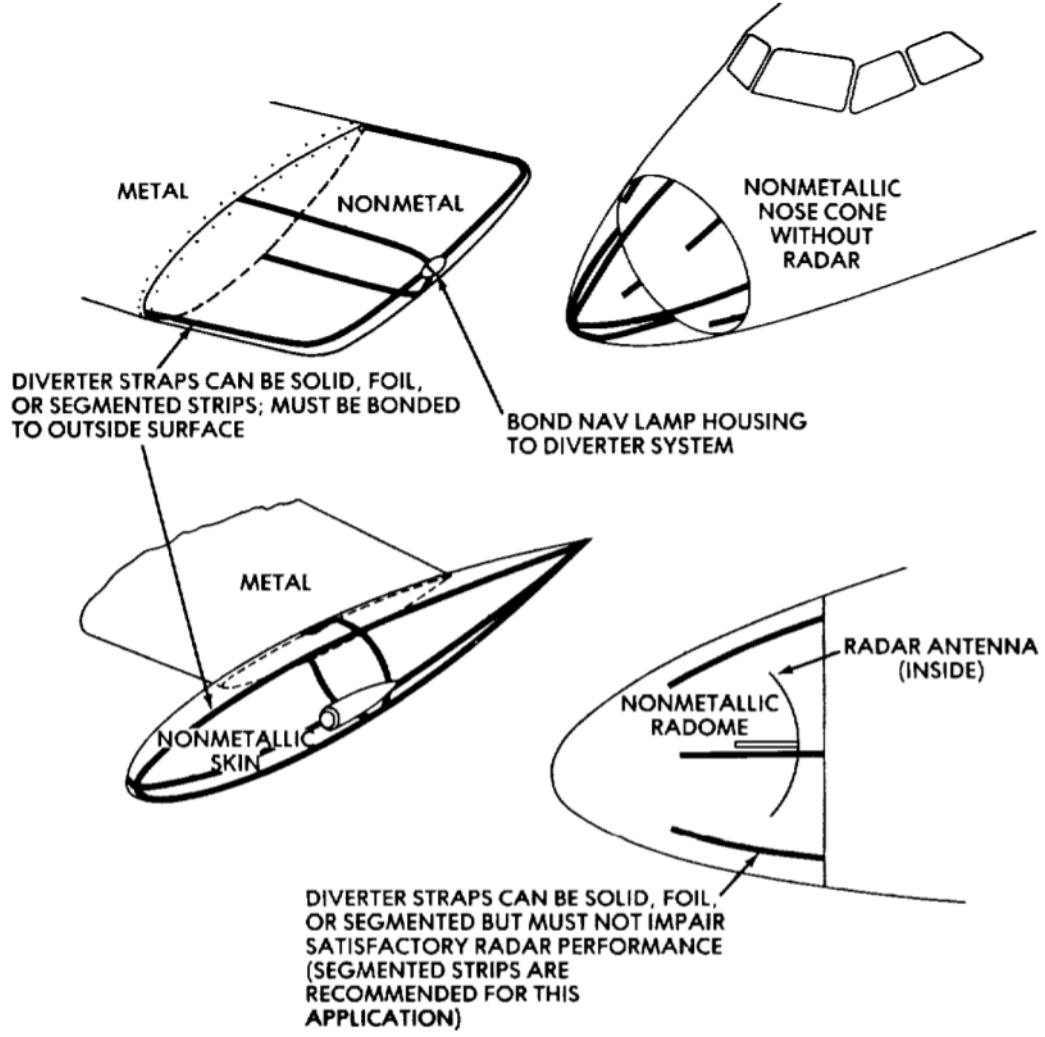


Figure 4.7: Arrangement of diverter straps on non-metallic structural components.

If the maximum inductive voltage along the diverter is greater than the skin-puncture voltage, the diverter will have to be moved a minimum displacement distance away from a point on the skin directly above the enclosed conductor. This distance may be written quantitatively in the following way:

if

$$Diverter\ inductive\ voltage \leq Skin\ puncture\ voltage \quad (4.3)$$

then

$$Minimum\ displdist\ [cm] = \frac{diverter\ inductive\ volt\ [kV] - skin\ puncture\ volt\ [kV]}{surface\ flashover\ voltage\ [kV]} \quad (4.4)$$

Table 4.1: TMPULSE BREAKDOWN VOLTAGES OF TYPICAL FIBERGLASS SKIN MATERIALS

| Skin construction  | Total Thickness | Breakdown Voltage |
|--|-----------------|-------------------|
| One fiberglass shee  | 0, 163 [cm]     | 21 [kV]           |
| Two filament-wound fiberglass tape skins enclosing polyimide foam filler | 1, 27 [cm]      | 150 [kV]          |
| Two fiberglass skins enclosing foam filler                               | 0, 99 [cm]      | 70 [kV]           |

This distance may also be expressed in terms of the diverter inductance and lightning current rate of rise as follows:

$$Minimumdisplacementdistance[cm] = \frac{L [\mu H] dI_L/dt [kA/\mu s] - Skinpuncturevoltage[kV]}{surface flashover voltage [kV]} \quad (4.5)$$

If a minimum displacement distance applies, then the diverter, to be effective, must be positioned somewhere between the minimum and the maximum displacement distances from a point directly above the enclosed conductor.

Clearly, the skin-puncture voltages of nonmetallic skins must be known before protective diverter systems can be designed.

The skin-puncture voltage for a particular nonmetallic skin construction is obtainable by impulse voltage breakdown tests, and is a function of the material type and thickness, as well as of layup patterns, core fillers, surface treatments, etc. Examples of skin puncture voltages determined from 1000[kV/μs] impulse tests are given in Table 4.1

# Chapter 5

## Conclusions

The main purpose of this thesis was to find a model built that, using different softwares, could describe in a realistic way the discharge process, in order to evaluate if a determined object could be the source for a streamer inception and then a leader propagation.

It has been illustrated in the previous sections how I managed to do it, joining different ideas and different models, conciliating them to obtain a simple simulation in which could be shown all the most important data in a discharge.

I tried to do it proceeding by step, adding every time something new and more complicated. At the end this model (mostly regarding the grounded structures) could be used to verify the endurance of the object if it finds itself in a high electrical field environment. If not, the model will show how the leader can propagate into the space, and the quantity of charge it can store.

Moreover, using my model, it is possible to evaluate how the radome of an aircraft could be transparent to the external electrical field.

Regarding this last point, this work is not complete, thus I'll apply this model and these studies in a laboratory environment to test some protection for military aircrafts built by *Airbus* in Cardiff, for the next two years.

# Acknowledgements

Carry out this thesis wasn't simple at all. Once I arrived in Cardiff the Coronavirus already spread into the UK and in all the Europe, so the life wasn't simple.

I've never been to the Cardiff University, and I never met personally all the HV group.

In any case, many people supporting me, firstly the two supervisors that followed me and gave me important suggestions: Professor Manu Haddad from the Cardiff University and Professor Roberto Turri from the Padova University. They helped me remotely in a so difficult period, besides all the difficulties, so I want to thank them. Moreover, prof Haddad has given to me an incredible chance to stay in Cardiff for two more years, working with the HV group and Airbus Defence and Space.

A special thank is for my family: if it wasn't for my parents, for their trust, I wouldn't achieve all these results I'm so proud of. They've always supported me, leaving me the choice to do what I love most. And I can't take into account my sister, that has always been an inspiration for me, and in the lockdown doesn't leave me alone, hosting me in her house in Exeter.

Last, but not least, I thank all my friends, long standings and new friends, for supporting me in the good and in the bad times.

# Bibliography

- [1] Giancarlo Pesavento, *Appunti di Alte Tensioni*.
- [2] Franklin A. Fisher and J. Anderson Plurner , *Lightning Protection of Aircraft*, Lightning Technologies Inc., (2nd edition), 2014
- [3] G. Mazzanti, *Dispense del Corso di Tecnica delle alte tensioni*.
- [4] B Bagheri<sup>1</sup> , J Teunissen<sup>1,2</sup> , U Ebert<sup>1,3</sup> , M M Becker<sup>4</sup> , S Chen<sup>3,5</sup> , O Ducasse<sup>6</sup>, O Eichwald<sup>6</sup> , D Loffhagen<sup>4</sup> , A Luque<sup>7</sup> , D Mihailova<sup>3</sup>, J M Plewa<sup>6</sup>, J van Dijk<sup>3</sup> and M Yousfi<sup>6</sup>, *Comparison of six simulation codes for positive streamers in air*, Plasma Sources Sci. Technol. 27 (2018)
- [5] P.Lalande, V.Mazur *A Physical Model of Branching in Upward Leaders.*, Physics, 2012
- [6] V. Mazur, L.H.Ruhnke *Model of Electric Charges in Thunderstorms and Associated Lightning*, Journal of Geophysical Research, vol. 103, n°. D18, pp. 23,299-23,308
- [7] Oscar Diaz, Vernon Cooray *Methodologies for the charge estimation in the leader corona region used in modeling long air gaps under positive voltage impulses*, ICLP (International Conference on Lightning Protection), 2016
- [8] L. Arevalo, V. Cooray *Preliminary study on the modeling of negative leader discharges*, Journal of Physics D Applied Physics, July 2011
- [9] M. Becerra, V. Cooray *A Simplified Physical Model to Determine the Lightning Upward Connecting Leader Inception*, IEEE Transactions on Power Delivery 21(2):897 - 908 · May 2006
- [10] R Morrow and J J Lowke *Streamer propagation in air*, J. Phys. D: Appl. Phys. 30 (1997) 614–627
- [11] O. Diaz, V. Cooray *Numerical modeling of electrical discharges in long air gaps tested with positive switching impulses*, IEEE Transactions on Plasma Science · February 2018
- [12] I. Gallimberti *The mechanism of the long spark formation*, Le J. Phys. Colloq., Vol. 40, No. C7, pp. C7-193-C7-250, 1979.
- [13] N. Goelian, P. Lalande, A. Bondiou-Clergerie, G. L. Bacchiega, A. Gazzani, and I. Gallimberti, *A simplified model for the simulation of positive-spark development in long air gaps*, J. Phys. D. Appl. Phys., Vol. 30, No. 17, pp. 2441–2452, 1997.



- [14] “*COMSOL multiphysics user guide (Version 5.4)*” COMSOL, AB, 2019.
- [15] Zhijun Li, Shengxin Huang, Jianwei Gu, Tianyu He “*A Contribution to the Investigation of Leader Tortuosity in Positive Long Rod-Plane Air Discharge*” IEEE Access, December 10, 2019.
- [16] C. Karch, M. Calomfirescu, M. Rothenhäusler, C. Brand, and H. Meister “*FFS: LIGHTNING STRIKE PROTECTION OF RADOMES – AN OVERVIEW* ” September 2017.